DETERMINATION OF SHADOWING EFFECTS USING THE P_1 TRANSPORT MODEL

by

WILLIAM WALTER PORATH

B. S., Kansas State University, 1961

A MASTER'S THESIS

submitted in partial fulfillment of the

requirements for the degree

MASTER OF SCIENCE

Department of Nuclear Engineering

KANSAS STATE UNIVERSITY
Manhattan, Kansas

1964

Approved by:

John D. Mingle

Major Professor

TABLE OF CONTENTS

TABLE OF CONTENTS (continued)

APPENDICES (continued)

NOMENCLATURE

A_{lm}	coefficient of Boltzmann equation defined by Eq. (A-18)
B_{lm}	coefficient of Boltzmann equation defined by Eq. (A-18)
C_{lm}	coefficient of Boltzmann equation defined by Eq. (A-19)
D_{lm}	coefficient of Boltzmann equation defined by Eq. (A-19)
D	diffusion coefficient (cm)
f_{lm}	angular flux (neutrons/sec-cm^2)
H	height of rod-moderator region (cm)
I_o (r)	ordinary Bessel function of imaginary argument
J_o (r)	ordinary Bessel function
J	neutron current (neutrons/sec-cm^2)
$P_{lm}(\underline{\Omega})$	associated Legendre polynomials
r	distance from the axis of the cylinder
R1	radius of absorber (inches)
R2	outer radius of moderator region (inches)
s	displacement in the direction of $\underline{\Omega}$
s_l	expansion coefficient defined by Eq. (A-11)
S'	source of thermal neutrons (neutrons/sec-cm^2)
S_{lm}	expansion coefficient defined by Eq. (A-13)
$U_o(\alpha r)$	a particular solution of Bessel's equation (see Appendix C)
α	separations equation constant defined by Eq. (26)
β	separations equation constant defined by Eq. (16)

γ	separations equation constant defined by Eq. (26)
∇	gradient operator
∇^2	Laplacian operator
λ	separations equation constant defined by Eq. (16)
λ_{tr}	transport mean free path (cm)
κ^2	ratio of macroscopic absorption cross section to diffusion coefficient (cm^{-2})
$\underline{\Omega}$	unit vector in the direction of the neutron motion
φ	angle between the projection of $\underline{\Omega}$ on the x-y plane and the direction of $\underline{r}$
ϕ	thermal neutron flux (neutrons/sec-cm^2)
σ	standard deviation
Σ	total macroscopic cross section (cm^{-1})
Σ_a	macroscopic absorption cross section (cm^{-1})
Σ_s	macroscopic scattering cross section (cm^{-1})
Σ_{tr}	macroscopic transport cross section (cm^{-1})
θ	angle between $\underline{\Omega}$ and the z axis
θ_o	angle between the unit vectors $\underline{\Omega}$ and $\underline{\Omega}'$

Subscripts

l	primary indices in the spherical harmonic expansion
m	secondary indices in the spherical harmonic expansion
1	absorber region
2	moderator region

INTRODUCTION

Within the active core volume, the various materials present compete with each other in the absorption of the neutrons present. In reactors that are assumed to be homogeneous, the ratios of the cross sections may be used to well describe the events that occur. However, in a reactor that is considered hetrogeneous, which is the usual case, the neutron flux, and hence the rate of absorptions and collisions, may vary greatly between the materials present.

Consider the case where an absorbing rod is separate from the moderating material. If an experimental determination is made of the neutron flux in the moderator and the rod, a depression of the flux within the rod will be evident. This depression, though expected, is greater than that predicted by a diffusion theory calculation using the value of the flux at the surface of the rod as the average flux inside the absorber. This phenomenon is called self-shielding or self-absorption, and it is due to the absorption of a considerable fraction of the incoming neutrons by the nuclei near the surface of the absorbing rod.

Some work has been done which treats self-shielding and capture of neutrons by cylindrical shapes surrounded by a scattering medium (4, 8, 9). Bartels (1) surveyed all the earlier literature (pre-1950) on self-shielding for various absorber geometries. He presented this information in graphical form along with the analytical expressions used

to construct the graphs. In each case, the problem of self-shielding was approached from the viewpoint of a self-absorption factor and an effective cross section. Dwork, et. al. (4) investigated self-shielding for an infinitely long, hollow cylinder. This group rigorously derived equations expressing the self-shielding in a hollow cylinder, and presented their results in graphical form. However, they too used a self-shielding factor and an effective cross section to account for the increased flux depression. Kushneriuk (8) investigated the problem of neutron capture by long cylinders. He arrived at an expression for the self-shielding correction in terms of the average flux in the rod and the unperturbed flux. So, in essence, an effective cross section was determined.

Thus, it appears that the conventional method of treating self-shielding is by determining an effective cross section for the absorber. Then, the proper neutron absorption is obtained by multiplying the average neutron flux inside the absorber by the effective cross section.

A different approach to the problem of self-shielding is one that relates the measured value of the cross section and the physical radius of the rod to an effective rod radius. That is, given a rod of known radius and cross section, an effective rod radius is determined so that the neutron absorption as calculated using the effective rod radius, the neutron flux at the surface of the rod, and the cross section, would match the experimentally determined flux depression.

Thus, to fully utilize the concept of an effective rod radius, one would like to have available graphs that relate the effective rod radius to some dimensionless parameter that is peculiar to the system under consideration. Since the product of the macroscopic absorption cross section and the rod radius is dimensionless, graphs involving this quantity as well as moderator properties would reduce the labor involved in the calculation of the thermal neutron flux level and the power distribution throughout the active core volume.

THEORY

A rigorous solution of the Boltzmann transport equation using spherical harmonics results in an expression for the flux that is an infinite series involving the associated spherical harmonics, i.e., the $P_{\ell m}(\Omega)$ or the associated Legendre polynomials. By considering only a finite number of terms in the series, an approximation to the value of the flux can be made. The accuracy of the approximation depends on the number of terms of the infinite series that are specified. These approximations are symbolically represented as P_ℓ approximations, where the value of ℓ denotes the order of the approximation; e.g., $\ell = 1$ is a first order approximation, $\ell = 2$ is a second order approximation, and so on. The subscript m ranges from $-\ell$ to $+\ell$. A more detailed discussion of the spherical harmonics solution of the Boltzmann transport equation in cylindrical geometry is presented in Appendix A, while a general treatment of this subject can be found in references (3, 5, 7, 11, 16).

The P_1 approximation results when the infinite series representation of the flux is terminated after two terms, $\ell = 0$ and $\ell = 1$. The three equations that are obtained lead to a solution for the flux that is identical with the result of ordinary diffusion theory (3, 7, 12, 16) except for the definition of D, the diffusion coefficient. For the P_1 approximation, the diffusion coefficient is defined as $1/(3\Sigma_{tr})$, while for diffusion theory, the diffusion coeffi-

cient is defined as $1/(3\Sigma_s)$. Keeping in mind this difference in notation, the mathematical methods associated with diffusion theory will be applied to the problem under consideration.

The geometry of this problem is shown in Figure 1. The center region, region I, represents an absorber. The z axis is co-linear with the axis of region I. Region II, which is concentric to region I, represents the moderator. The source is located in the x-y plane, and it can assume any configuration, i.e., point source, plane source, discrete sources, and so forth.

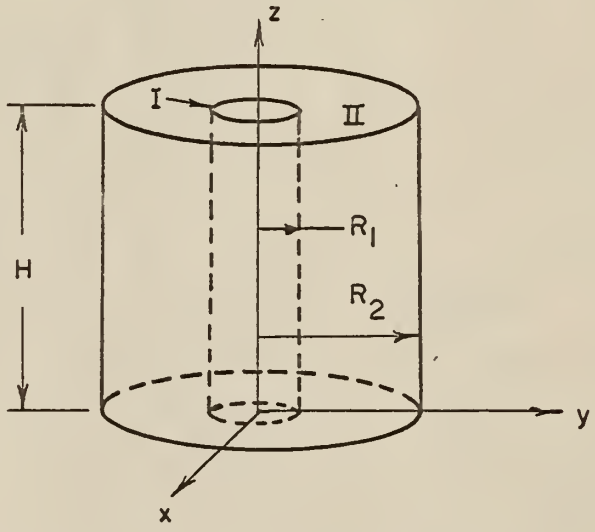

Figure 1. Coordinate System

As neutrons from the source diffuse in the positive z direction, a depression of the neutron flux in region I, the absorber region, is apparent when the flux is plotted as a function of r, the distance from the z axis, on any given z plane. The depression is caused by the excess absorption of neutrons in region I over that of region II. However, the

magnitude of the flux depression due to these absorptions is greater than would be predicted by diffusion theory.

The increase in the flux depression is the result of self-absorption within the absorbing media. That is, the incident neutron flux will be decreased by absorptions at the surface of the media which decreases the number of neutrons available for absorption as the neutrons diffuse inward through the absorber. To obtain the true absorption rate, the flux could be determined as a function of $\underline{r}$, multiplied by the macroscopic absorption cross section, and the product integrated over the volume of the absorber. This method is cumbersome and difficult to use (1). A simpler procedure would be to devise an effective cross section to multiply the flux at the surface of the absorber to yield the correct neutron absorption (4). A third method of obtaining the proper neutron absorption, and the method of this work, is by increasing the radius of a fictitious absorbing media while allowing the macroscopic absorption cross section of this media to remain its measured value.

Thus, for an absorber with a given macroscopic absorption cross section, an effective absorber radius can be calculated by varying the radius of the fictitious absorber until the function that best describes the flux within this absorber fits the measured values of the flux with the minimum least squared error. Keeping the above in mind, the mathematical theory of this problem will now be presented.

Using the subscript "1" for the absorber and the subscript "2" for the moderator, the equations to be satisfied are

$$\nabla^2 \phi_1 - \kappa_1^2 \phi_1 = 0 \tag{1}$$

and

$$\nabla^2 \phi_2 - \kappa_2^2 \phi_2 = 0 \tag{2}$$

where

$$\kappa_1^2 = \Sigma_{a_1}/D_1 ; \qquad \kappa_2^2 = \Sigma_{a_2}/D_2 \tag{3}$$

and

$$D_1 = 1/(3\Sigma_{tr_1}) ; \qquad D_2 = 1/(3\Sigma_{tr_2}). \tag{4}$$

In order to obtain a unique solution to Eqs. (1) and (2), boundary conditions must be applied. For this type of problem, the boundary conditions are well known (3, 5, 6, 7, 11, 12) and straight forward. The flux, ϕ, must be finite and non-negative throughout the region of diffusion. This condition is clear since the flux can never be infinite or negative. However, it can be zero. At interfaces between media with different diffusion properties, the net neutron current densities and the neutron fluxes are equal. Finally, the neutron flux must go to zero at the extrapolated boundary. The extrapolated boundary is defined as the physical boundary plus $0.71\lambda_{tr}$, where, in general, λ_{tr} is small compared to the dimension of the physical boundary.

The following five equations will express mathematically the above boundary conditions:

1. $\phi_1(0,z) \neq \infty$ (5)

2. $\phi_2(R2,z) = 0$ (6)

3. $\phi_1(r,H) = \phi_2(r,H) = 0$ (7)

4. $\phi_1(R1,z) = \phi_2(R1,z)$ (8)

5. $D_1 \nabla \phi_1(R1,z) = D_2 \nabla \phi_2(R1,z)$. (9)

The boundary condition at the x-y plane depends upon the source configuration. For this problem it will be assumed that the source is a plane isotropic source emitting S' neutrons per second per centimeter squared. Thus, the following two boundary conditions are obtained:

6. $S'/2 = S = -D_1 \left.\frac{\partial \phi_1}{\partial z}\right|_{z=0}$ (10)

7. $S'/2 = S = -D_2 \left.\frac{\partial \phi_2}{\partial z}\right|_{z=0}$. (11)

The Laplacian operator, ∇^2 , for cylindrical coordinates with no θ dependence is written as

$$\nabla^2 = \frac{\partial^2}{\partial r^2} + \frac{1}{r}\frac{\partial}{\partial r} + \frac{\partial^2}{\partial z^2}. \quad (12)$$

Using this, Eq. (1) for region I becomes

$$\frac{\partial^2 \phi_1}{\partial r^2} + \frac{1}{r}\frac{\partial \phi_1}{\partial r} + \frac{\partial^2 \phi_1}{\partial z^2} - \kappa_1^2 \phi_1 = 0. \quad (13)$$

If the variables are separable, a solution of the form

$$\phi(r,z) = R(r)\,Z(z) \tag{14}$$

is attempted. Utilizing Eq. (14) in Eq. (13) produces

$$\frac{1}{R}R'' + \frac{1}{rR}R' + \frac{1}{Z}Z'' - \gamma_1^2 = 0. \tag{15}$$

Because the first two terms are functions of r alone, they must be equal to a constant, β^2. By similar reasoning, the third term is equal to a constant, λ^2. Thus Eq. (15) becomes

$$\beta^2 + \lambda^2 - \gamma_1^2 = 0 \tag{16}$$

and this equation will be called the separations constants equation.

Now, examining the individual terms of Eq. (15), it is seen that

$$\frac{1}{R}R'' + \frac{1}{rR}R' = \beta^2 \tag{17}$$

and

$$\frac{1}{Z}Z'' = \lambda^2. \tag{18}$$

A solution of Eq. (17) is

$$R(r) = A I_o(\beta r) + B K_o(\beta r) \tag{19}$$

while a solution for Eq. (18) is

$$Z(z) = C \sinh \lambda z + E \cosh \lambda z. \tag{20}$$

Thus, the complete solution before the application of the boundary conditions is

$$\phi_1(r,z) = [A I_o(\beta r) + B K_o(\beta r)][C \sinh \lambda z + E \cosh \lambda z]. \quad (21)$$

In order that Eq. (5) be satisfied

$$B = 0. \quad (22)$$

Changing the argument of Eq. (20) from λz to $\lambda(H-z)$, which is valid for a slab geometry coordinate, Eq. (7) is satisfied if

$$E = 0. \quad (23)$$

Thus,

$$\phi_1(r,z) = A I_o(\beta r) \sinh \lambda(H-z). \quad (24)$$

Applying the same procedures to region II, the solution to Eq. (2) may be written as

$$\phi_2(r,z) = [F J_o(\alpha r) + G Y_o(\alpha r)][M \sinh \gamma z + N \cosh \gamma z] \quad (25)$$

where the separations constants equation for this region is

$$-\alpha^2 + \gamma^2 - \mu^2 = 0. \quad (26)$$

The choice of sign on the α^2 term is determined by the type of solution desired in the outer region. Application of Eqs. (6) and (7) to Eq. (25) produces

$$\phi_2(r,z) = B[J_o(\alpha r) - T Y_o(\alpha r)] \operatorname{Sinh} \gamma(H-z) \tag{27}$$

where

$$T = J_o(\alpha R2)/Y_o(\alpha R2) . \tag{28}$$

Now, an auxiliary function $U_o(\alpha r)$ is defined (2) as

$$U_o(\alpha r) \equiv J_o(\alpha r)Y_o(\alpha R2) - Y_o(\alpha r) J_o(\alpha R2). \tag{29}$$

Some of the properties of this function are discussed in Appendix C. Using Eq. (29), Eq. (27) becomes

$$\phi_2(r,z) = B^* U_o(\alpha r) \operatorname{Sinh} \gamma(H-z) \tag{30}$$

where

$$B^* = B/Y_o(\alpha R2).$$

When boundary condition four, Eq. (8), is applied to Eqs. (24) and (30), it is seen that

$$A I_o(\beta R1) \operatorname{Sinh} \lambda(H-z) = B^* U_o(\alpha R1) \operatorname{Sinh} \gamma(H-z) \tag{31}$$

or writing Eq. (31) in a different form

$$K_1 \operatorname{Sinh} \lambda(H-z) = K_2 \operatorname{Sinh} \gamma(H-z). \tag{32}$$

Rearrangement of Eq. (32) gives

$$K_3 = \frac{\operatorname{Sinh} \lambda(H-z)}{\operatorname{Sinh} \gamma(H-z)} . \tag{33}$$

Eq. (33) implies that, regardless of the value of z,

the left-hand side of the equation is always equal to the same constant. In order for this to be true, λ and γ would have to be equal. Thus, Eq. (26) may be written as

$$-\alpha^2 + \lambda^2 - \gamma_2^2 = 0 \,. \tag{34}$$

When boundary conditions four and five, Eqs. (8) and (9), are applied to Eqs. (24) and (30)

$$A\, I_o(\beta R1) = B^* U_o(\alpha R1) \tag{35}$$

and

$$D_1 A \beta\, I_1(\beta R1) = -D_2 B^* \alpha\, U_1(\alpha R1) \,. \tag{36}$$

Dividing Eq. (36) by (35)

$$\frac{D_1 \beta\, I_1(\beta R1)}{I_o(\beta R1)} = -\frac{D_2 \alpha\, U_1(\alpha R1)}{U_o(\alpha R1)} \,. \tag{37}$$

Solving Eq. (37) for β gives

$$\beta = -\frac{\alpha\, U_1(\alpha R1)}{U_o(\alpha R1)} \cdot \frac{D_2\, I_o(\beta R1)}{D_1\, I_1(\beta R1)} \,. \tag{38}$$

Examination of Eq. (38) reveals that it is transcendental in nature and requires an iterative type of solution to determine the constants α and β. But in solving for α and β, it must be remembered that they are related by Eqs. (16) and (34); i.e.,

$$\alpha^2 = \gamma_1^2 - \gamma_2^2 - \beta^2 \,. \tag{39}$$

Because of the periodicity of the functions $J_o(r)$ and $Y_o(r)$ that compose the function $U_o(r)$, an infinity of solutions is obtained for Eq. (38). Therefore, Eq. (39) now becomes

$$\alpha_n^2 = \mathcal{K}_1^2 - \mathcal{K}_2^2 - \beta_n^2 \tag{40}$$

and the expressions for the fluxes are now written as

$$\phi_1(r,z) = \sum_{n=o}^{\infty} A_n I_o(\beta_n r) \operatorname{Sinh} \lambda_n (H-z) \tag{41}$$

and

$$\phi_2(r,z) = \sum_{n=o}^{\infty} B_n^* U_o(\alpha_n r) \operatorname{Sinh} \lambda_n (H-z). \tag{42}$$

The subscript "n" on λ is because of the infinity of values of α and β .

The application of boundary conditions six and seven, Eqs. (10) and (11), yield

$$S = D_1 \sum_{n=o}^{\infty} A_n \lambda_n I_o(\beta_n r) \operatorname{Cosh} \lambda_n H \tag{43}$$

and

$$S = D_2 \sum_{n=o}^{\infty} B_n^* \lambda_n U_o(\alpha_n r) \operatorname{Cosh} \lambda_n H. \tag{44}$$

Utilizing the orthogonality relations for Bessel functions, the coefficients for Eq. (43) are obtained in the usual manner. Thus

$$\sum_{p=o}^{\infty} \int_o^{R1} S\, r\, J_o(\beta_p r)\, dr = \lambda_n D_1 \sum_{p=o}^{\infty} \sum_{n=o}^{\infty} \int_o^{R1} A_n r\, J_o(\beta_p r) I_o(\beta_n r) \operatorname{Cosh} \lambda_n H\, dr \tag{45}$$

so that

$$A_n = \frac{S\, J_1(\beta_n R1)}{\frac{D_1 \lambda_n}{2}\{J_o(\beta_n R1) I_1(\beta_n R1) + J_1(\beta_n R1) I_o(\beta_n R1)\} \operatorname{Cosh} \lambda_n H} \tag{46}$$

if $S \neq S(r)$. Similarly, applying the orthogonality relations for $U_o(\alpha_n r)$ as developed in Appendix C, the coefficients B_n can be determined. Thus

$$\sum_{p=0}^{\infty} \int_{R1}^{R2} S\, r\, U_o(\alpha_p r)\, dr = \left\{D_2 \sum_{p=0}^{\infty} \sum_{n=0}^{\infty} \int_{R1}^{R2} B_n^* \lambda_n r\, U_o(\alpha_p r)\, U_o(\alpha_n r)\, dr\right\} \operatorname{Cosh} \lambda_n H \tag{47}$$

so that

$$B_n^* = \frac{S\left\{\frac{2}{\pi} + R1\, k_1 U_o(\alpha_n R1)\right\}}{\frac{D_2 \lambda_n}{2}\left\{\left(\frac{2}{\pi}\right)^2 - (\alpha_n^2 + k_1^2)[R1\, U_o(\alpha_n R1)]^2\right\} \operatorname{Cosh} \lambda_n H} \tag{48}$$

if $S \neq S(r)$ and as before

$$B_n^* = B_n / Y_o(\alpha_n R2) \tag{49}$$

where

$$k_1 = -\frac{\alpha_n U_o'(\alpha_n R1)}{U_o(\alpha_n R1)} \qquad \text{(See Appendix C).} \tag{50}$$

Another set of source boundary conditions that might be of interest is one where the source is considered to be zero at the x-y plane in the absorber, while the source in this position in the moderator remains as described by Eq. (11).

To describe the boundary conditions for this new source condition, the partial neutron current equations

are used. That is,

$$J_+(z)\Big|_{z=0} = 0 \qquad \text{for } 0 \leqslant r \leqslant R1 \quad \text{(Region I)} \tag{51}$$

$$J_+(z)\Big|_{z=0} = S \qquad \text{for } R1 < r \leqslant R2 \quad \text{(Region II)} \tag{52}$$

where the partial neutron current in the positive direction is defined as (6)

$$J_+(z) = \frac{\phi}{4} - \frac{D}{2}\frac{\partial \phi}{\partial z}. \tag{53}$$

Using Eqs. (41) and (42) as definitions for ϕ_1 and ϕ_2 respectively, the following two equations are obtained:

$$\sum_{n=0}^{\infty} \frac{A_n I_o(\beta_n r) \operatorname{Sinh} \lambda_n H}{4} + \frac{D_1}{2}\sum_{n=0}^{\infty} A_n \lambda_n I_o(\beta_n r) \operatorname{Cosh} \lambda_n H = 0 \tag{54}$$

and

$$\sum_{n=0}^{\infty} \frac{B_n^* U_o(\alpha_n r) \operatorname{Sinh} \lambda_n H}{4} + \frac{D_2}{2}\sum_{n=0}^{\infty} B_n^* U_o(\alpha_n r) \lambda_n \operatorname{Cosh} \lambda_n H = S. \tag{55}$$

Working first with Eq. (54), it is seen that

$$\sum_n A_n I_o(\beta_n r)\left\{\operatorname{Sinh} \lambda_n H + 2D_1 \lambda_n \operatorname{Cosh} \lambda_n H\right\} = 0. \tag{56}$$

If β_n is real, $I_o(\beta_n r)$ is never equal to zero, and a trivial solution is obtained if $A_n = 0$. Therefore, the bracketed term must equal zero. After transposing, the bracketed term may be written as

$$\tanh \lambda_n H = -2 D_1 \lambda_n . \tag{57}$$

Since the hyperbolic tangent is always greater than or equal to zero if its argument is positive, the possible solutions to Eq. (57) are

$$\lambda_n = 0 ; \qquad \lambda_n = i \xi_n . \tag{58}$$

When $\lambda_n = 0$, solution of Eq. (18) yields

$$Z = C_1 + C_2 z . \tag{59}$$

Application of Eq. (7) leads to

$$Z = C_1 (1 - z/H) = C_3 (H - z) \tag{60}$$

and the flux equation for the absorber is written as

$$\phi_1 = \sum_n A_n I_0(\beta_n r)(H - z). \tag{61}$$

Utilizing the boundary condition at the interface, Eq. (8)

$$\sum_n A_n I_0(\beta_n R1)(H - z) = \sum_n B_n^* U_0(\alpha_n R1) \sinh \gamma_n (H - z) \tag{62}$$

or

$$\sum_n \frac{A_n I_0(\beta_n R1)}{B_n^* U_0(\alpha_n R1)} = \frac{\sinh \gamma_n (H - z)}{H - z} . \tag{63}$$

Since the left-hand side is a constant, the above implies that, regardless of the value of z , the

right-hand side is equal to a constant. For this to be true, γ_n must equal zero so that the solution of Eq. (2) will yield the same result as the solution of Eq. (7) when λ_n is equal to zero.

However, from physical consideration of the system, it is known that the attenuation of the flux in the z direction is exponential and not linear as these results suggest. Thus, one must conclude that the solution $\lambda_n = 0$ does not well describe the physical situation and is invalid.

Now consider the case when λ_n is imaginary and let $\lambda_n = i\,\xi_n$; then Eq. (57) becomes

$$\operatorname{Tan} \xi_n H = -2D_1 \xi_n . \tag{64}$$

An examination of a plot of the tangent reveals that an infinity of solutions to Eq. (64) are possible. Because the form of the flux equation with $\lambda_n = i\,\xi_n$ is

$$\phi_1 = \sum_n A_n I_o(\beta_n r)[i \operatorname{Sin} \xi_n(H-z)] \tag{65}$$

negative imaginary values of A_n are necessary to obtain positive values of ϕ_1 . Hence, the argument of the sine term must be positive.

Application of the interface boundary condition, Eq. (8), leads to the condition that

$$\sum_n \frac{A_n I_o(\beta_n R1)}{B_n^* U_o(\alpha_n R1)} = \frac{\operatorname{Sinh} \gamma_n(H-z)}{\operatorname{Sin} \xi_n(H-z)} , \tag{66}$$

Again, it is evident that the right-hand side is equal to a constant which implies that γ_n is imaginary, so that once more $\lambda_n = \gamma_n$.

The sine distribution in the z direction does not contradict the physical situation. Since the model chosen calls for a plane source of monoenergetic neutrons at the source plane, the value of the neutron flux at the source plane should be largest and decrease to zero at the extrapolated height of the system. The sine function as defined fulfills these conditions.

To determine the form of the A_n coefficients, the interface boundary condition, Eq. (8), must be applied, and the A_n's can then be expressed in terms of the B_n^*'s. Therefore, the forms of the coefficients B_n^* must be determined. Working with Eq. (55), rearrangement yields, after the substitution of sine and cosine for hyperbolic sine and cosine,

$$4S = \sum_n B_n^* U_o(\alpha_n r)[\sin \lambda_n H + 2D_2 \lambda_n \cos \lambda_n H] \qquad (67)$$

where the bracketed term is some constant, C_n say. Applying the orthogonality relation for $U_o(\alpha_n r)$ as developed in Appendix C

$$4S\int_{R1}^{R2} r\, U_o(\alpha_j r)\, dr = \sum_n \int_{R1}^{R2} B_n^* r\, U_o(\alpha_j r)\, U_o(\alpha_n r)\, C_n\, dr \qquad (68)$$

which becomes

$$B_j^* = \frac{4S\left[\frac{2}{\pi} + R1\, k_1\, U_o(\alpha_j R1)\right]}{\frac{C_n}{2}\left[\left(\frac{2}{\pi}\right)^2 - (\alpha_j^2 + k_1^2)\left\{R1\, U_o(\alpha_j R1)\right\}^2\right]} \,. \tag{69}$$

Thus, it is seen that the coefficients B_j^* are similar in form to those obtained from Eq. (48). Now Eq. (8) is applied to find A_n:

$$\sum_n A_n I_o(\beta_n R1)(i \sin \xi_n(H-z)) = \sum_n B_n^* U_o(\alpha_n R1)(i \sin \xi_n(H-z)) \tag{70}$$

and

$$A_n = \frac{B_n^* U_o(\alpha_n R1)}{I_o(\beta_n R1)} \tag{71}$$

where B_n^* is defined by Eq. (69).

A second approach to formulating this source condition is by use of the net current equation at the source plane; i.e.,

$$\begin{aligned} J(z)\big|_{z=0} &= 0 \qquad && 0 \leq r \leq R1 \\ J(z)\big|_{z=0} &= S \qquad && R1 < r \leq R2 \end{aligned} \tag{72}$$

where $J(z)$ is defined (6) as

$$J(z) = -D \nabla \phi. \tag{73}$$

Using Eq. (41) and (42) as definitions of ϕ_1 and ϕ_2 the following equations are obtained:

$$D_1 \sum_n A_n I_o(\beta_n r)\, \lambda_n \cosh \lambda_n H = 0 \tag{74}$$

and

$$D_2 \sum_n B_n^* U_o(\alpha_n r)\, \lambda_n \operatorname{Cosh} \lambda_n H = S . \tag{75}$$

Examination of Eq. (74) reveals that trivial solutions are obtained if either $A_n = 0$ or $\lambda_n = 0$. Assuming that β_n is real, $I_o(\beta_n r)$ is never equal to zero. Thus, λ_n must be imaginary for a solution to exist. Letting $\lambda_n = i\,\xi_n$, Eq. (74) becomes

$$D_1 \sum_n A_n I_o(\beta_n r)(i\,\xi_n \operatorname{Cos} \xi_n H) = 0 . \tag{76}$$

The roots of this equation occur at

$$\xi_n = (2n+1)\pi/2H , \tag{77}$$

By arguments similar to those used to obtain Eq. (66), it can be shown that γ_n must also be imaginary. Thus, Eq. (75) becomes

$$D_2 \sum_n B_n^* U_o(\alpha_n r)(i\,\xi_n \operatorname{Cos} \xi_n H) = S . \tag{78}$$

Applying the orthogonality condition for $U_o(\alpha r)$ as developed in Appendix C

$$S \int_{R1}^{R2} r\, U_o(\alpha_j r)\, dr = D_2 \sum_n B_n^* i\,\xi_n \operatorname{Cos} \xi_n H \int_{R1}^{R2} r\, U_o(\alpha_j r)\, U_o(\alpha_n r)\, dr \tag{79}$$

which becomes

$$B_j^* = \frac{S\left[\frac{2}{\pi} + k_1 R1\, U_o(\alpha_j R1)\right]}{\frac{i\,\xi_n \operatorname{Cos} \xi_n H}{2}\left[\left(\frac{2}{\pi}\right)^2 - (\alpha_j^2 + k_1^2)\{R1\, U_o(\alpha_j R1)\}^2\right]} . \tag{80}$$

Application of the interface boundary condition, Eq. (8), yields an expression for A_n. Thus,

$$\sum_n A_n I_o(\beta_n R1)(i\xi_n \sin \xi_n (H-z)) = \sum_n B_n^* U_o(\alpha_n R1)(i\xi_n \sin \xi_n (H-z)) \tag{81}$$

and

$$A_n = \frac{B_n^* U_o(\alpha_n R1)}{I_o(\beta_n R1)} . \tag{82}$$

where B_n^* is defined by Eq. (80).

The net current source condition may be a more accurate description of the events that occur at the source plane than the partial current source condition since the net current equation accounts for neutrons that enter into the source region and then reenter the rod-moderator region. The partial current equation considers only those neutrons that are moving in the proper direction and assumes that all events that direct neutrons in the opposite direction are losses. The fact that the net current condition has implied that an imaginary source is necessary definitely will hinder its physical application although it is an interesting mathematical criterion. Therefore, the partial current boundary condition would normally be utilized.

Thus, for the case of a known plane isotropic source of neutrons located in the x-y plane, the value of the effective rod radius can be determined analytically by solving, using a trial and error iterative procedure, Eqs. (38), (40), (46),

and (48). If the value of the source is unknown, the effective rod radius can be determined numerically by fitting an experimentally determined flux plot by a method of least squares while varying the rod radius to reduce the least square error to a minimum. An IBM 1620 computer program that determines the effective rod radius and the unknown coefficients in the flux equations is described in Appendix F.

EXPERIMENTAL PROCEDURE

To determine the effective rod radius, one must first obtain, by a suitable method, an experimental flux plot in the absorber and moderator region. A method of doing this, and the method employed in this work, involved the use of gold wire and gold foil in conjunction with absorber rods of two different diameters utilized with a graphite thermal column of a nuclear reactor.

The absorbing rod used to obtain the data for the flux plot was cut into three sections. Ideally, these sections were of such a length that the end effects due to the length of the sections were negligible, and the center section of the rod was of sufficient length that the z dependence of the flux was eliminated.

Slots were cut into each end of the center section of the rod, and these slots were of sufficient depth and width that they accommodated both the foil and the wire. The wire or foil when in position extended from the edge of the special graphite stringer completely through the absorber rod. With the wire and rod in place in the stringer, it was then placed into the graphite thermal column and the irradiation period was begun.

For the case where two different rod diameters were used, the stringer was constructed so that when the one rod was being used to amass the data, a graphite rod of the same material as the stringer was placed in the groove for the

second rod. The purpose of the graphite rod was to eliminate the void space that would have been present when only one rod was placed in the stringer.

At the conclusion of the period of irradiation, the reactor was shut down, and the special stringer was removed from the thermal column. The stringer was then placed in a guarded area to permit the short lived isotopes of the absorber rod to decay away. After a suitable cooling off period, the wires or foils were removed from the rod-stringer assembly and transported to the counting facility.

To count the wire, a wire counting facility was needed. This facility consisted of a wire guide to measure the position of the wire in relation to the center of the rod and a Geiger counting tube. The counting tube was shielded to prevent the beta radiation from scattering and streaming into the sensitive volume of the tube.

A foil counting facility similar to the one constructed to count the wire was feasible, but a more simple arrangement was employed. The foil was taped to a piece of graph paper and then cut into small strips at appropriate intervals. These strips were then placed on a special plancet that insured reproducible geometry with respect to the counting tube, and the small foils were then counted using a gas flow proportional counter.

ANALYSIS OF DATA

In the theoretical development of the two region P_1 transport model, it was shown that an analytic expression for the neutron flux in both regions can be determined for a given absorber radius once a source condition is established. However, to determine the effective rod radius, it was necessary to fit a set of experimental data with the proper expressions for the flux while varying the absorber radius. An IBM 1620 computer program was written for this purpose, and it is described in Appendix F.

The effective rod radius was determined by a trial and error procedure which strived to minimize the sum of the weighted squares of the residuals between the experimental values and the values calculated from the theoretical expressions for the neutron flux in both regions. The weighting function used was that one which required that the residual between the calculated value at any point and the experimental measurement should lie within the statistical standard deviation.

Another point considered in the fitting of the experimental data was the number of harmonics necessary to best fit the data. Provision was made in the computer program to accommodate up to five harmonics. However, the inclusion of more than three harmonics was deemed inadvisable since the accuracy of the data did not warrant a more precise analysis.

All of the data were analyzed using one harmonic, and

two different situations were considered in the analysis. In one case, the value obtained from the solution of the transcendental equation $\varkappa/\Sigma = \tanh \varkappa/\Sigma_s$ was used for $\varkappa$ in the rod; in the second case, the diffusion theory value for $\varkappa$ in the rod, $\varkappa = (3\Sigma_a\Sigma_s)^{\frac{1}{2}}$, was employed. The purpose of this approach was to show the difference between asymptotic theory and the P_1 transport theory in the absorbing media, since diffusion theory is true only when $\Sigma_a \ll \Sigma_s$.

Three particular sets of data were analyzed using two and three harmonics to see what effect, if any, the additional terms would have on the value of the least square error. In each of these cases, the value used for $\varkappa$ in the rod was that obtained from asymptotic theory.

RESULTS AND CONCLUSIONS

The analysis of the data for this work was identified by the following notation and parallels the notation used in the tables of original data found in Appendix D:

Case 1. One inch rod with gold wire near source.

Case 2. One inch rod with gold wire away from source.

Case 3. One inch rod with gold foil near source.

Case 4. One inch rod with gold foil away from source.

Case 5. Two inch rod with gold wire near source.

Case 6. Two inch rod with gold wire away from source.

The phrases "near source" and "away from source" refer to the position of the gold foil or wire with respect to the reactor core during the period of irradiation. Thus, "near source" signifies that the foil (or wire) was placed in the special graphite stringer in the position nearest the core, and "away from source" signifies that the foil (or wire) was placed in the special graphite stringer in the position farthest from the source (See Figure 23 in Appendix D).

The Tabulation of Results was further subdivided by the letters A, B, C, and D to indicate the method of analysis. These letters have the following meaning:

A. Data analyzed using one harmonic and the value of λ_1 obtained from asymptotic theory.

B. Data analyzed using one harmonic and the value of λ_1 obtained from diffusion theory.

C. Data analyzed using two harmonics and the value of

$\varkappa_1$ obtained from asymptotic theory.

D. Data analyzed using three harmonics and the value of $\varkappa_1$ obtained from asymptotic theory.

For example, the results listed as Case 3B signify that the data recorded using the gold foil positioned in the stringer nearest the core were analyzed using one harmonic and the diffusion theory value for $\varkappa$ in the rod.

Table 1 presents a tabulation of the results, identified by the preceding notation, obtained for the value of the effective rod radius, R_{eff}, for both the one inch and the two inch diameter steel rod using the IBM 1620 computer program described in Appendix F. Figures 2 through 20 graphically illustrate the variation of the flux in the absorbing rod and moderator calculated by the least square analysis as compared to the experimental data.

For the analysis that utilized the value of $\varkappa$ in the rod obtained from the solution of the transcendental equation $\varkappa/\Sigma = \tanh \varkappa/\Sigma_s$, in only two instances did the value obtained for R_{eff} exceed the value of the physical rod radius. Both of these cases involved the one inch rod. In one instance, specifically Case 4, the value obtained for R_{eff} was not consistent with the values obtained in the other cases for the one inch rod. However, the validity of this data was questioned at the time it was recorded because the gold foil was noted to be out of position when it was removed from the special stringer. In both cases involving the two inch rod, the value

of R_{eff} was less than the rod radius. Thus, one must conclude from these results that this method of analysis was not too satisfying from the stand point of an effective rod radius. Although the calculated rod radius was greater than the physical radius of the rod in two instances, the majority of the results led to the conclusion that the absorbing rod was smaller in size than its actual measurement. Thus, the accuracy of the experimental data has left something to be desired.

In the analysis that used the diffusion theory value for $\varkappa$ in the rod, the value obtained for R_{eff} in all cases was smaller than the rod radius. This result was not too surprising since diffusion theory is known (11) to be faulty in regions where Σ_a is of the same order of magnitude as Σ. Hence, this method of calculating the effective rod radius was less satisfying than the first and should not be used to determine the effective rod radius.

When more than one harmonic was included in the analysis of the data, the general result was that the value of R_{eff} increased and the least square error decreased. In one particular case utilizing the one inch rod, Case 1, the value of R_{eff} calculated using one harmonic increased from 0.4604 inch to 0.5063 inch by using three harmonics while the least square error decreased from 541.4 to 352.1 respectively. The results of Case 2 present a more definite illustration of how the additional terms of the multi-harmonic analysis reduced the value of the least square error. For this case, the value of R_{eff} calculated using one harmonic increased

from 0.5072 inch to 0.5488 inch for two harmonics and then decreased to 0.5138 inch for three harmonics. The value of the least square error in these three instances varied from 234.8 to 88.5 to 99.8 respectively.

The result that the inclusion of two or three harmonics improved the value of the least square error indicates that the foil or wire were too near the source and/or the end of the rod, and this resulted in the significance of the higher order harmonic terms. If the foil or wire had been located at a greater distance from the reactor core and if the rod had been longer, these terms would have been insignificant compared to the fundamental mode, one harmonic.

Case 2 results emphasize this fact. The wire used to record the data was located away from the core which means that it was ten inches farther from the core than was the wire that was located near the core, Case 1. For Case 2 the minimum least square error and the maximum value for R_{eff} occurred using two harmonics to analyze the data. Thus, it appears that this little increase in distance was sufficient to reduce the effect of the third harmonic on the value of the flux.

The results for the multi-harmonic analysis of the two inch rod data were totally unexpected. Case 6 was selected for analysis since it presented the best prospect for producing an R_{eff} on the order of the physical dimension of the rod judging from the results obtained for Case 1 and Case 2.

For two harmonics, the desired result was obtained when the value of the least square error decreased and R_{eff} increased from the values obtained for one harmonic. However, when the three harmonic analysis was attempted, the value of both the least square error and R_{eff} decreased. Thus, it appears that, as with Case 2, the wire was located far enough from the core to reduce the harmonic content of the flux to two harmonics, but the data were insufficiently accurate to produce the expected results.

It was also noted in the results of the multi-harmonic analysis that the sign on the term associated with the fundamental mode was negative in all cases, and that the second harmonic was the dominant term. Referring to Appendix G, it can be seen that the signs on the coefficients of the flux equations are exactly opposite what one's intuition would suggest; i.e., one would expect the fundamental mode, the first harmonic, to be dominant and have positive coefficients, while the higher harmonics would be smaller in magnitude and have either positive or negative signs. Hence, it would appear that the original data were not as accurate as they could have been.

In the graphs of the original data, it was noticed from the beginning that unexpected peaks were evident in the moderating region. At first it was thought that these peaks were due to the location of the control rods used to bring the reactor to critical. But, in a later irradiation, these rods

were withdrawn completely and different ones were employed to cause the reactor to become critical and the peaks were still present. No explanation for these peaks was found when the data were recorded, and none is offered at this time.

Summarizing the results, it was seen that values for R_{eff} greater than the physical dimension of the rod were obtained in a few cases, and in these cases, the magnitude of the flux depression was very close to that obtained experimentally. For the cases in which R_{eff} was found to be less than the actual rod dimension, in one instance the data were known to be invalid, and in the others, the results were inconclusive since a multi-harmonic analysis of the data was not conducted.

Thus, it would appear that the concept of an effective rod radius was reasonable, but it will require much more investigation to produce graphs of the type that are needed to fully utilize this concept. Great care must be exercised when data for this type of experiment are recorded, and the location of the detecting material in relation to the reactor core is also important. To analyze the data for this type of investigation, computers of greater speed than the IBM 1620 would be very advantageous, especially for the multi-harmonic analysis. Examination of other materials and various rod sizes using the ideas embodied in this work would provide an excellent starting place for future experimentation.

TABLE I

Tabulation of Results								
Case Number	A		B		C		D	
	R_{eff} (Inches)	Least Squared Error	R_{eff} (Inches)	Least Squared Error	R_{eff} (Inches)	Least Squared Error	R_{eff} (Inches)	Least Squared Error
1	0.4604	541.4	0.4232	596.8	0.4947	401.6	0.5063	352.1
2	0.5072	234.8	0.4726	261.0	0.5488	88.5	0.5138	99.8
3	0.5297	968.1	0.4933	894.0	—	—	—	—
4	0.3955	2592.2	0.3637	2819.5	—	—	—	—
5	0.7406	2375.8	0.6854	2783.1	—	—	—	—
6	0.8404	1678.2	0.7789	2116.5	0.8585	1546.2	0.8068	871.1

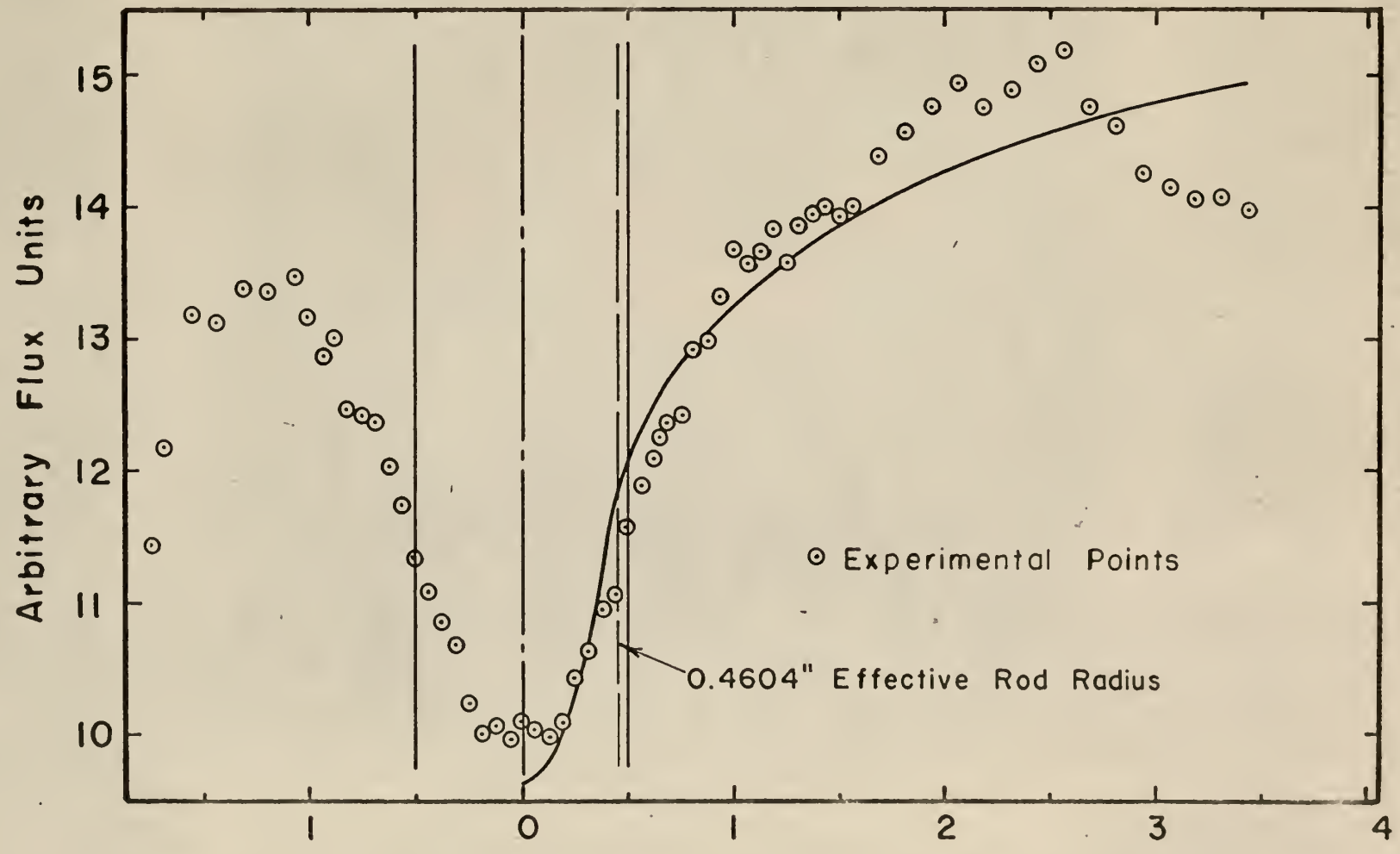

Fig.2 Flux Calculated by Least Squares Analysis Case 1A

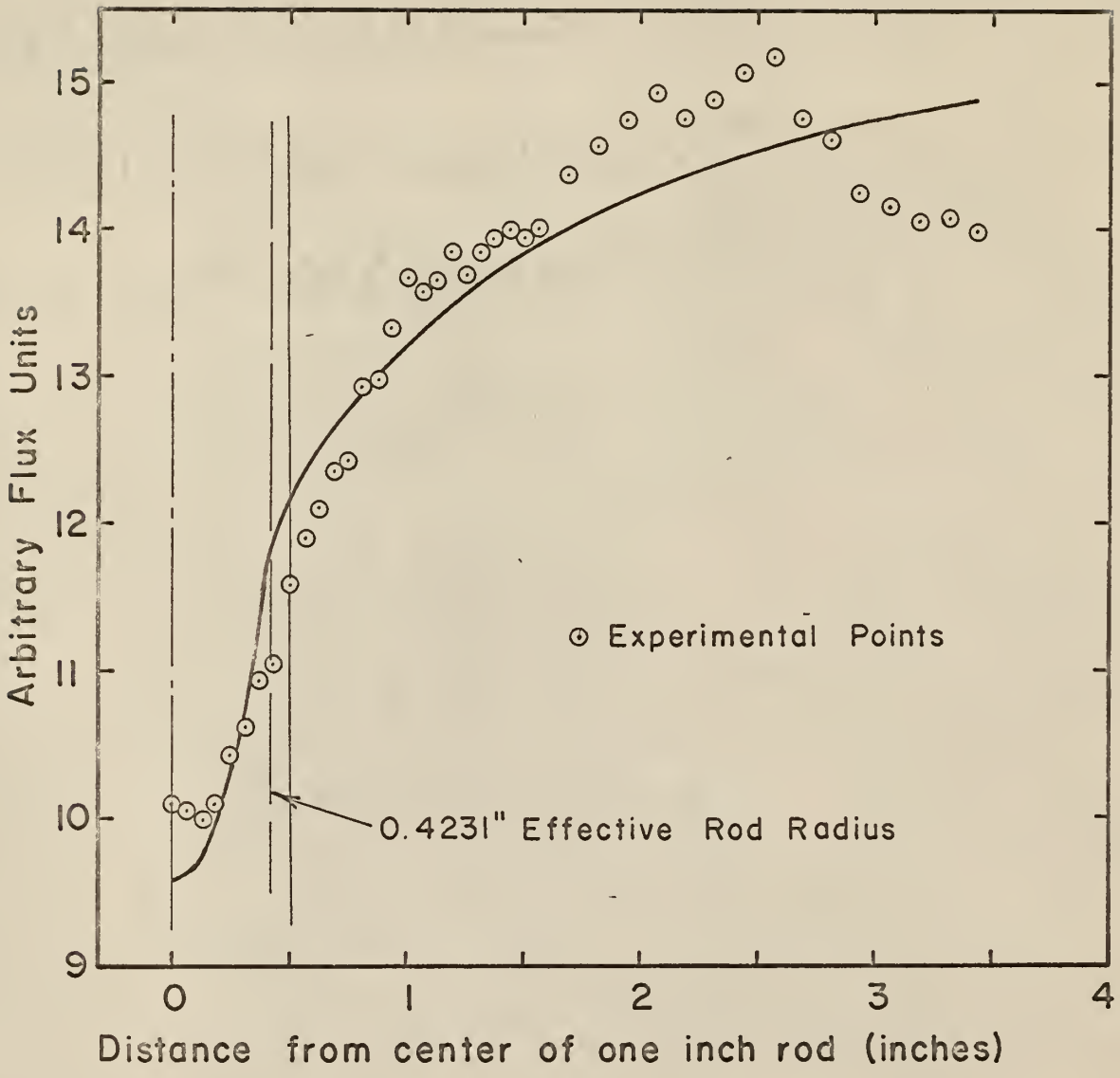

Fig.3 Flux Calculated by Least Squares Analysis Case 1B

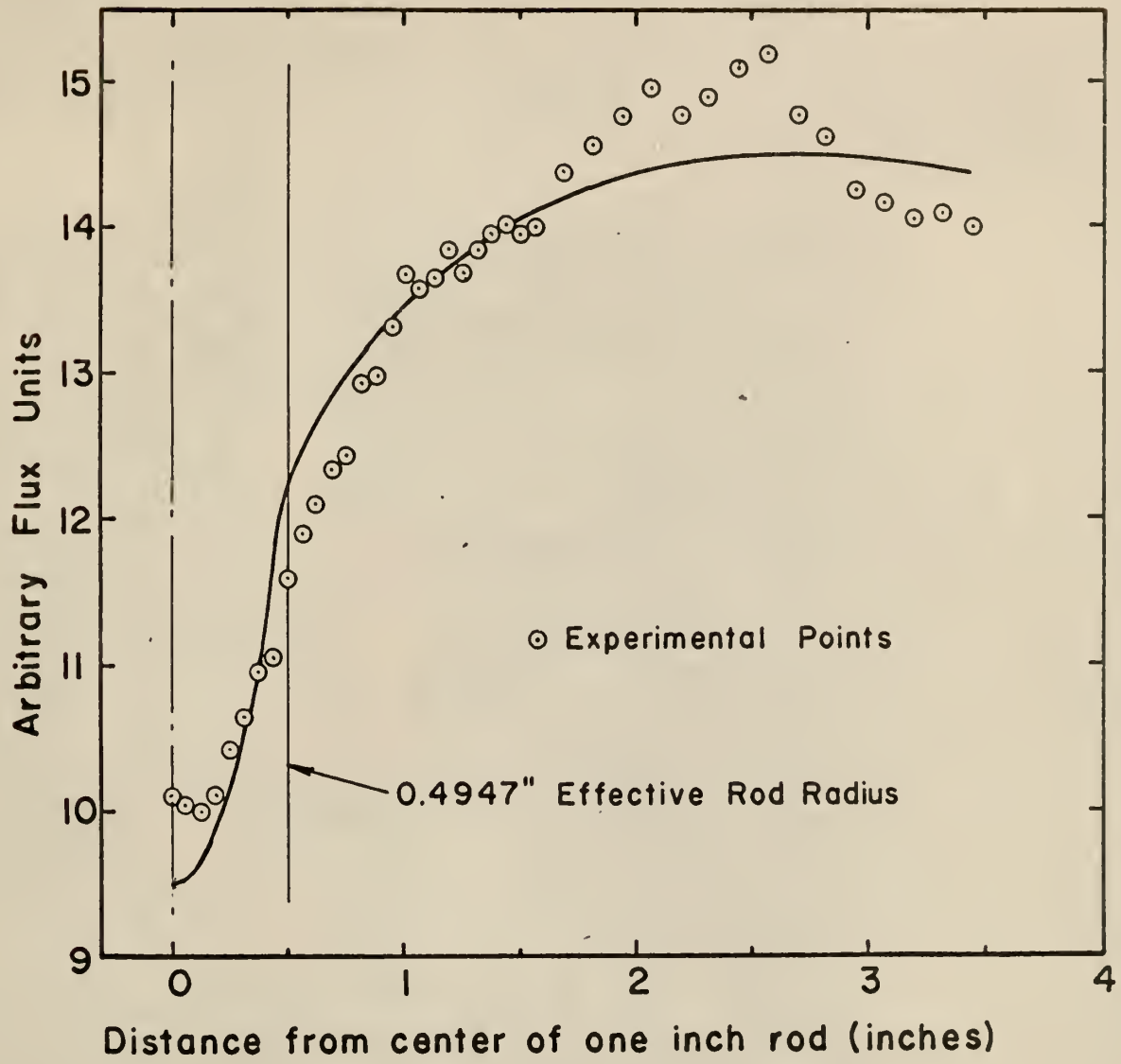

Fig.4 Flux Calculated by Least Squares Analysis Case IC

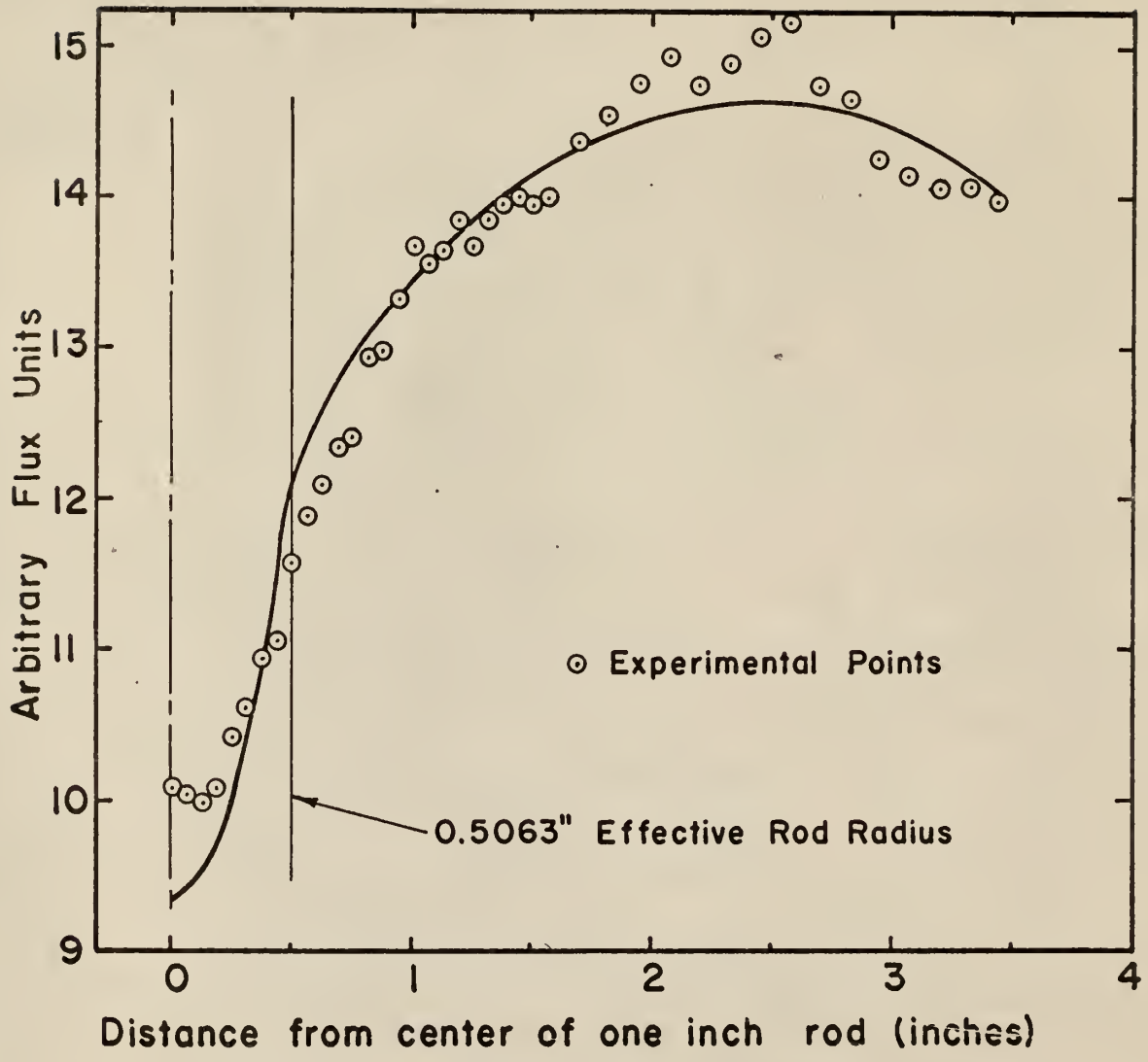

Fig. 5 Flux Calculated by Least Squares Analysis Case 1D

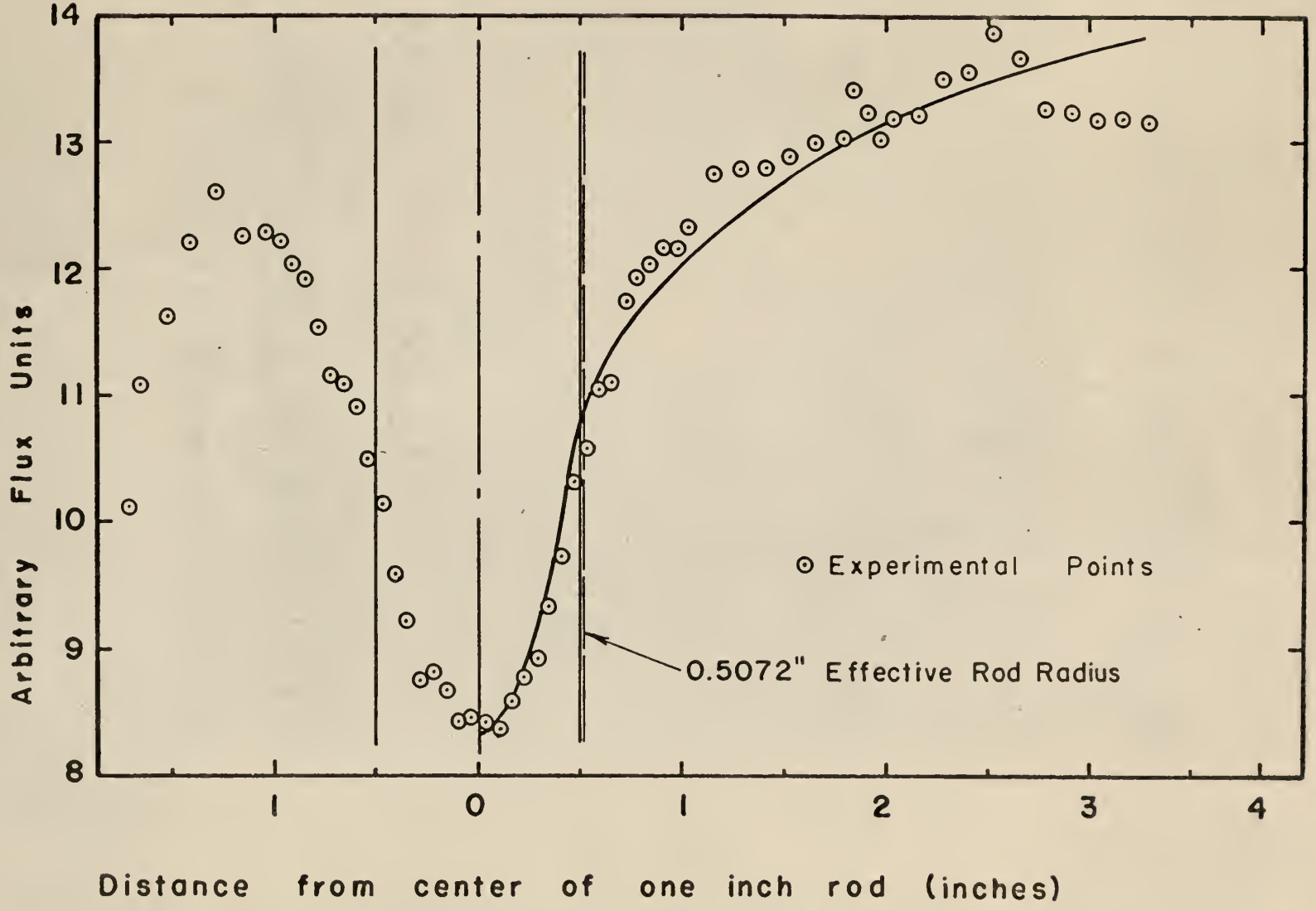

Fig.6 Flux Calculated by Least Squares Analysis Case 2A

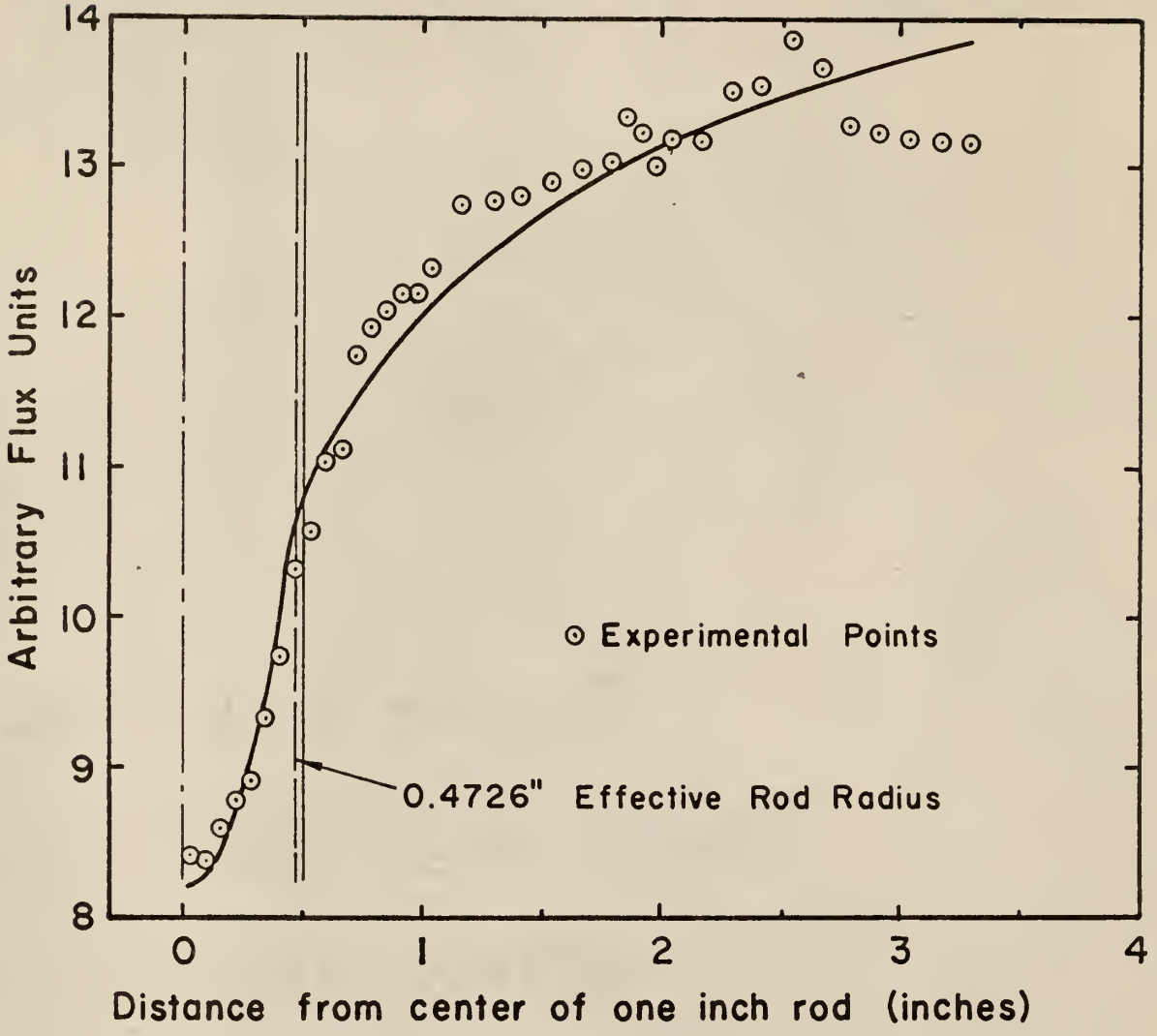

Fig. 7 Flux Calculated by Least Squares Analysis Case 2B

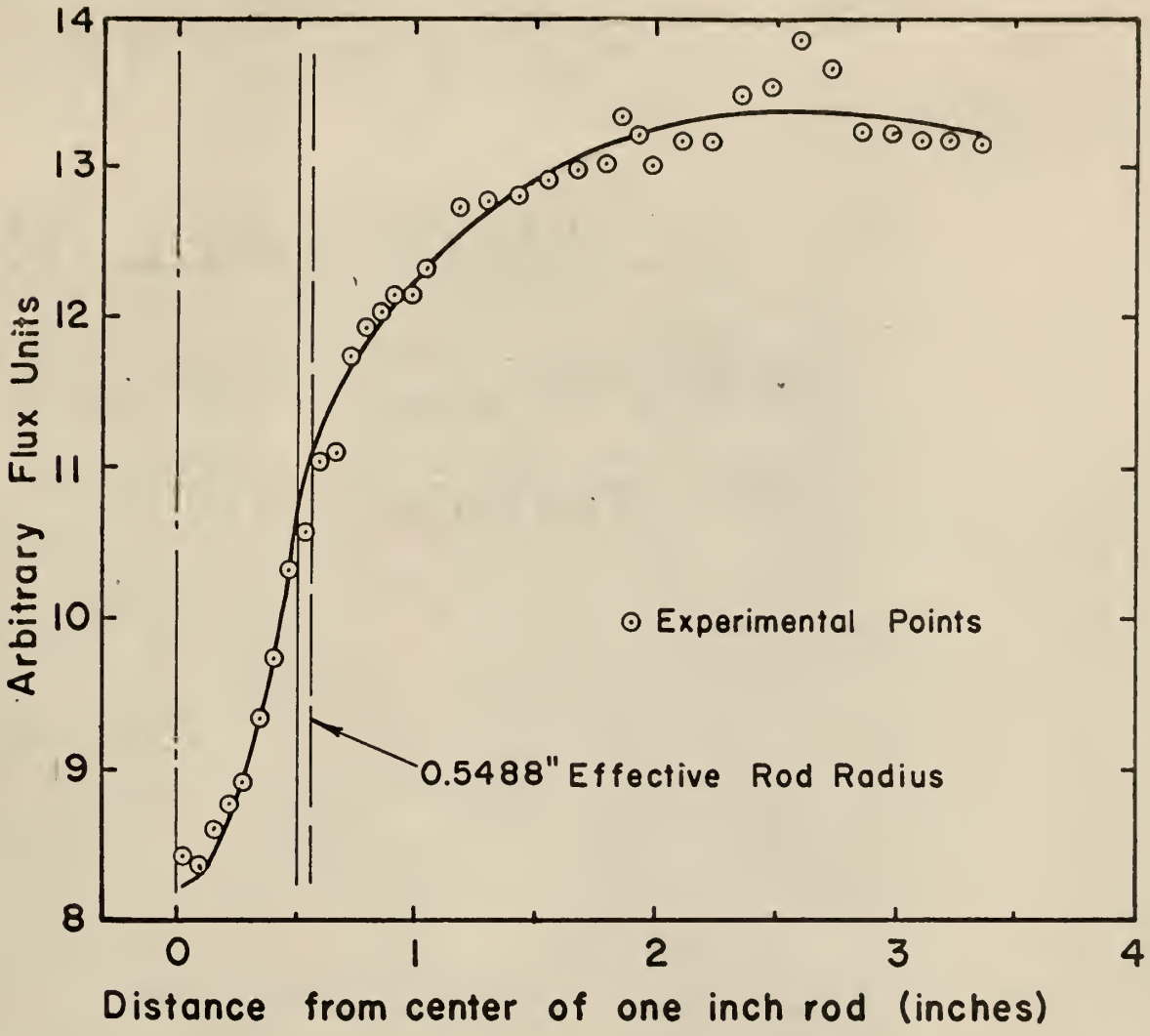

Fig. 8 Flux Calculated by Least Squares Analysis Case 2C

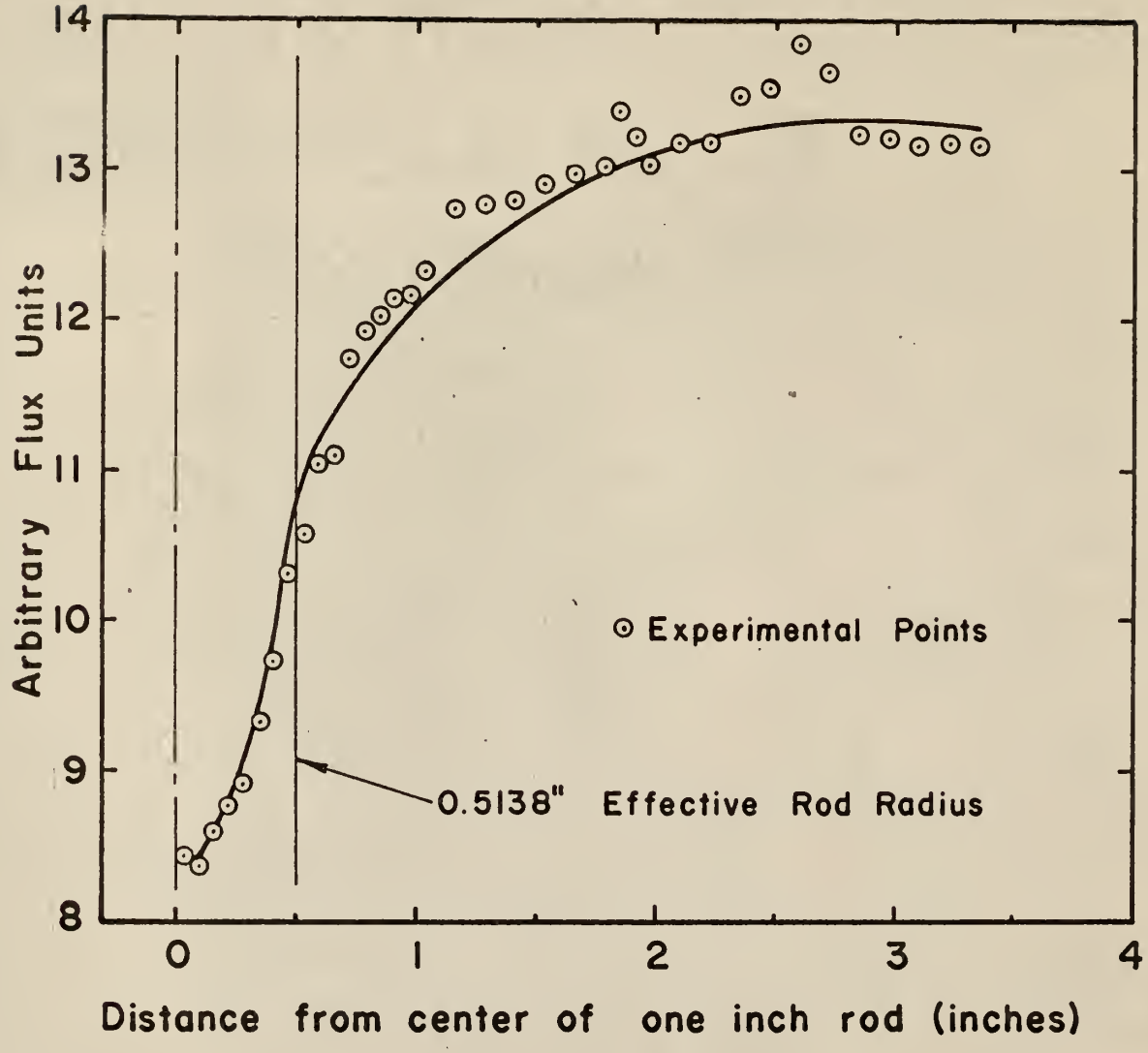

Fig.9 Flux Calculated by Least Squares Analysis Case 2D

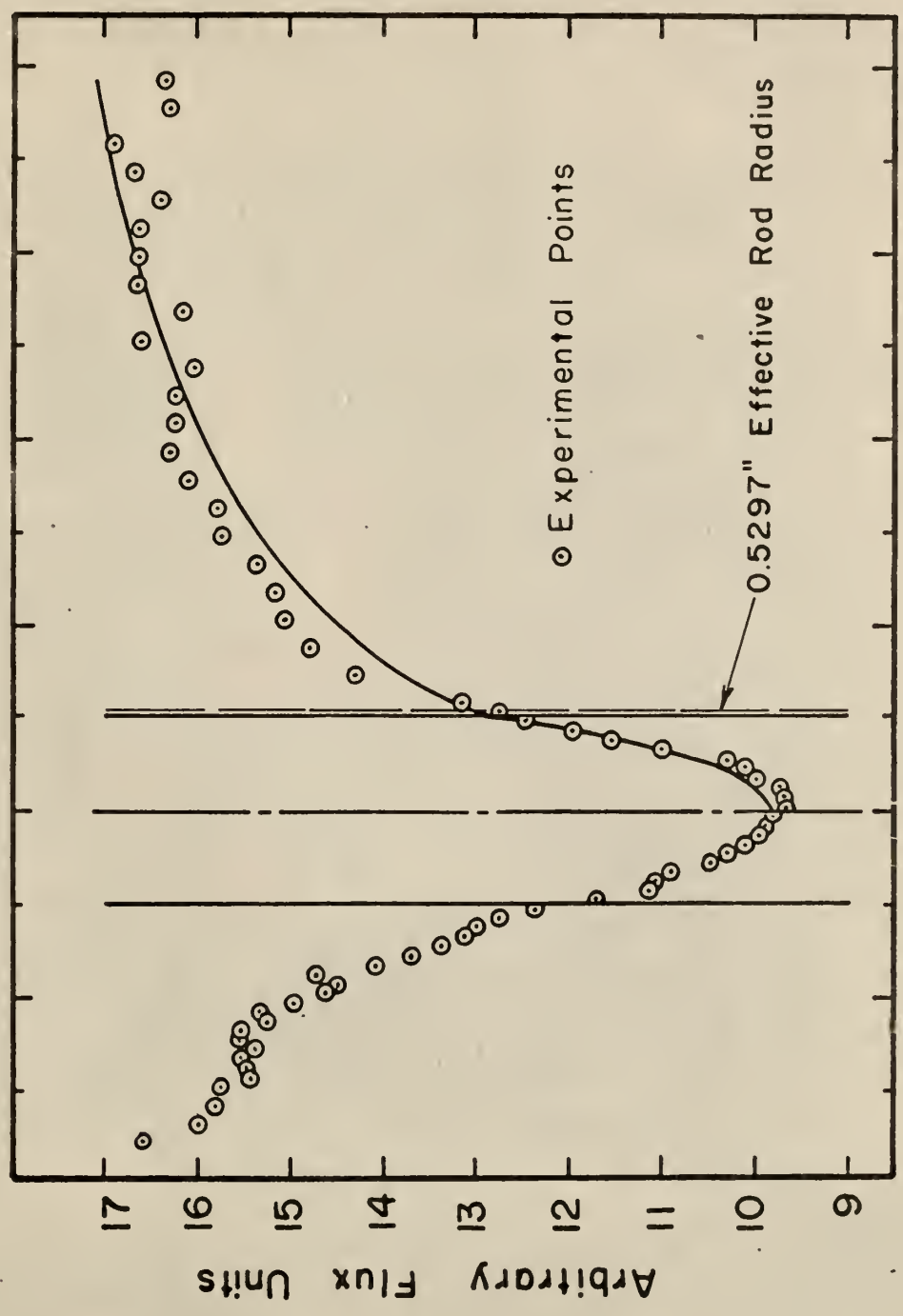

Fig. 10 Flux Calculated by Least Squares Analysis Case 3A

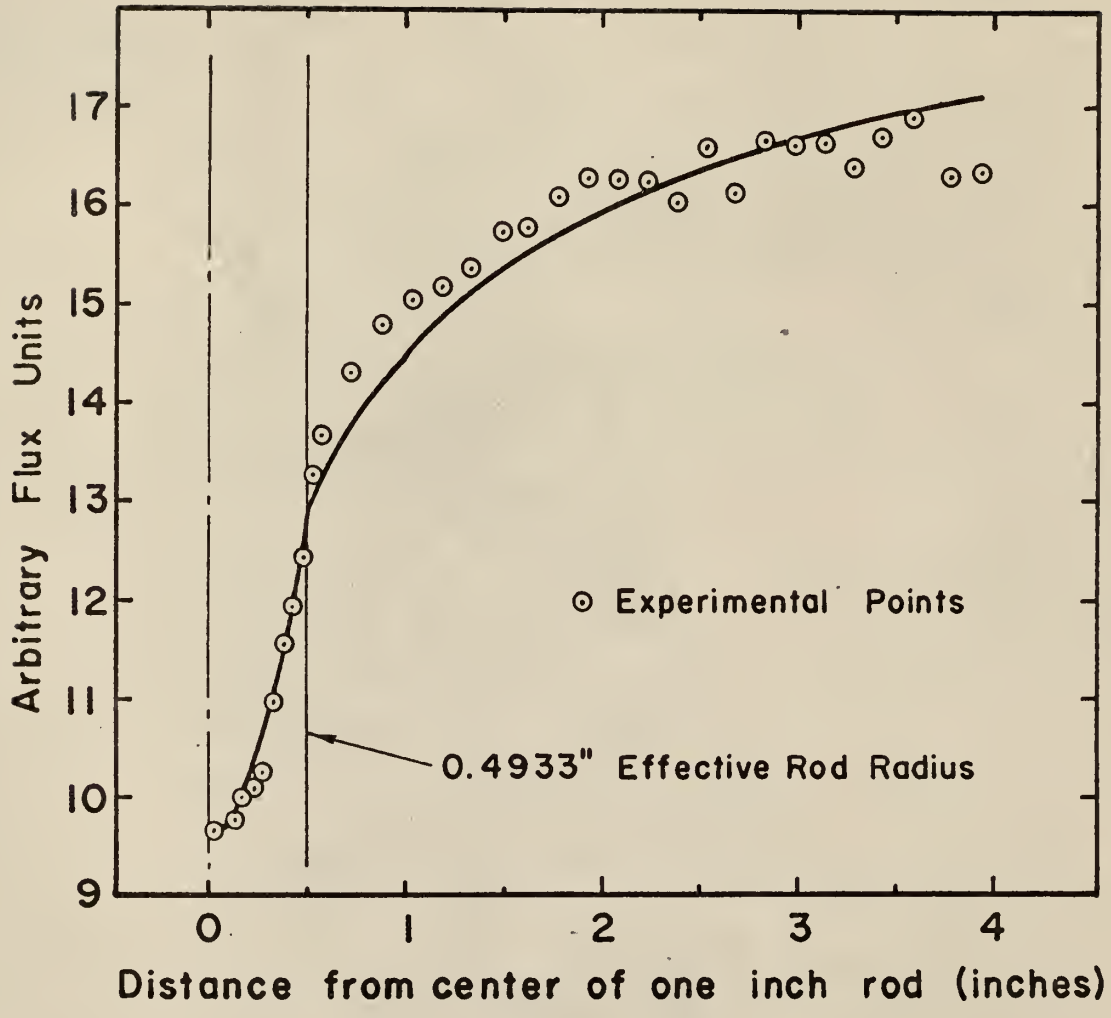

Fig.11 Flux Calculated by Least Squares Analysis
Case 3B

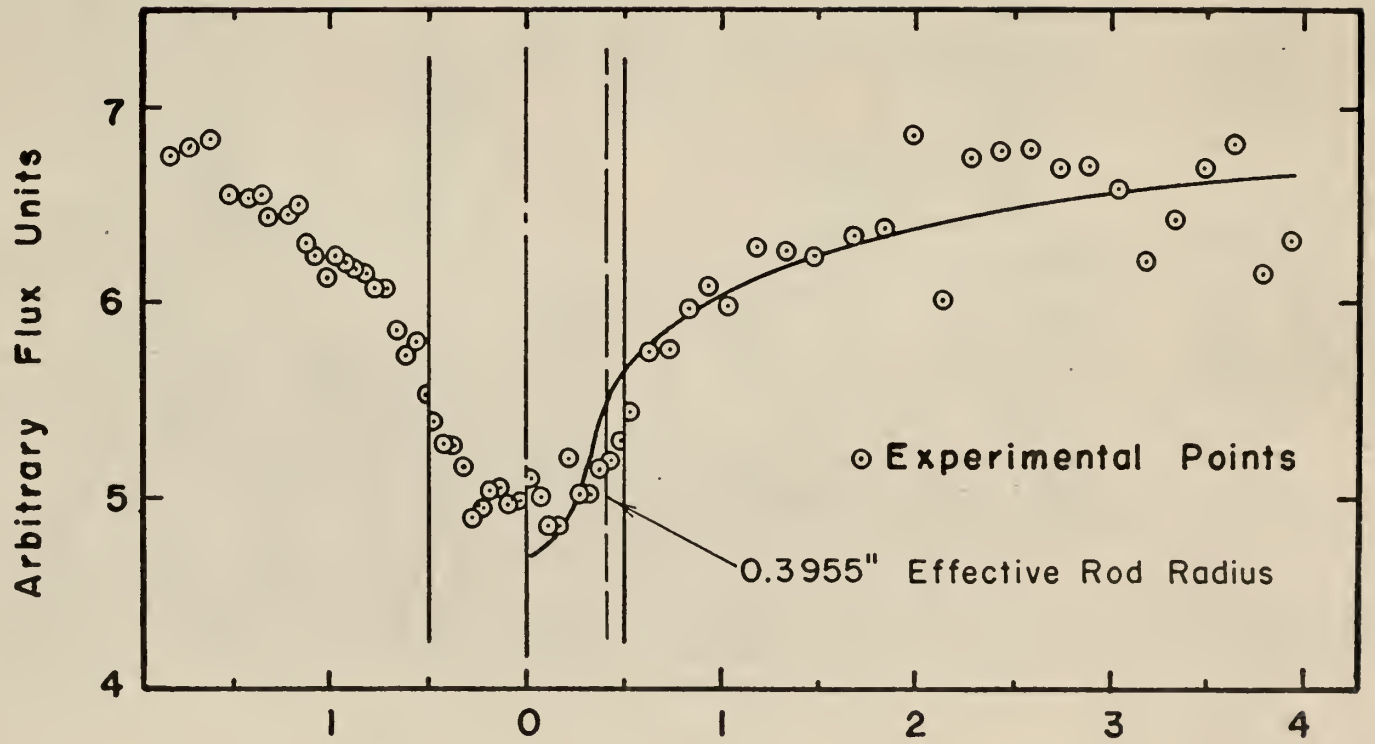

Fig.12 Flux Calculated by Least Squares Analysis Case 4A

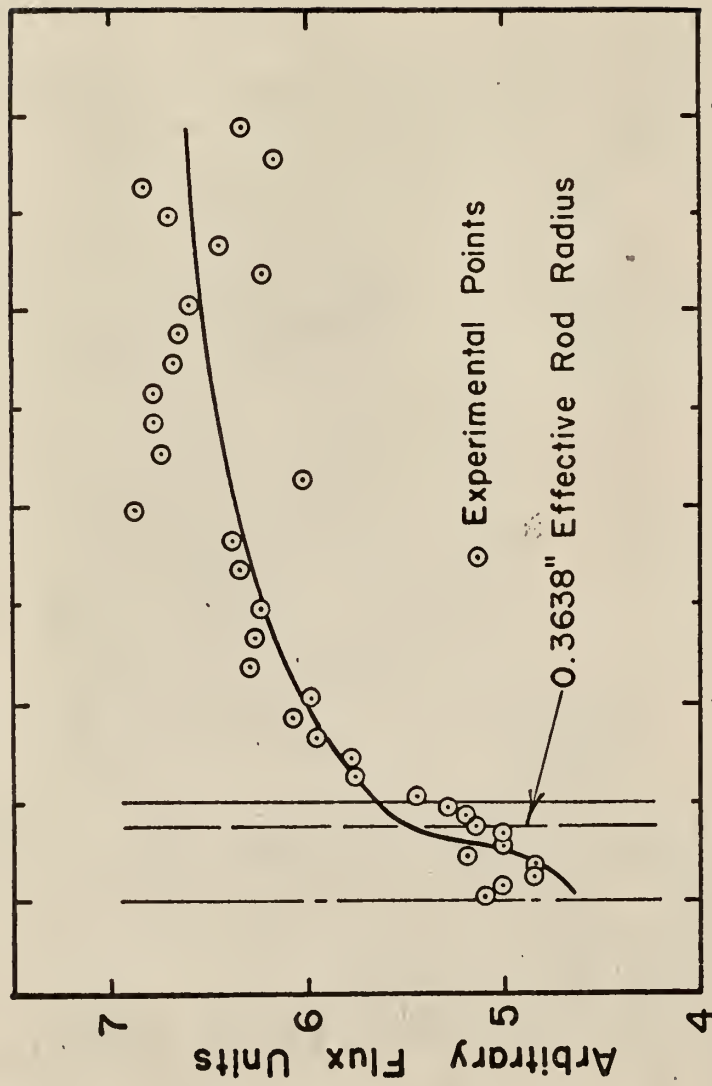

Fig.13 Flux Calculated by Least Squares Analysis
Case 4B

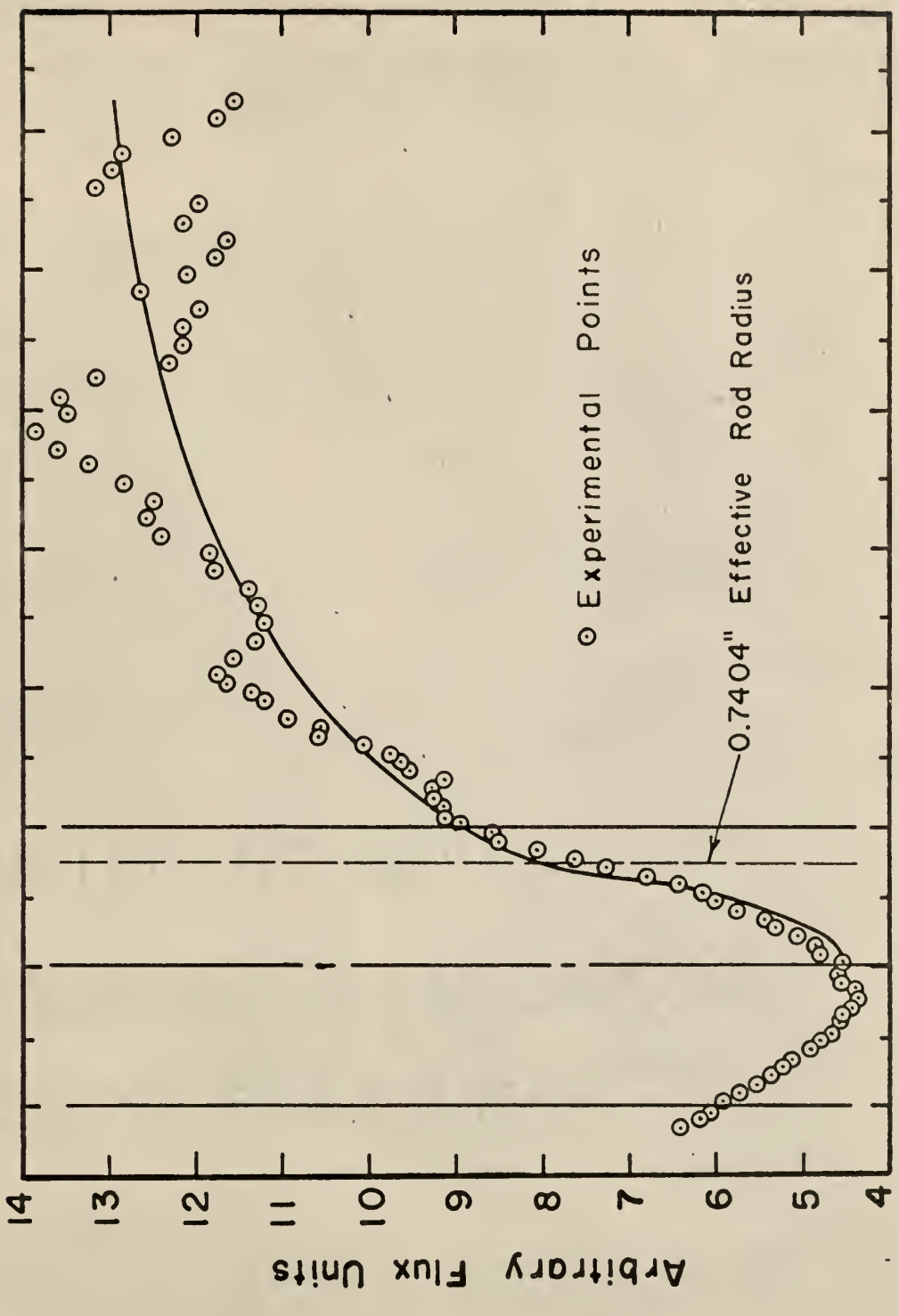

Fig.14 Flux Calculated by Least Squares Analysis Case 5A

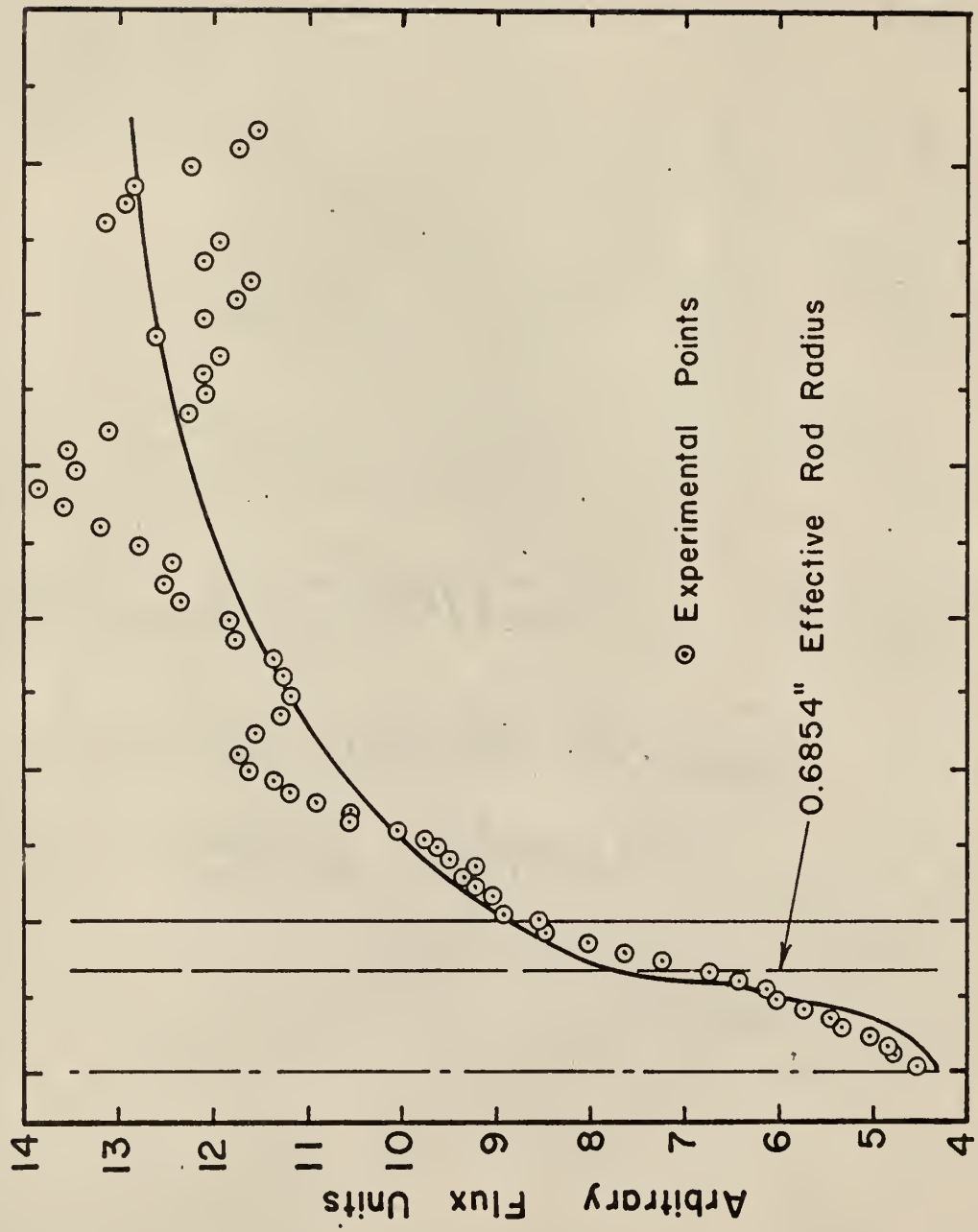

Fig.15 Flux Calculated by Least Squares Analysis
Case 5B

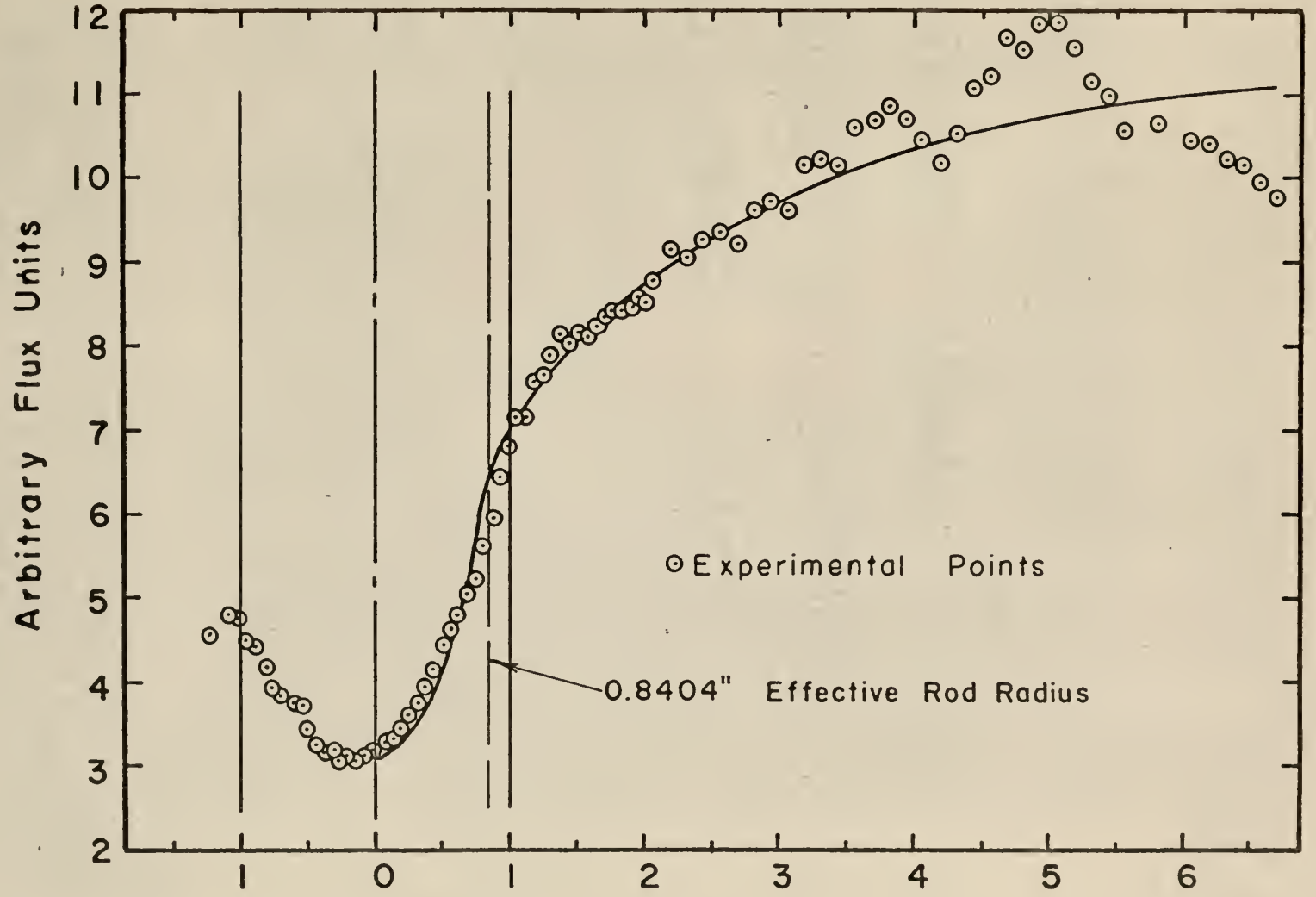

Fig.16 Flux Calculated by Least Squares Analysis Case 6A

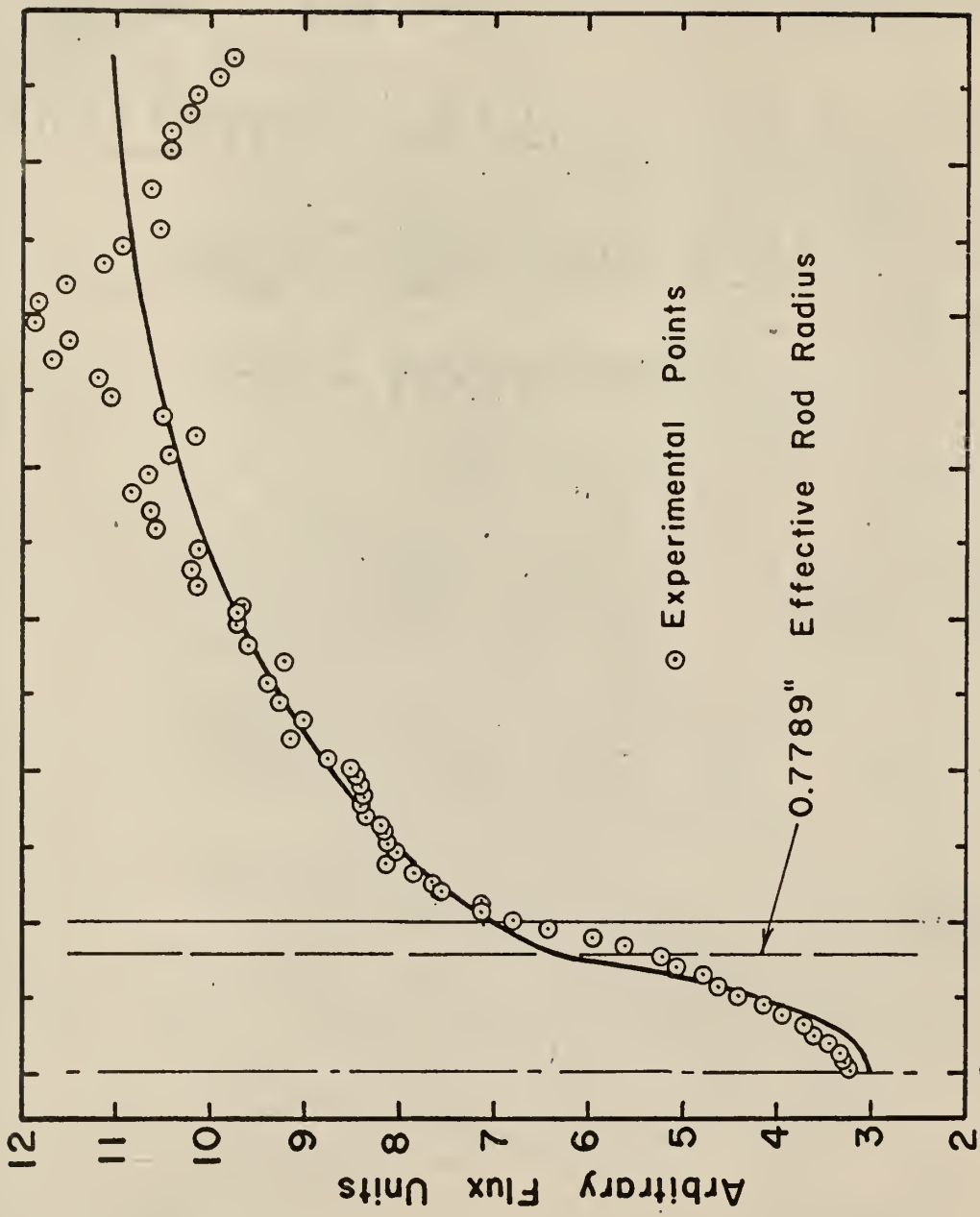

Fig.17 Flux Calculated by Least Squares Analysis
Case 6B

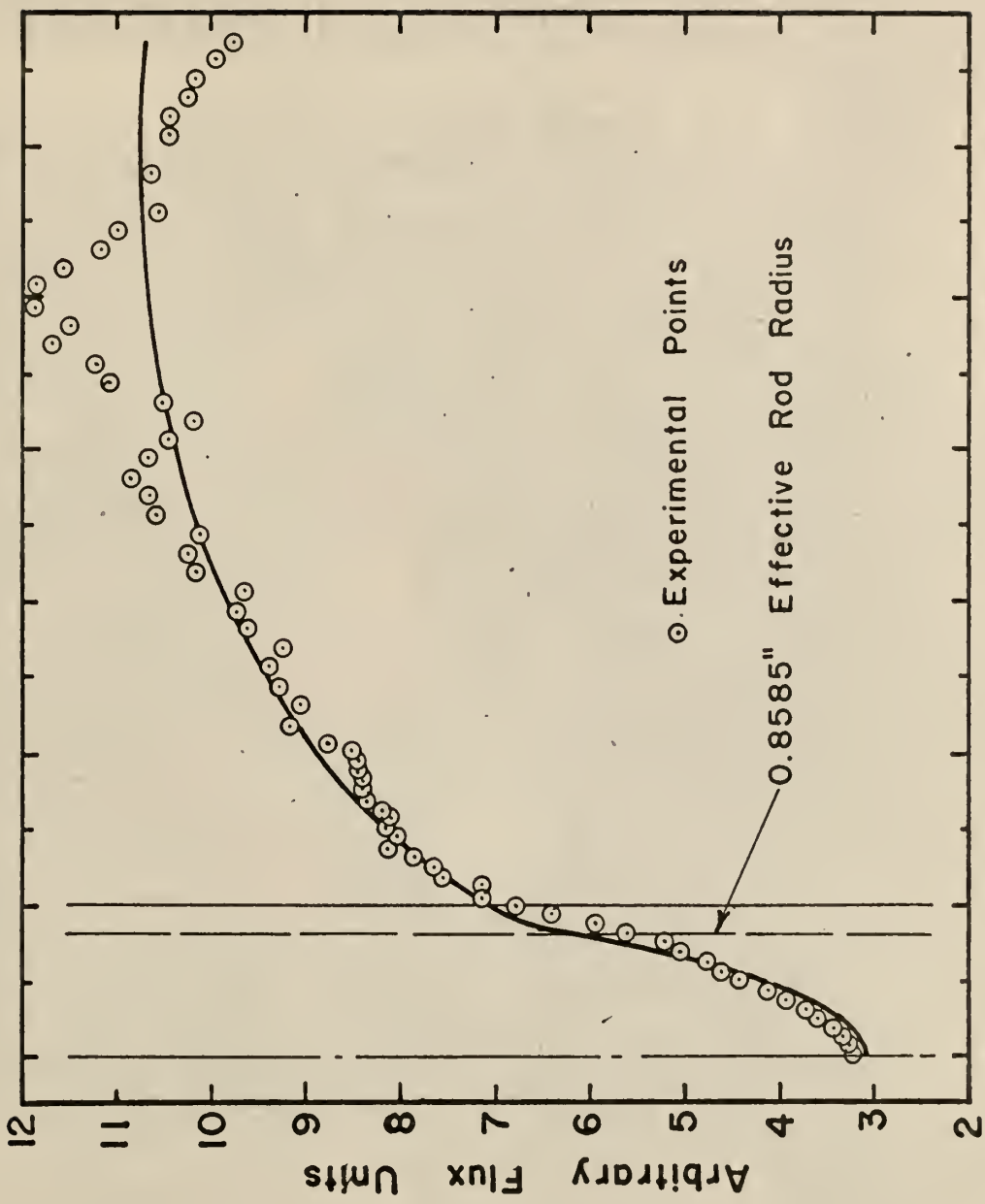

Fig. 18 Flux Calculated by Least Squares Analysis
Case 6C

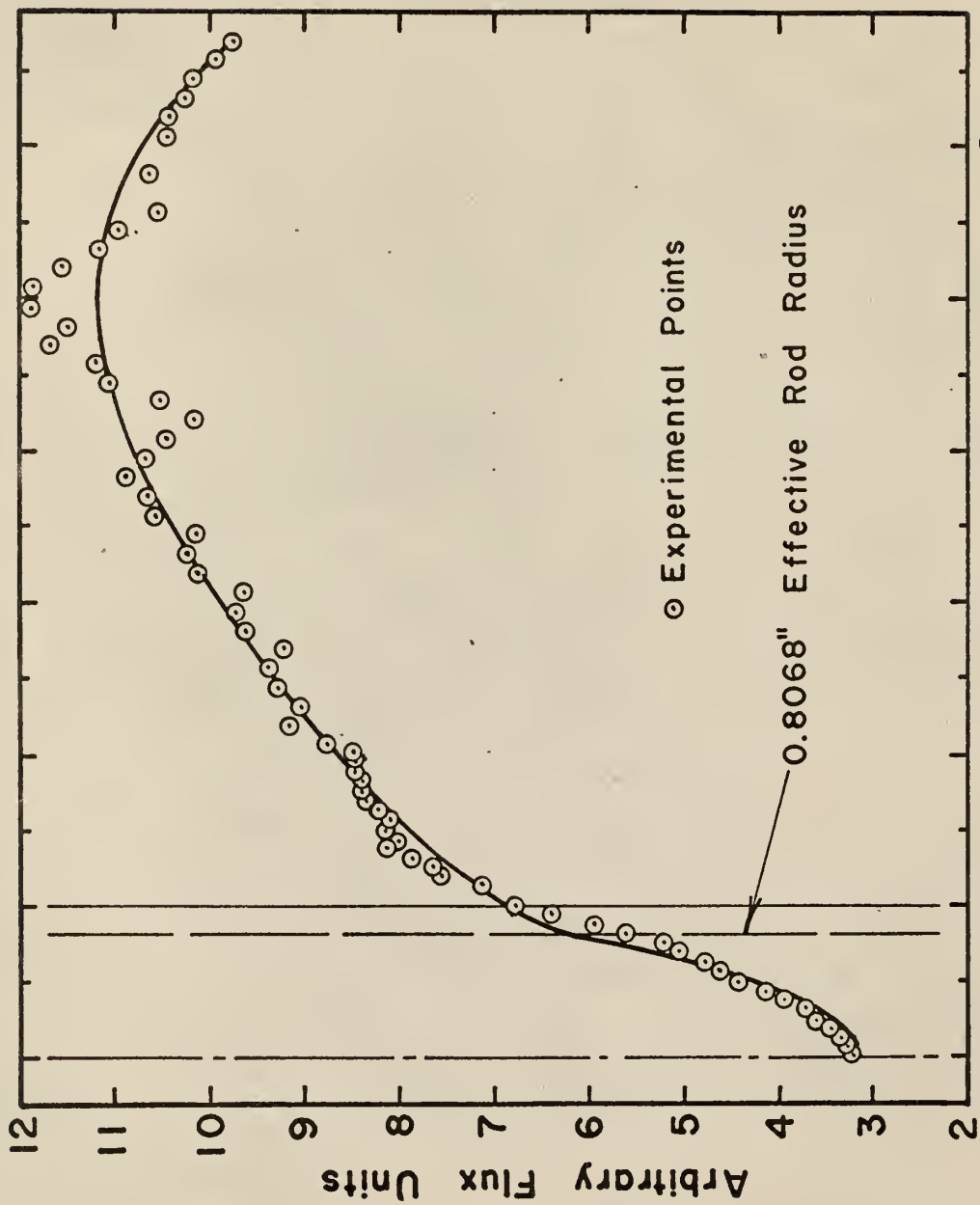

Fig. 19 Flux Calculated by Least Squares Analysis
Case 6D

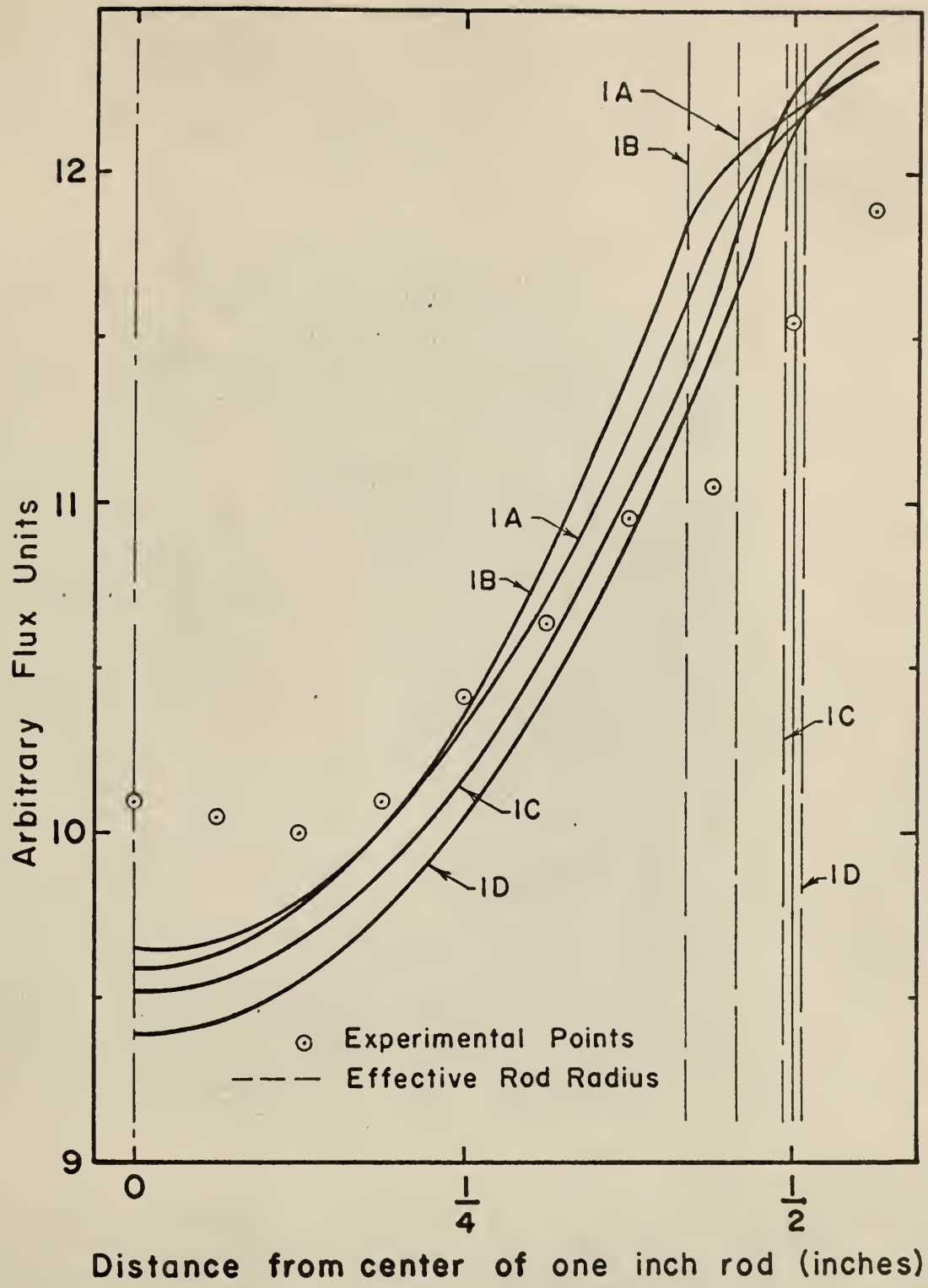

Fig.20 Comparison of Flux in Rod Calculated by Least Squares Analysis for Case I

Suggestions for Further Work

For the concept of an effective rod radius to be of use, graphs relating the dimensionless parameter $\Sigma_a R1$ to the effective rod radius should be available. To construct graphs of this type and to determine the empirical representation for these graphs, various combinations of rod radius and absorber material should be investigated.

Since the primary problem in the determination of the effective rod radius is in the calculation of the coefficients in the flux equations, other representations for these terms could be examined. More rigorous boundary conditions, e.g., no return current at the outer boundary, might be examined to see what effect, if any, they would have on the value of the effective rod radius.

Because P_1 transport theory is just slightly more accurate than elementary diffusion theory, investigations considering higher order P_n calculations should prove of interest. Some work has already been done in this area (13), but there is still much to be accomplished. This type of analysis is somewhat more difficult, but the improvement in the accuracy of the results should more than compensate for the extra labor involved.

ACKNOWLEDGMENT

The author wishes to express his sincere appreciation to the Kansas State University Engineering Experiment Station for its financial support and to the Atomic Energy Commission, who, through its fellowship program, made possible the opportunity for this study. Sincere gratitude is extended to Dr. Martin Grotenhuis who made available the facilities of the International School of Nuclear Science and Engineering for the recording of the data, and to the Association of Midwest Universities who provided the financial support for the work performed at the International School. Heartfelt thanks are extended to Dr. John O. Mingle of the Department of Nuclear Engineering for his guidance, encouragement, and help throughout this work, and to the other staff members for their particular contributions. Particular gratitude is extended to Dr. William R. Kimel, Head of the Department of Nuclear Engineering, for his advice and encouragement during the course of this work. Also thanks are given to Mr. Fred Prohammer who, through Dr. Kimel, suggested this problem.

LITERATURE CITED

1. Bartels, W. K. C.
   Self-Absorption of Monoenergetic Neutrons. KAPL-336, 1950.

2. Carslaw, H. S., and J. C. Jaeger.
   Conduction of Heat in Solids. Oxford: Clarendon Press, 1959.

3. Davison, B.
   Neutron Transport Theory. Oxford: Clarendon Press, 1957.

4. Dwork, J., P. L. Hoffman, H. Hurwitz, and E. F. Clancy.
   Self-Shielding Factors for Infinitely Long Hollow Cylinders. KAPL-1262, 1955.

5. Galanin, A. D.
   Thermal Reactor Theory. Translated from the Russian by J. B. Sykes. New York: Pergamon Press Inc., 1960.

6. Glasstone, W.
   Principles of Nuclear Reactor Engineering. Princeton: Van Nostrand, 1955.

7. Glasstone, W., and M. E. Edlund.
   The Elements of Nuclear Reactor Theory. Princeton: Van Nostrand, 1952.

8. Kushneriuk, S. A.
   Neutron Capture by Long Cylindrical Bodies Surrounded by Predominantly Scattering Media. AECL-462, 1957.

9. Kushneriuk, S. A., and C. McKay.
   Neutron Density in an Infinite, Non-Capturing Medium Surrounding a Long Cylindrical Body Which Scatters and Captures Neutrons. AECL-137, 1954.

10. Lennox, D. H., and C. N. Kelber.
    Summary Report on the Hazards of the Argonaut Reactor. ANL-5647, 1956.

11. Megreblian, R. V., and D. K. Holmes.
    Reactor Analysis. New York: McGraw-Hill, 1960.

12. Murray, R. L.
    Nuclear Reactor Physics. London: Macmillan and Company Inc., 1959.

13. Noble, L. D.
Unpublished work and private communication.
Kansas State University, 1962.

14. Scarborough, J. B.
Numerical Mathematical Analysis. Baltimore: Johns Hopkins, 1950.

15. Sturm, W. J., and D. A. Daavettila.
Argonaut Reactor Data Book. ANL-6258, 1961.

16. Weinberg, A. M., and E. P. Wigner.
The Physical Theory of Neutron Chain Reactors.
Chicago: University of Chicago, 1958.

APPENDICES

APPENDIX A

Derivation of the Boltzmann Transport Equation in Cylindrical Geometry

Following the notation of Weinberg and Wigner (16), the Boltzmann transport equation for the monoenergetic, steady state system is given as

$$\underline{\Omega} \cdot \text{grad}\, f(\underline{r},\underline{\Omega}) + f(\underline{r},\underline{\Omega})\,\Sigma(\underline{r}) = S(\underline{\Omega}) + \int d\underline{\Omega}'\, f(\underline{r},\underline{\Omega})\,\Sigma_s(\underline{\Omega}' \rightarrow \underline{\Omega}) \qquad \text{(A-1)}$$

where

$\underline{\Omega}$ is the unit vector in the direction of the neutron motion,

$f(\underline{r},\underline{\Omega})\, d\underline{r}\, d\underline{\Omega}$ is the angular flux; i.e., it is the number of neutrons in the volume element $d\underline{r}$ around $\underline{r}$ whose directions of motion lie in the solid angle $d\underline{\Omega}$ about $\underline{\Omega}$ times the speed v,

$d\underline{\Omega}$ is the differential solid angle,

Σ is the total cross section ($\Sigma = \Sigma_a + \Sigma_s$) ,

$\Sigma_s(\underline{\Omega}' \rightarrow \underline{\Omega})$ is the scattering cross section for changing $\underline{\Omega}'$ into the direction $d\underline{\Omega}$ about $\underline{\Omega}$,

$\underline{\Omega} \cdot \text{grad}\, f$ is the directional derivative of f in the direction $\underline{\Omega}$; i.e., if the coordinate s is extended in the direction $\underline{\Omega}$, then

$$\underline{\Omega} \cdot \text{grad}\, f = \frac{\partial f}{\partial s} . \qquad \text{(A-2)}$$

For a system with cylindrical symmetry and which is infinite in the z direction, the angular flux, f, depends on three variables. In the notation of Weinberg and Wigner (16), these variables are:

r -- the distance from the axis of the cylinder, the z axis

θ -- the angle between $\underline{\Omega}$ and z; and

φ -- the angle between the projection of $\underline{\Omega}$ on the x-y plane and the direction of r.

The geometry of the above described system is shown in Figure 21.

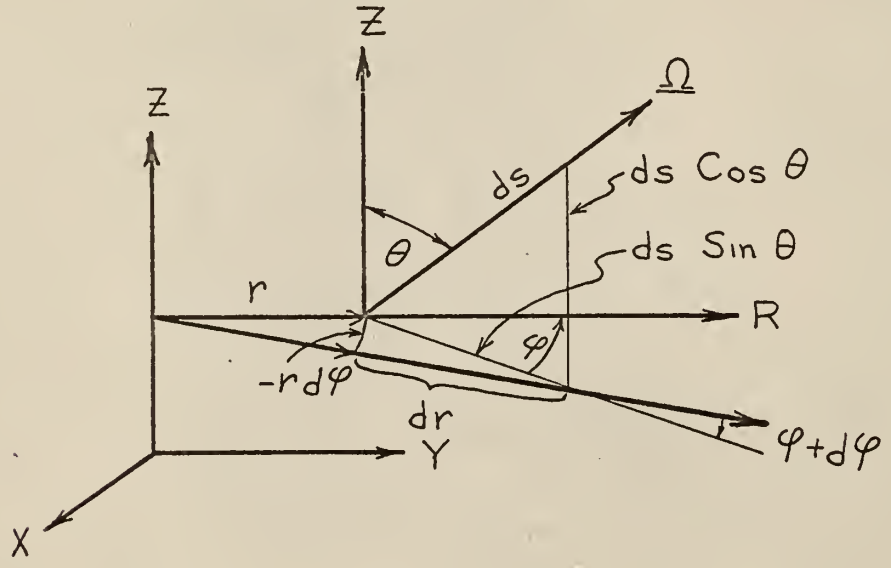

Figure 21. Cylindrical Geometry Coordinate System

Note that when $d\varphi$ is small

$$\mathrm{Sin}(\varphi+d\varphi) = \mathrm{Sin}\,\varphi$$

$$\mathrm{Cos}(\varphi+d\varphi) = \mathrm{Cos}\,\varphi .$$

Thus,

$$-r\,d\varphi = ds\,\mathrm{Sin}\,\theta\,\mathrm{Sin}\,\varphi \tag{A-3}$$

and

$$dr = ds\,\mathrm{Sin}\,\theta\,\mathrm{Cos}\,\varphi\,. \tag{A-4}$$

Then

$$\frac{d\varphi}{ds} = -\frac{1}{r}\,\mathrm{Sin}\,\theta\,\mathrm{Sin}\,\varphi \tag{A-5}$$

and

$$\frac{dr}{ds} = \mathrm{Sin}\,\theta\,\mathrm{Cos}\,\varphi. \tag{A-6}$$

From Eq. (A-2) $\underline{\Omega}\cdot \mathrm{grad}\, f = \frac{\partial f}{\partial s}$.

Since

$$f = f(r, \varphi) \tag{A-7}$$

then

$$\frac{\partial f}{\partial s} = \frac{\partial f}{\partial r}\cdot\frac{dr}{ds} + \frac{\partial f}{\partial \varphi}\cdot\frac{d\varphi}{ds} \tag{A-8}$$

so that

$$\frac{\partial f}{\partial s} = \frac{\partial f}{\partial r}[\mathrm{Sin}\,\theta\,\mathrm{Cos}\,\varphi] + \frac{\partial f}{\partial \varphi}\left[-\frac{1}{r}\,\mathrm{Sin}\,\theta\,\mathrm{Sin}\,\varphi\right], \tag{A-9}$$

The substitution of Eq. (A-8) and Eq. (A-9) into Eq. (A-1) yields

$$\sin\theta\cos\varphi\frac{\partial f(r,\theta,\varphi)}{\partial r}-\frac{1}{r}\sin\theta\sin\varphi\frac{\partial f(r,\theta,\varphi)}{\partial r}+$$

$$\Sigma(r)f(r,\theta,\varphi)=S(r,\theta,\varphi)+ \tag{A-10}$$

$$\int d\underline{\Omega}\,\Sigma_s(r,\cos\theta_o)f(r,\theta,\varphi)$$

which is the monoenergetic Boltzmann transport equation in cylindrical geometry with z and φ symmetry.

To transform the Boltzmann equation to a more convenient form for computation, expand $\Sigma_s(r,\cos\theta_o)$, $f(r,\theta,\varphi)$ and $S(r,\theta,\varphi)$ in spherical harmonics noting that Σ_s only depends on θ_o, the angle between $\underline{\Omega}$ and $\underline{\Omega}'$. Thus

$$\Sigma_s(r,\cos\theta_o)=\sum_{l=0}^{\infty}s_l P_l(\cos\theta_o) \tag{A-11}$$

$$f(r,\theta,\varphi)=\sum_{l=0}^{\infty}\sum_{m=-l}^{l}f_{lm}P_{lm}(\underline{\Omega}) \tag{A-12}$$

$$S(r,\theta,\varphi)=\sum_{l=0}^{\infty}\sum_{m=-l}^{l}S_{lm}P_{lm}(\underline{\Omega}) \tag{A-13}$$

where one form of $P_{lm}(\underline{\Omega})$ is given by

$$P_{lm}(\underline{\Omega})=\frac{e^{im\varphi}(-\sin\theta)^m}{(l!)2^l}\left\{\frac{(l-m)!}{(l+m)!}\right\}^{\frac{1}{2}}\frac{d^{l+m}(\cos^2\theta-1)^l}{(d\cos\theta)^{l+m}}. \tag{A-14}$$

In order that the spherical harmonics can be fully utilized, the following relations for this special use should be noted:

$$P_{l,-m}(\underline{\Omega})=(-1)^m P_{lm}(\underline{\Omega})^* \tag{A-15}$$

where the * indicates the complex conjugate;

the orthogonality relation for Legendre polynomials;

$$\int d\underline{\Omega}\, P_{l'm'}(\underline{\Omega})\, P_{lm}(\underline{\Omega})^{*} = \frac{4\pi}{2l+1}\,\delta_{ll'}\,\delta_{mm'} \tag{A-16}$$

the addition theorem for Legendre polynomials;

$$P_l(\mathrm{Cos}\,\theta_0) = \sum_{m=-l}^{l} P_{lm}(\underline{\Omega})\, P_{lm}(\underline{\Omega}')^{*} \tag{A-17}$$

and finally, the recursion relations for the Legendre polynomials

$$\mathrm{Sin}\,\theta e^{i\varphi} = \frac{1}{2l+1}\left[2(2l-1)C_{lm}P^{(\underline{\Omega})}_{l-1,m+1} - 2(2l+3)A_{lm}P^{(\underline{\Omega})}_{l+1,m+1}\right] \tag{A-18}$$

$$\mathrm{Sin}\,\theta e^{i\varphi} = \frac{1}{2l+1}\left[2(2l+3)B_{lm}P^{(\underline{\Omega})}_{l+1,m-1} - 2(2l+1)D_{lm}P^{(\underline{\Omega})}_{l-1,m-1}\right] \tag{A-19}$$

where

$$A_{lm} = \frac{\left[(l+m+1)(l+m+2)\right]^{\frac{1}{2}}}{2(2l+3)} \qquad B_{lm} = \frac{\left[(l-m+1)(l-m+2)\right]^{\frac{1}{2}}}{2(2l+3)}$$

$$C_{lm} = \frac{\left[(l-m-1)(l-m)\right]^{\frac{1}{2}}}{2(2l+1)} \qquad D_{lm} = \frac{\left[(l+m-1)(l+m)\right]^{\frac{1}{2}}}{2(2l+1)} .$$

The substitution of Eqs. (A-11), (A-12), and (A-13) into Eq. (A-10) leads to

$$\mathrm{Sin}\,\theta\,\mathrm{Cos}\,\varphi\sum_{l=0}^{\infty}\sum_{m=-l}^{l} P_{lm}(\underline{\Omega})\frac{\partial f_{lm}^{(r)}}{\partial r} - \frac{1}{r}\,\mathrm{Sin}\,\theta\,\mathrm{Sin}\,\varphi\sum_{l=0}^{\infty}\sum_{m=-l}^{l} f_{lm}^{(r)}\frac{\partial P_{lm}^{(\underline{\Omega})}}{\partial \varphi}$$

$$+\sum_{l=0}^{\infty}\sum_{m=-l}^{l} f_{lm}^{(r)} P_{lm}(\underline{\Omega})\,\Sigma(r) = \sum_{l=0}^{\infty}\sum_{m=-l}^{l} S_{lm} P_{lm}(\underline{\Omega}) \tag{A-20}$$

$$+\int d\underline{\Omega}\, f_{lm}^{(r)} P_{lm}(\underline{\Omega})\sum_{l=0}^{\infty}\sum_{m=-l}^{l} s_l P_{lm}(\underline{\Omega})\, P_{lm}(\underline{\Omega}')^{*}.$$

Now multiply Eq. (A-20) by $P_{l'm'}(\underline{\Omega})^{*}d\underline{\Omega}$ and integrate

over all $\underline{\Omega}$. Examining each term, starting with the right-hand side, keeping in mind the orthogonality relation, it can be shown that:

$$\iint f_{lm}(r) P_{lm}(\underline{\Omega}) P_{l'm'}(\underline{\Omega})^* d\underline{\Omega} \sum_{l=0}^{\infty} \sum_{m=-l}^{l} s_l P_{lm}(\underline{\Omega}) P_{lm}(\underline{\Omega}')^* d\underline{\Omega} = \tag{A-21}$$

$$[4\pi/(2l+1)]^2 f_{lm}(r) s_l$$

$$\int \sum_{l=0}^{\infty} \sum_{m=-l}^{l} S_{lm} P_{lm}(\underline{\Omega}) P_{l'm'}(\underline{\Omega})^* d\underline{\Omega} = [4\pi/(2l+1)] S_{lm} \tag{A-22}$$

$$\int \sum_{l=0}^{\infty} \sum_{m=-l}^{l} f_{lm}(r) P_{lm}(\underline{\Omega}) \Sigma(r) P_{l'm'}(\underline{\Omega})^* d\underline{\Omega} = [4\pi/(2l+1)] f_{lm}(r) \Sigma(r) . \tag{A-23}$$

For the first term on Eq. (A-20), write $\cos\varphi$ in exponential form and then substitute the recursion relations Eqs. (A-18) and (A-19). Thus

$$\int \sin\theta \cos\varphi \sum_{l=0}^{\infty} \sum_{m=-l}^{l} P_{lm}(\underline{\Omega}) P_{l'm'}(\underline{\Omega})^* d\underline{\Omega} \frac{\partial f_{lm}(r)}{\partial r} =$$

$$\int \sin\theta [(e^{i\varphi} + e^{-i\varphi})/2] \sum_{l=0}^{\infty} \sum_{m=-l}^{l} P_{lm}(\underline{\Omega}) P_{l'm'}(\underline{\Omega})^* d\underline{\Omega} \frac{\partial f_{lm}(r)}{\partial r} =$$

$$\int \sum_{l=0}^{\infty} \sum_{m=-l}^{l} \frac{1}{2} \frac{\partial f_{lm}(r)}{\partial r} d\underline{\Omega} P_{l'm'}(\underline{\Omega})^* \frac{1}{2l+1} \Big\{ [2(2l-1) C_{lm} P_{l-1,m+1}(\underline{\Omega}) - \tag{A-24}$$

$$2(2l+3) A_{lm} P_{l+1,m+1}(\underline{\Omega})] + [2(2l+3) B_{lm} P_{l+1,m-1}(\underline{\Omega}) - 2(2l-1) D_{lm} P_{l-1,m-1}(\underline{\Omega})] \Big\} =$$

$$\frac{4\pi}{2l+1} \Big[C_{lm} \frac{\partial f_{l-1,m+1}(r)}{\partial r} - A_{lm} \frac{\partial f_{l+1,m+1}(r)}{\partial r} + B_{lm} \frac{\partial f_{l+1,m-1}(r)}{\partial r} - D_{lm} \frac{\partial f_{l-1,m-1}(r)}{\partial r} \Big] .$$

The second term of Eq. (A-20) is handled in a like manner.

From Eq. (A-14) it is seen that

$$\frac{\partial P_{lm}(\underline{\Omega})}{\partial \varphi} = i m P_{lm}(\underline{\Omega}). \tag{A-25}$$

Thus

$$\int \frac{1}{r} \sin\theta \sin\varphi \sum_{l=0}^{\infty} \sum_{m=-l}^{l} f_{lm}(r) P_{l'm'}(\underline{\Omega})^* d\underline{\Omega} \frac{\partial P_{lm}(\underline{\Omega})}{\partial \varphi} =$$

$$\int \frac{1}{r} \sin\theta [(e^{i\varphi} - e^{-i\varphi})/2i] \sum_{l=0}^{\infty} \sum_{m=-l}^{l} f_{lm}(r) P_{l'm'}(\underline{\Omega})^* d\underline{\Omega}\, i m P_{lm}(\underline{\Omega}) =$$

$$\int \sum_{l=0}^{\infty} \sum_{m=-l}^{l} \frac{f_{lm}(r)}{r} P_{l'm'}(\underline{\Omega})^* d\underline{\Omega} \frac{im}{2i(2l+1)} \{[2(2l-1)C_{lm} P_{l-1,m+1}(\underline{\Omega}) - \tag{A-26}$$

$$2(2l+3)A_{lm} P_{l+1,m+1}(\underline{\Omega})] - [2(2l+3)B_{lm} P_{l+1,m-1}(\underline{\Omega}) - 2(2l-1)D_{lm} P_{l-1,m-1}(\underline{\Omega})]\} =$$

$$[4\pi/(2l+1)]\left\{C_{lm} f_{l-1,m+1}(r) \frac{m+1}{r} - A_{lm} f_{l+1,m+1}(r) \frac{m+1}{r} - B_{lm} f_{l+1,m-1}(r) \frac{m-1}{r} + D_{lm} f_{l-1,m-1}(r) \frac{m-1}{r}\right\}.$$

Regrouping Eqs. (A-21), (A-22), (A-24) and (A-25) in the proper order, the spherical harmonics form for the Boltzmann transport equation in cylindrical coordinates is obtained

$$A_{lm}\left[\frac{d}{dr} + \frac{m+1}{r}\right] f_{l+1,m+1}(r) - B_{lm}\left[\frac{d}{dr} - \frac{m-1}{r}\right] f_{l+1,m-1}(r) - \tag{A-27}$$

$$C_{lm}\left[\frac{d}{dr} + \frac{m+1}{r}\right] f_{l-1,m+1}(r) + D_{lm}\left[\frac{d}{dr} - \frac{m-1}{r}\right] f_{l-1,m-1}(r) +$$

$$f_{lm}(r)\Sigma(r) = S_{lm} + [4\pi/(2l+1)] f_{lm}(r) s_l .$$

APPENDIX B

Derivation of the P_1 Transport Equation in Cylindrical Geometry

In order to derive the P_1 transport model for cylindrical geometry, the Boltzmann transport equation must be utilized. The solution of this equation can be found in many references (3, 5, 7, 11, 12, 16). The form of the Boltzmann equation that will be used in the derivation is that one found in Weinberg and Wigner (16) page 276 for a cylinder infinite in the z direction and for monoenergetic neutrons. The equation has the form

$$A_{\ell m}\left[\frac{\partial}{\partial r}+\frac{m+1}{r}\right]f_{\ell+1,m+1}-B_{\ell m}\left[\frac{\partial}{\partial r}-\frac{m-1}{r}\right]f_{\ell+1,m-1}-C_{\ell m}\left[\frac{\partial}{\partial r}+\frac{m+1}{r}\right]f_{\ell-1,m+1}$$
$$+D_{\ell m}\left[\frac{\partial}{\partial r}-\frac{m-1}{r}\right]f_{\ell-1,m-1}+\frac{4\pi}{2\ell+1}s_{\ell}f_{\ell m}-\Sigma f_{\ell m}+S_{\ell m}=0 \qquad \text{(B-1)}$$

where

$$A_{\ell m}=\frac{\{(\ell+m+2)(\ell+m+1)\}^{1/2}}{2(2\ell+3)} \qquad B_{\ell m}=\frac{\{(\ell-m+1)(\ell-m+2)\}^{1/2}}{2(2\ell+3)}$$

$$C_{\ell m}=\frac{\{(\ell-m-1)(\ell-m)\}^{1/2}}{2(2\ell-1)} \qquad D_{\ell m}=\frac{\{(\ell+m-1)(\ell+m)\}^{1/2}}{2(2\ell-1)}$$

For the P_1 approximation, $\ell = 0, 1$ while $-\ell \leqslant m \leqslant +\ell$. The $f_{\ell m}$ equals zero for $\ell \geqslant 2$, and when $\ell = -1$. Because the medium of interest is assumed to be purely diffusing, the source term, $S_{\ell m}$, equals zero. In the P_1 approximation, scattering is assumed to be linearly anisotropic so that $s_0 \neq 0$ and $s_1 \neq 0$ while all other $s_\ell = 0$.

Because of the cylindrical symmetry around the z axis, the only $f_{\ell m}$ of interest are those where $\ell + m =$ even. All other $f_{\ell m}$ are neglected. (The equations for $\ell + m =$ even are independent of the $\ell + m =$ odd so that no part of a particular solution is omitted.)

Keeping the preceding facts in mind along with the property that, because of symmetry in the φ direction, $f_{\ell,-m} = (-1)^m f^*_{\ell m}$, the following equations are obtained:
When $\ell = 0$, $m = 0$

$$\frac{\sqrt{2}}{3}\left[\frac{\partial}{\partial r} + \frac{1}{r}\right] f_{11} + 4\pi s_0 f_{00} - \Sigma f_{00} = 0 . \qquad \text{(B-2)}$$

When $\ell = 1$, $m = 1$

$$\frac{\sqrt{2}}{2}\frac{\partial f_{00}}{\partial r} + \frac{4\pi s_1 f_{11}}{3} - \Sigma f_{11} = 0 . \qquad \text{(B-3)}$$

Solving Eq. (B-3) for f_{11}

$$f_{11} = \frac{\sqrt{2}}{2}\frac{\partial f_{00}}{\partial r} \cdot \frac{1}{\Sigma - \frac{4\pi s_1}{3}} \qquad \text{(B-4)}$$

and using the definition for Σ_{tr} that is found in (16), Eq. (B-4) becomes

$$f_{11} = \frac{\sqrt{2}}{2}\frac{\partial f_{00}}{\partial r} \cdot \frac{1}{\Sigma_{tr}} . \qquad \text{(B-5)}$$

Substitution of Eq. (B-5) into Eq. (B-2) and assuming Σ_{tr} is spacially independent leads to

$$\frac{1}{3\Sigma_{tr}}\left[\frac{\partial^2}{\partial r^2} + \frac{1}{r}\frac{\partial}{\partial r}\right] f_{00} + (4\pi s_0 - \Sigma) f_{00} = 0 . \qquad \text{(B-6)}$$

Noting that $4\pi s_o - \Sigma = -\Sigma_a$ and defining

$$D \equiv \frac{1}{3\Sigma_{tr}} \tag{B-7}$$

for the P_1 approximation, Eq. (B-6) becomes

$$D\nabla^2 f_{oo} - \Sigma_a f_{oo} = 0 \tag{B-8}$$

where

$$\phi_{TOTAL} = 4\pi f_{oo} \tag{B-9}$$

and ∇^2 is the well known Laplacian operator.

Thus, the P_1 transport equation is identical in form with the thermal diffusion equation except for the definition of D, the diffusion coefficient.

The net current in the r direction can also be obtained using the preceding method and equations. When $\ell = 1$, $m = -1$, Eq. (B-1) becomes

$$-\frac{\sqrt{2}}{2}\frac{\partial f_{oo}}{\partial r} + \frac{4\pi S_1}{3} f_{1,-1} - \Sigma f_{1,-1} = 0. \tag{B-10}$$

Now subtract Eq. (B-10) from Eq. (B-3) and obtain

$$\sqrt{2}\frac{\partial f_{oo}}{\partial r} + \frac{4\pi S_1}{3}[f_{11} - f_{1,-1}] - \Sigma[f_{11} - f_{1,-1}] = 0. \tag{B-11}$$

Using the previous definition of Σ_{tr}, Eq. (B-11) becomes

$$\sqrt{2}\frac{\partial f_{oo}}{\partial r} - \Sigma_{tr}[f_{11} - f_{1,-1}] = 0. \tag{B-12}$$

Now use Eq. (B-7) to define D and rearrange Eq. (B-12) into the form

$$J(r) = -D\nabla f_{oo} = \frac{2^{-1/2}}{3}[f_{1,-1} - f_{11}] \tag{B-13}$$

where ∇ represents the gradient operator in cylindrical coordinates with no φ or z dependence.

APPENDIX C

The Orthogonality Condition for $U_0(\alpha r)$

$U_0(\alpha r)$ is a solution of Bessel's equation

$$\frac{1}{r}\frac{d}{dr}\left(r\frac{d\omega}{dr}\right) + \alpha^2\omega = 0 \tag{C-1}$$

where the boundary condition

$$\omega(b) = 0 \tag{C-2}$$

has been applied. For this case

$$\omega(r) = U_0(\alpha r) \equiv J_0(\alpha r)Y_0(\alpha b) - Y_0(\alpha r)J_0(\alpha b) . \tag{C-3}$$

Let $U_0(\alpha r)$ be a solution of Eq. (C-1) and let $U_0(\beta r)$ be a solution of

$$\frac{1}{r}\frac{d}{dr}\left(r\frac{d\nu}{dr}\right) + \beta^2\nu = 0 \tag{C-4}$$

where $\nu(r) = U_0(\beta r)$. Multiply Eq. (C-1) by ν and Eq. (C-4) by ω and subtract Eq. (C-4) from Eq. (C-1). Thus

$$\begin{aligned}(\beta^2 - \alpha^2) r\nu\omega &= \nu\frac{d}{dr}\left(r\frac{d\omega}{dr}\right) - \omega\frac{d}{dr}\left(r\frac{d\nu}{dr}\right) \\ &= \frac{d}{dr}\left[r\left(\nu\frac{d\omega}{dr} - \omega\frac{d\nu}{dr}\right)\right] .\end{aligned} \tag{C-5}$$

Now multiply Eq. (C-5) by rdr and integrate over (a,b), the interval of interest.

Thus

$$(\beta^2-\alpha^2)\int_a^b r v\omega\, dr = \int_a^b \frac{d}{dr}\left[r\left(v\frac{d\omega}{dr} - \omega\frac{dv}{dr}\right)\right] dr$$

$$= \left[r\left(v\frac{d\omega}{dr} - \omega\frac{dv}{dr}\right)\right]_a^b . \qquad \text{(C-6)}$$

From the preceding definitions of v and ω it is easily seen that both v and ω are zero when evaluated at the upper limit. Thus, evaluating Eq. (C-6) at the lower limit

$$(\beta^2-\alpha^2)\int_a^b r v\omega\, dr =$$

$$-a\left\{U_o(\beta a)\left[-\alpha U_o'(\alpha a)\right] - U_o(\alpha a)\left[-\beta U_o'(\beta a)\right]\right\} \qquad \text{(C-7)}$$

where

$$\frac{d\omega}{dr} = -\alpha\left[J_1(\alpha r)\, Y_o(\alpha b) - Y_1(\alpha r)\, J_o(\alpha b)\right]$$

$$= -\alpha U_o'(\alpha r) = -\alpha U_1(\alpha r) \qquad \text{(C-8)}$$

and

$$\frac{dv}{dr} = -\beta\left[J_1(\beta r)\, Y_o(\beta b) - Y_1(\beta r)\, J_o(\beta b)\right]$$

$$= -\beta U_o'(\beta r) = -\beta U_1(\beta r) . \qquad \text{(C-9)}$$

Eq. (C-7) can be rearranged into the form

$$(\beta^2-\alpha^2)\int_a^b r v\omega\, dr = k_o\left[\alpha U_o'(\alpha a) + k_1 U_o(\alpha a)\right] \qquad \text{(C-10)}$$

where

$$k_o = a U_o(\beta a) \qquad \text{(C-11)}$$

$$k_1 = -\beta U_o'(\beta a)/U_o(\beta a) , \qquad \text{(C-12)}$$

Now, if α and β are positive roots of the equation

$$\alpha U_o'(\alpha a) + k_1 U_o(\alpha a) = 0 \qquad \text{(C-13)}$$

then

$$\int_a^b r v \omega \, dr = \int_a^b r U_o(\beta r) U_o(\alpha r) \, dr = 0 \qquad \text{(C-14)}$$

which is the orthogonality condition for $U_o(\alpha r)$.

In order to evaluate the integral

$$\int_a^b r U_o^2(\alpha r) \, dr$$

take Eq. (C-1) and multiply it by $2r \frac{d\omega}{dr}$:

$$2r \frac{d\omega}{dr} \cdot \frac{d}{dr}\left(r \frac{d\omega}{dr}\right) + 2r \frac{d\omega}{dr} r \alpha^2 \omega = 0. \qquad \text{(C-15)}$$

Rearranging the terms of Eq. (C-15) yields

$$\frac{d}{dr}\left(r \frac{d\omega}{dr}\right)^2 + \alpha^2 r^2 \frac{d}{dr}(\omega^2) = 0. \qquad \text{(C-16)}$$

Now multiply Eq. (C-16) by dr and integrate over (a,b), the region of orthogonality:

$$\int_a^b \frac{d}{dr}\left(r \frac{d\omega}{dr}\right)^2 dr + \alpha^2 \int_a^b r^2 \frac{d}{dr}(\omega^2) \, dr = 0. \qquad \text{(C-17)}$$

Integrating the second term by parts and the straight forward integration of the first term yields

$$\left[\left(r \frac{d\omega}{dr}\right)^2\right]_a^b + \alpha^2 \left[r^2 \omega^2\right]_a^b - 2\alpha^2 \int_a^b r \omega^2 \, dr = 0. \qquad \text{(C-18)}$$

Rearranging Eq. (C-18) and evaluating the expressions for ω^2 and $\left(\frac{d\omega}{dr}\right)^2$ at the limits yields the following

equation:

$$2\alpha^2\int_a^b r\,U_o^2(\alpha r)\,dr = \tag{C-19}$$

$$b^2\alpha^2 U_1^2(\alpha b) - a^2\alpha^2 U_1^2(\alpha a) - a^2\alpha^2 U_o^2(\alpha a)\,.$$

From Murray (12), the Wronskian relation is given as

$$J_o(X)\,Y_1(X) - J_1(X)\,Y_o(X) = -\frac{2}{\pi X}\,. \tag{C-20}$$

Using Eq. (C-8) as a definition for $U_1(\alpha b)$, it is easily seen that

$$U_1(\alpha b) = \frac{2}{\alpha\pi b} \tag{C-21}$$

and by applying the definition for $U_1(\alpha a)$ as given in Eq. (C-13), Eq. (C-19) becomes

$$\int_a^b r\,U_o^2(\alpha r)\,dr = \frac{1}{2\alpha^2}\left\{\frac{4}{\pi^2} - a^2\alpha^2\left[\frac{k_1^2}{\alpha^2}U_o^2(\alpha a) + U_o^2(\alpha a)\right]\right\} \tag{C-22}$$

$$= \frac{1}{2\alpha^2}\left\{\frac{4}{\pi^2} - a^2\alpha^2 U_o^2(\alpha a)\left[\frac{k_1^2}{\alpha^2} + 1\right]\right\}.$$

Another integral that must be considered is

$$\int_a^b r\,U_o(\alpha r)\,dr\,. \tag{C-23}$$

Writing the equivalent expression for $U_o(\alpha r)$, the integral becomes

$$\int_a^b rU_o(\alpha r)\,dr = \int_a^b r\left[J_o(\alpha r)\,Y_o(\alpha b) - Y_o(\alpha r)\,J_o(\alpha b)\right]dr\,. \tag{C-24}$$

Performing the indicated integration:

$$\int_a^b r\, U_o(\alpha r)\, dr = \left\{\frac{r}{\alpha}\left[J_1(\alpha r) Y_o(\alpha b) - Y_1(\alpha r) J_o(\alpha b)\right]\right\}_a^b$$

$$= \left[\frac{r}{\alpha} U_1(\alpha r)\right]_a^b \qquad (C\text{-}25)$$

$$= \frac{b}{\alpha} U_1(\alpha b) - \frac{a}{\alpha} U_1(\alpha a) .$$

Substituting the value for $U_1(\alpha b)$ from Eq. (C-21) and the value for $U_1(\alpha a)$ from Eq. (C-13), Eq. (C-25) becomes

$$\int_a^b r\, U_o(\alpha r)\, dr = \frac{2}{\pi\alpha^2} + \frac{a}{\alpha^2} k_1 U_o(\alpha a) , \qquad (C\text{-}26)$$

Further discussion of the properties of this function can be found in Carslaw and Jaeger (2).

APPENDIX D

Experimental Facilities

The experimental facilities used to compile the preliminary data employed in this work were the Argonaut Training Reactor of the International School of Nuclear Science and Engineering located at Argonne National Laboratory. The use of these facilities was made possible through the courtesy and cooperation of the International School of Nuclear Science and Engineering and the Association of Midwestern Universities. It is noted that the experimental phase of this work was completed before the Kansas State University TRIGA MARK II Reactor went critical.

A complete description of the Argonaut reactor can be found in references (10, 15). The following will be a short account of the actual facilities used.

The foils were irradiated in the external graphite thermal column. The thermal column is an extension of the reactor reflector graphite, and it is four feet by five feet in cross section by six feet long. It is composed of assorted lengths of machined reactor grade graphite four inches in cross section. A total of fifteen removable horizontal stringers are available for access in the direction of the core. The J-10 stringer was the one in which the experimental measurements were made. It is located on the vertical and horizontal center line of the core.

The core of the Argonaut reactor system is annular in design, and it is reflected internally and externally with graphite. The fuel elements are hetrogeneous and consist of BORAX-type fuel plates (15) in rectangular assemblies three by six inches. Light water serves as the moderator in and surrounding each fuel box while graphite moderator pieces separate the individual fuel boxes.

Because of the annular design of the core, the core can be loaded with fuel in two different configurations for power runs: a one slab loading or a two slab loading. The one slab loading consists of six fuel boxes placed in the annulus separated only by the graphite moderator pieces. When a two slab loading is required, an identical configuration of fuel elements is located diametrically opposite the initial loading.

The critical loading of the two slab system is approximately four kilograms of U-235 at 20% enrichment. With this loading the reactor will normally operate in the range of one to one hundred watts. The reactor can operate continuously at one kilowatt and is capable of operation at a maximum thermal power of ten kilowatts.

For this particular work, a one slab loading was used, and the fuel elements were placed in position nearest the thermal column; as shown in Figure 22.

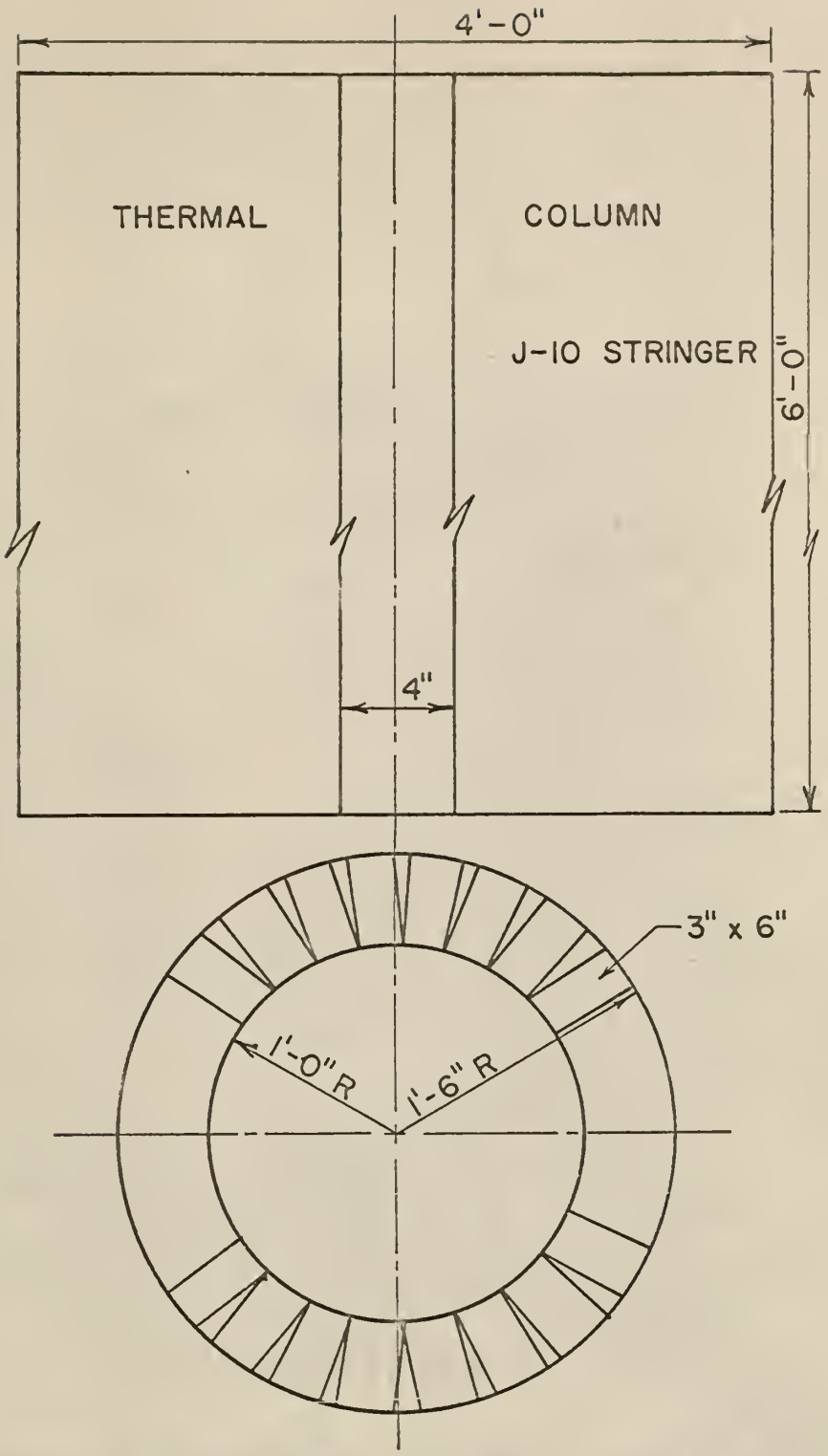

FIG. 22 ARGONAUT CORE AND THERMAL COLUMN SKETCH.

Experimental Procedure

The data compiled for this work were taken by the method outlined in the main body, and the pertinent details will be presented here.

The absorber rods were steel measuring one inch and two inches in diameter. The gold wire was used to record data for both the one inch and the two inch rod while the gold foil was used only in conjunction with the one inch rod. Both rods were cut into three sections; the center section was ten inches long; the forward section, the section nearest the core, was six inches long; and the aft section was eight inches long (see figure 23).

The center section had a slot, 1/32 inch wide by 9/32 inch deep, located on the center line of the rod cut into each end. Into each slot, one gold wire or one gold foil was placed depending on the phase of the experiment. The wire or foil was of such a length that it extended from the edge of the special graphite stringer to approximately one inch beyond the edge of the rod when the rod was in place in the stringer. The special stringer, with a graphite rod in the position of the steel rod not being used, was then placed in position for the irradiation. The wire or foil was irradiated for a period of one hour while the reactor was operated at a power level of 100 watts.

The reactor was shut down at the conclusion of the irradiation period by a "scram" procedure, and the time at

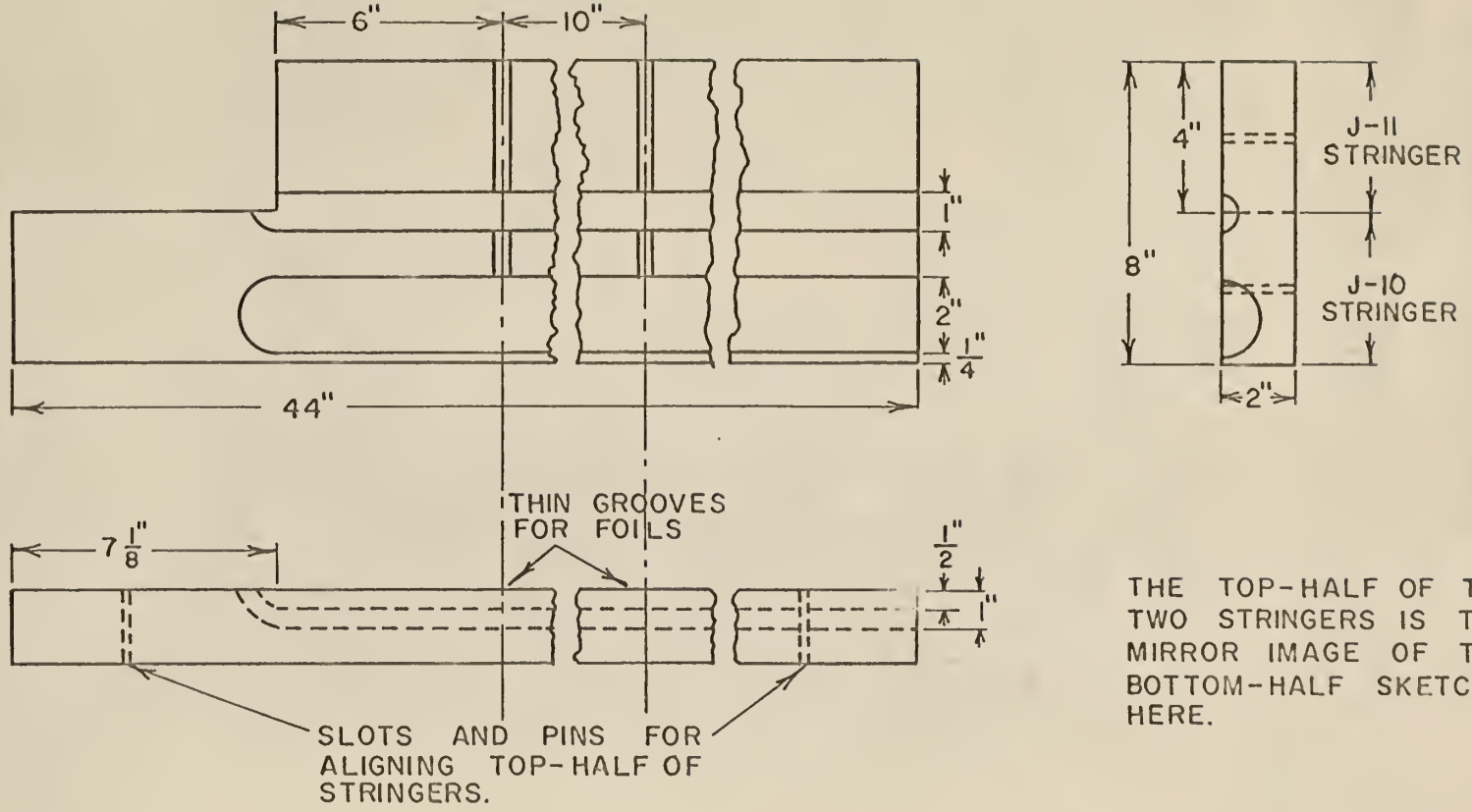

FIG. 23 SPECIAL STRINGER FOR IRRADIATING GOLD FOIL AND GOLD WIRE.

which this occurred was recorded. Following the shut down, the special stringer was removed from the thermal column, and allowed to cool off. The wires, or foils, were then removed from the stringer and transported to the counting facility which was located at some distance from the irradiation facility.

The wire was counted as described previously. The counting tube was an end window Geiger-Mueller type. As the wire was advanced under the G-M tube, it was always moved a sufficient distance to prevent counting a portion of the same section of the wire twice. At large distances from the center of the rod, the wire was advanced in steps of one-eighth inch. In the immediate vicinity of the rod, the step was reduced to one-sixteenth inch, the diameter of the hole in the wire guide. This increment was maintained until the wire was advanced past the region where the rod had been positioned. At each position where a count was taken, the time when the counting began was recorded.

The foil counting procedure was that one described previously. The foil was taped to a piece of graph paper having ten divisions per one-half inch. The foil was then cut into narrow strips approximately 0.050 inches wide. These small strips of foil were then placed on a special plancet and counted using a gas flow proportional counter. At large dis-

tances from the rod, the small strips were counted every quarter inch. In the proximity of the rod, each individual strip was counted. At each position where a count was taken, the time when the counting period began was recorded.

Counting Facilities

The facility used to count the irradiated gold wire was one that had been previously constructed by the International Institute specifically designed to count irradiated wires. The apparatus consisted of an Argonne scaler, a Nuclear Chicago Model 3031B Geiger-Mueller counting chamber, and a wire guide.

The wire guide and counting chamber were so constructed that only a small section of the wire could be "seen" by the end window G-M tube. The portion of the wire guide below the G-M tube was constructed of lead to prevent radiation from the wire from being scattered into the counting region of the tube; see Figure 24.

The equipment had been checked by a member of the Laboratory staff, and it was found to operate best at a voltage of 1400 volts with a discriminator setting of 175. When a Chi-square test was run using a standard beta ray source, the equipment was found to be operating with a high confidence probability, 80%.

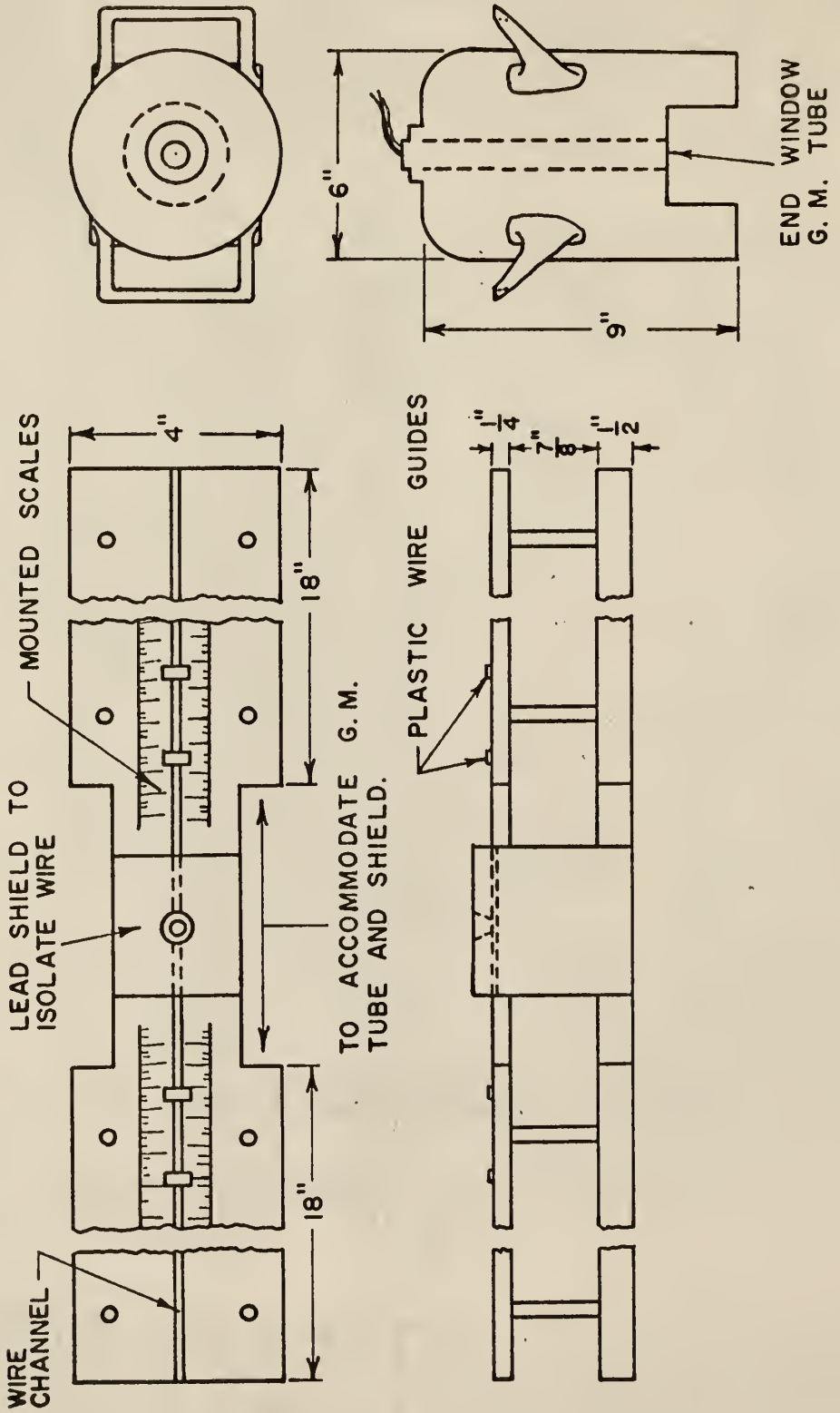

FIG. 24 WIRE COUNTING EQUIPMENT.

To count the gold foil, a gas flow proportional counter and a scaler were used. The scaler was the Argonne type, and the counting chamber was a lead shielded "pig" type into which a continuous flow of P-10 gas, a mixture of 10% methane and 90% argon, was passed to maintain the background radiation level as low as possible.

A member of the Laboratory staff had checked this apparatus and found that it operated best at a voltage of 3150 volts with a discriminator setting of 50. When a Chi-square test was run using a standard beta ray source, this equipment was found to be operating with a high confidence probability, 80%.

Treatment of Raw Data

The data for each gold wire and gold foil were corrected for the background counts, the decay of the sample that occurred previous to being counted, and the dead time of the counting equipment. These corrected data are listed in Tables 2 through 7 in the form of counts per minute. The deviation reported is the standard deviation of a single observation. Each sample was counted for a sufficient length of time to reduce the standard error to approximately 1%. An IBM 1620 computer program was used to make the corrections, and the program is described in Appendix E.

The data points near the outer boundary of the graphite stringer were rejected for the determination of the effective rod radius because they were not consistent with the remainder of the data.

Description of Tables

The tables of the original data, Tables 2 through 7, are identified by the following notation:

Case 1. One inch rod with gold wire near source.

Case 2. One inch rod with gold wire away from source.

Case 3. One inch rod with gold foil near source.

Case 4. One inch rod with gold foil away from source.

Case 5. Two inch rod with gold wire near source.

Case 6. Two inch rod with gold wire away from source.

The phrases "near source" and "away from source" refer to the location of the gold foil or wire with respect to the reactor core during the period of irradiation. Thus, near source means that the foil (or wire) was placed in the special graphite stringer in the position nearest the core. Away from source means that the foil (or wire) was placed in the special graphite stringer in the position farthest from the core.

The data in these tables have been corrected for the background counts, the decay of the sample that occurred

previous to being counted, and the dead time of the counting equipment. The deviation that is reported is the standard deviation of a single observation.

TABLE 2.
ORIGINAL DATA FOR CASE 1

DISTANCE FROM CENTER OF ONE INCH ROD (INCHES)	COUNTS PER MINUTE	STANDARD DEVIATION
.00000	10115	102
.06250	10058	101
.12500	10001	101
.18750	10112	102
.25000	10438	103
.31250	10636	104
.37500	10950	106
.43750	11062	106
.50000	11593	109
.56250	11892	110
.62500	12100	111
.68750	12358	112
.75000	12423	112
.81250	12935	115
.87500	12982	115
.93750	13321	116
1.00000	13671	118
1.06250	13568	117
1.12500	13658	118
1.18750	13840	118
1.25000	13682	118
1.31250	13859	118
1.37500	13949	119
1.43750	13992	119
1.50000	13958	119
1.56250	14007	119
1.68750	14375	120
1.81250	14562	121
1.93750	14762	122
2.06250	14941	123
2.18750	14768	122
2.31250	14894	122
2.43750	15080	123
2.56250	15188	124
2.68750	14766	122
2.81250	14617	121
2.93750	14260	120
3.06250	14167	119
3.18750	14060	119
3.31250	14086	119
3.43750	13980	118

TABLE 3.
ORIGINAL DATA FOR CASE 2

DISTANCE FROM CENTER OF ONE INCH ROD (INCHES)	COUNTS PER MINUTE	STANDARD DEVIATION
.03125	8434	94
.09375	8387	94
.15625	8613	95
.21875	8783	96
.28125	8921	97
.34375	9346	99
.40625	9744	101
.46875	10325	104
.53125	10585	105
.59375	11045	107
.65625	11114	108
.71875	11754	110
.78125	11938	111
.84375	12039	112
.90625	12158	112
.96875	12164	112
1.03125	12326	113
1.15625	12740	115
1.28125	12775	115
1.40625	12807	115
1.53125	12916	115
1.65625	12982	115
1.78125	13033	116
1.84375	13406	117
1.90625	13234	116
1.96875	13004	115
2.03125	13189	116
2.15625	13188	116
2.28125	13508	117
2.40625	13545	117
2.53125	13863	119
2.65625	13660	118
2.78125	13257	116
2.90625	13230	116
3.03125	13174	116
3.15625	13179	116
3.28125	13161	115

TABLE 4.
ORIGINAL DATA FOR CASE 3

DISTANCE FROM CENTER OF ONE INCH ROD (INCHES)	COUNTS PER MINUTE	STANDARD DEVIATION
.02500	9677	46
.07500	9714	48
.12500	9739	49
.17500	10016	48
.22500	10092	47
.27500	10293	47
.32500	10996	59
.37500	11552	49
.42500	11947	56
.47500	12470	57
.52500	13268	63
.57500	13660	60
.72500	14317	64
.87500	14796	67
1.02500	15031	62
1.17500	15177	62
1.32500	15374	70
1.47500	15737	70
1.62500	15797	66
1.77500	16105	75
1.92500	16307	66
2.07500	16260	69
2.22500	16216	70
2.37500	16024	64
2.52500	16604	78
2.67500	16145	69
2.82500	16651	73
2.97500	16622	67
3.12500	16636	71
3.27500	16398	64
3.42500	16706	68
3.57500	16916	77
3.77500	16315	63
3.92500	16356	71

TABLE 5.
ORIGINAL DATA FOR CASE 4

DISTANCE FROM CENTER OF ONE INCH ROD (INCHES)	COUNTS PER MINUTE	STANDARD DEVIATION
.02500	5114	29
.07500	5019	20
.12500	4857	25
.17500	4852	20
.22500	5205	30
.27500	5024	22
.32500	5025	22
.37500	5157	23
.42500	5194	26
.47500	5287	26
.52500	5441	24
.62500	5766	29
.72500	5780	25
.82500	5975	26
.92500	6079	31
1.02500	5988	26
1.17500	6293	28
1.32500	6276	28
1.47500	6248	31
1.67500	6340	32
1.82500	6396	29
1.97500	6875	30
2.12500	6020	30
2.27500	6743	31
2.42500	6781	39
2.57500	6789	34
2.72500	6682	30
2.87500	6710	33
3.02500	6598	30
3.17500	6225	31
3.32500	6443	36
3.47500	6707	31
3.62500	6825	31
3.77500	6165	29
3.92500	6324	26

TABLE 6.
ORIGINAL DATA FOR CASE 5

DISTANCE FROM CENTER OF TWO INCH ROD (INCHES)	COUNTS PER MINUTE	STANDARD DEVIATION
.03125	4555	48
.09375	4805	50
.15625	4867	50
.21875	5079	51
.28125	5330	52
.34375	5442	53
.40625	5754	54
.46875	6022	56
.53125	6163	56
.59375	6427	57
.65625	6779	59
.71875	7273	71
.78125	7640	72
.84375	8035	74
.90625	8508	76
.96875	8589	77
1.03125	8962	78
1.09375	9019	79
1.15625	9026	79
1.21875	9225	80
1.28125	9354	80
1.34375	9223	80
1.40625	9512	81
1.46875	9621	81
1.53125	9745	82
1.59375	10079	102
1.65625	10580	105
1.71875	10556	105
1.78125	10938	106
1.84375	11198	108
1.90625	11360	109
1.96875	11631	110
2.09375	11719	110
2.21875	11569	110
2.34375	11299	108
2.46875	11202	108
2.59375	11271	108
2.71875	11392	109
2.84375	11782	111
2.96875	11820	111
3.09375	12374	113
3.21875	12529	114

TABLE 6. CONTINUED
ORIGINAL DATA FOR CASE 5

DISTANCE FROM CENTER OF TWO INCH ROD (INCHES)	COUNTS PER MINUTE	STANDARD DEVIATION
3.34375	12462	114
3.46875	12799	115
3.59375	13211	117
3.71875	13599	119
3.84375	13865	120
3.96875	13446	118
4.09375	13554	119
4.21875	13132	117
4.34375	12289	113
4.46875	12119	113
4.59375	12134	113
4.71875	11941	112
4.84375	12627	115
4.96875	12103	113
5.09375	11778	111
5.21875	11621	110
5.34375	12122	113
5.46875	11979	112
5.59375	13159	118
5.71875	12965	117
5.84375	12845	116
5.96875	12249	113
6.09375	11762	111
6.21875	11543	110

TABLE 7.
ORIGINAL DATA FOR CASE 6

DISTANCE FROM CENTER OF TWO INCH ROD (INCHES)	COUNTS PER MINUTE	STANDARD DEVIATION
.00000	3232	43
.06250	3301	43
.12500	3303	43
.18750	3465	44
.25000	3613	45
.31250	3729	46
.37500	3957	47
.43750	4134	48
.50000	4427	49
.56250	4638	50
.62500	4792	51
.68750	5074	53
.75000	5219	62
.81250	5620	64
.87500	5963	65
.93750	6424	74
1.00000	6806	76
1.06250	7147	78
1.12500	7141	78
1.18750	7582	80
1.25000	7644	81
1.31250	7873	82
1.37500	8135	83
1.43750	8029	82
1.50000	8164	83
1.56250	8112	93
1.62500	8208	93
1.68750	8348	94
1.75000	8408	94
1.81250	8401	94
1.87500	8432	94
1.93750	8480	94
2.00000	8510	94
2.06250	8784	96
2.18750	9154	98
2.31250	9048	97
2.43750	9279	98
2.56250	9392	99
2.68750	9229	98
2.81250	9617	100
2.93750	9734	100
3.06250	9644	100

TABLE 7. CONTINUED
ORIGINAL DATA FOR CASE 6

DISTANCE FROM CENTER OF TWO INCH ROD (INCHES)	COUNTS PER MINUTE	STANDARD DEVIATION
3.18750	10159	103
3.31250	10230	103
3.43750	10158	102
3.56250	10593	105
3.68750	10667	105
3.81250	10848	106
3.93750	10693	105
4.06250	10443	104
4.18750	10195	102
4.31250	10518	104
4.43750	11081	107
4.56250	11202	107
4.68750	11697	109
4.81250	11512	108
4.93750	11884	110
5.06250	11852	110
5.18750	11562	109
5.31250	11152	107
5.43750	10988	106
5.56250	10576	104
5.81250	10664	104
6.06250	10477	103
6.18750	10443	103
6.31250	10254	102
6.43750	10185	102
6.56250	9948	100
6.68750	9791	100

APPENDIX E

IBM 1620 Program to Correct Raw Data

This computer program was written to correct the raw counted data for background counts, the counter dead time, and the decay of the sample previous to being counted. The program was written in FORTRAN I, and it utilized the automatic floating point subroutines EXP and SQRT. The logic diagram and the object program are given in this section.

Input for this program consisted of the experimental value of the counts, the length of time, in minutes, that elapsed to record the counts, the value of the exponent for the decay correction, and the number of the sample being corrected. A base value was also included to permit the counts to be based on any desired length of time. The data for each point was punched on a single card according to the specified format statement and read into the computer after the object program and the subroutines had been stored.

The output can be in either punched or typed form depending on the setting of sense switch two. One output card was punched for each input card that was read. The output consisted of the corrected count rate, the number of the sample that was corrected, and the standard deviation of the count rate.

The operating time for this program was approximately one second to correct one data point.

To correct the raw data counts recorded using the gold foil, a separate program was written. This program accounted for the variation in the weights of the individual foils.

The input for this program was identical to that of the program that processed the wire data except the weight of the foil, in milligrams, was included. The data for each point are punched on a single card according to the specified format statement and read into the computer after the object program and the subroutines had been stored.

The output for this program was identical to that of the wire data processing program. The operating time for this program was approximately one second per data point.

Table 8. Input Data For the IBM 1620 Raw Wire Data Correction Program

Symbol	Explanation
BASE	Length of time on which the count rate is based in minutes
CR	Total number of counts recorded for the sample
M	Length of the counting period in minutes
E	Exponent for the decay correction, λt
N	Sample Number

Table 9. Input Data For the IBM 1620 Raw Foil Data Correction Program

Symbol	Explanation
CR	Total number of counts recorded for the sample
M	Length of the counting period in minutes
E	Exponent for decay correction, λt
N	Sample number
WT	Sample weight in milligrams

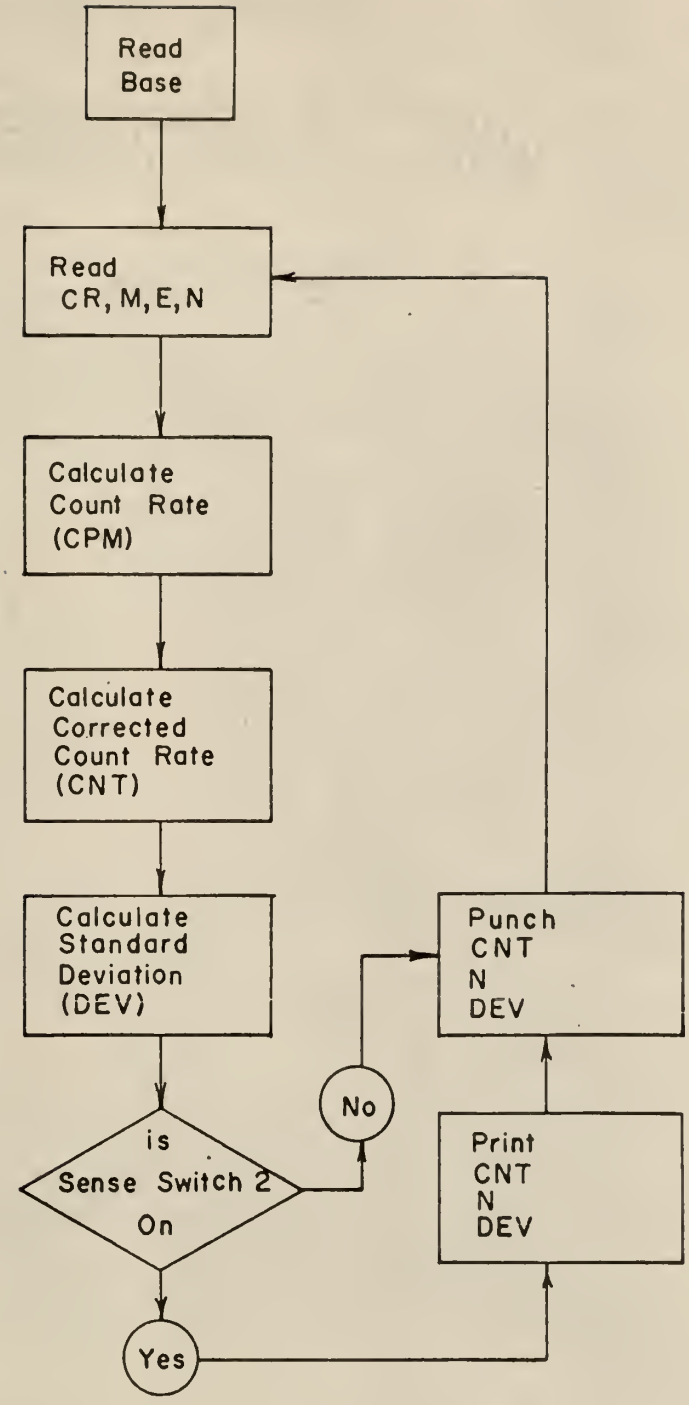

Logic Diagram for IBM 1620 Program for Processing Wire Data

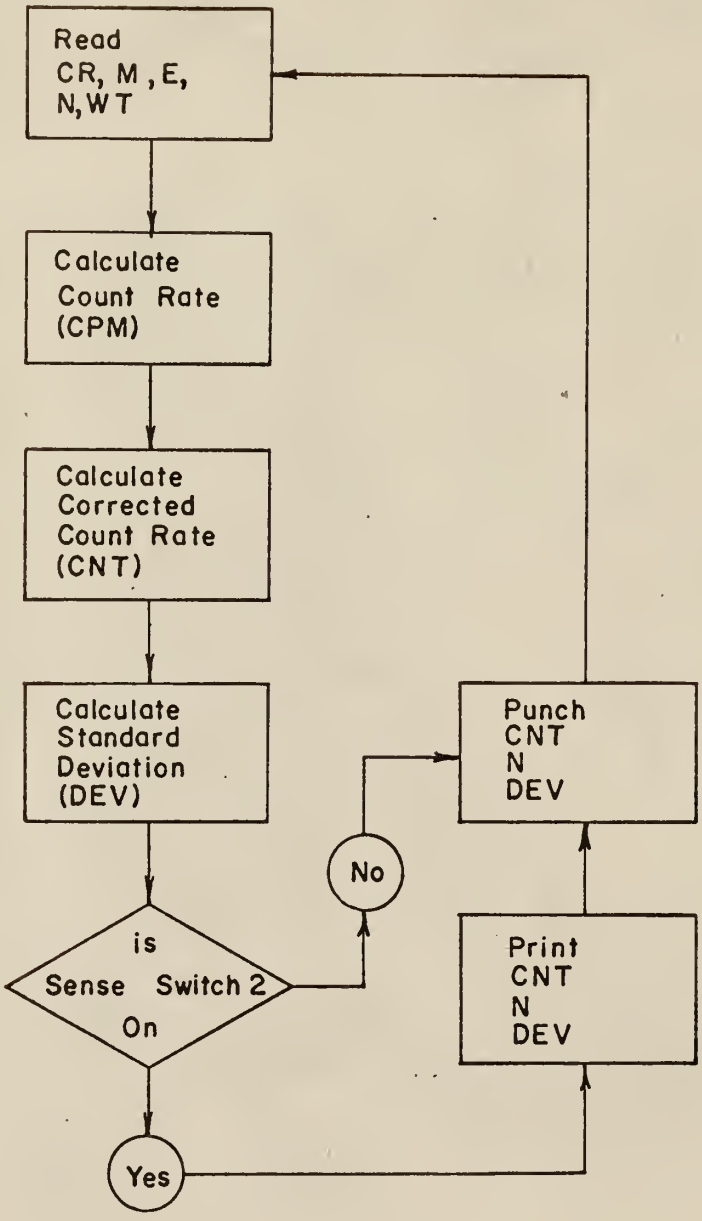

Logic Diagram for IBM 1620 Program for Processing Foil Data

```
C     PROGRAM FOR PROCESSING THE WIRE DATA
    1 FORMAT (E10.4,I5,E10.4,I5)
    2 FORMAT (E14.7,I6,E14.7)
      B=28.3833333
      READ1, BASE
   20 READ1,CR,M,E,N
      TIME=M
      CPM=CR/TIME
      CCRPM=CPM/(1.-CPM*4.E-6)
      CON=BASE*EXP(E)
      CNT=(CCRPM-B)*CON
      DEV=SQRT((CCRPM+B)*TIME)*CON/TIME
      IF(SENSE SWITCH 2)21,22
   21 PRINT2,CNT,N,DEV
   22 PUNCH2,CNT,N,DEV
      GO TO 20
      END
```

```
C     PROGRAM FOR PROCESSING RIBBON DATA
    1 FORMAT (E10.4,I5,E10.4,I5,E10.4)
    2 FORMAT (E14.7,I6,E14.7)
      SIGWS=6.25E-4
      B=15.0
   20 READ1,CR,M,E,N,WT
      TIME=M
      CPM=CR/TIME
      ENT=CPM/(1.-CPM*6.745E-8)
      EN=(ENT-B)*TIME
      CNT=2.*EN*EXP(E)/(WT*TIME)
      SIGNS=(ENT+B)*TIME
      DEV=CNT*SQRT(SIGNS/(EN**2)+SIGWS/(WT**2))
      IF(SENSE SWITCH 2)21,22
   21 PRINT2,CNT,N,DEV
   22 PUNCH2,CNT,N,DEV
      GO TO 20
      END
```

APPENDIX F

Description and Explanation of the IBM 1620 Computer Program to Determine the Effective Rod Radius From a Set of Experimental Data

To determine the effective rod radius from the experimental data, it is necessary to select a method to calculate the coefficients in the flux equations

$$\phi_i^R(r) = \sum_{i,j} A_j I_o(\beta_j r_i) \qquad \text{(F-1)}$$

and

$$\phi_i^M(r) = \sum_{i,j} [B_j J_o(\alpha_j r_i) + Y_o(\alpha_j r_i) C_j] \qquad \text{(F-2)}$$

where j is summed over the number of harmonics included in the analysis of the data, and i is the position at which the flux was measured. To calculate these coefficients, the method of weighted least squares is used.

A weighting factor in a least squares problem may be utilized in two ways: one, by requiring that the sum of the weighted residuals squared be a minimum; or two, by requiring that the residual between the calculated value at any point should lie within the statistical standard deviation of the experimental measurement. A weighting factor of unity satisfies the first method best. Scarborough (14) points out that the residuals squared are best weighted with the reciprocal of the standard deviation, $1/\sigma^{-2}$, if the second method is to

be satisfied.

Recall from the theory section that the constants α_j and β_j are related by the equations

$$\beta_j^2 = \mathcal{H}_1^2 - \mathcal{H}_2^2 - \alpha_j^2 \tag{F-3}$$

$$\frac{I_o(\beta_j R1)}{D_1 \beta_j I_1(\beta_j R1)} = -\frac{J_o(\alpha_j R1) - T Y_o(\alpha_j R1)}{D_2 \alpha_j (J_1(\alpha_j R1) - T Y_1(\alpha_j R1))} \tag{F-4}$$

where $T = J_o(\alpha_j R1)/Y_o(\alpha_j R1)$ and $\mathcal{H}_1^2$ and $\mathcal{H}_2^2$ are constants of the rod and the moderator.

Thus, it is evident that for a given value of R1 and R2, the simultaneous solution of Eqs. (F-3) and (F-4) will yield a proper value for α_j and β_j . In order to begin the calculation with a reasonable value for α_j and β_j , an initial value for α_j is estimated by using the boundary condition that the flux goes to zero at the outer boundary, R2.

Once the value of α_j and β_j for a given R1 is determined, the unknown coefficients in the flux equations are calculated by the method of least squares. The equation that must be solved is

$$E = \sum_i W_i (\phi_i - \sum_j M_{ji})^2 \tag{F-5}$$

where

$$M_{ji} = A_j I_o(\beta_j r_i) \qquad 0 \leqslant r \leqslant R1 \tag{F-6}$$

$$M_{ji} = B_j J_o(\alpha_j r_i) + C_j Y_o(\alpha_j r_i) \qquad R1 < r \leqslant R2 . \tag{F-7}$$

In order that this method might fully be utilized, it is necessary to express all the unknown coefficients in terms of one of their number. The coefficient B_j is selected as the main unknown. Using the boundary condition that

$$\phi_i^M(R2) = 0 \tag{F-8}$$

$$\phi_i^M(R1) = \phi_i^R(R1) \tag{F-9}$$

the expressions for C_j and A_j are obtained:

$$C_j = -B_j J_o(\alpha_j R2)/Y_o(\alpha_j R2) \tag{F-10}$$

$$A_j = B_j[J_o(\alpha_j R1) - T_j Y_o(\alpha_j R1)]/I_o(\beta_j R1) \tag{F-11}$$

where $T_j = J_o(\alpha_j R2)/Y_o(\alpha_j R2)$.

Operating on Eq. (F-5) in the usual manner, the equation for the determination of the unknown coefficients is obtained:

$$\sum_j B_j \sum_i W_i M_{ji} M_{ki} = \sum_i W_i \phi_i M_{ki} \tag{F-12}$$

where

$$M_{ki} = \left\{[J_o(\alpha_k R1) - T_k Y_o(\alpha_k R1)]/I_o(\beta_k R1)\right\} I_o(\beta_k r_i) \qquad 0 \leq r \leq R1 \tag{F-13}$$

$$M_{ki} = J_o(\alpha_k r_i) - T_k Y_o(\alpha_k r_i) \qquad R1 < r \leq R2 \tag{F-14}$$

and as before

$$T_k = J_o(\alpha_k R2)/Y_o(\alpha_k R2). \tag{F-15}$$

After the coefficients A_j, B_j, and C_j are obtained, the least squared error is calculated using Eq. (F-5). This value is stored, R1 is incremented, and the procedure is repeated, starting with the determination of α_j and β_j.

The value of R1 is incremented twice from the original value, and the least squared error at each of these values of R1 is subtracted in the manner of forward differences. These differences, along with the average value of the radii used to obtain the errors are then used to determine a straight line that intersects the axis of the graph, Δ Error vs. R1, at the position of an estimate of the minimum on the error curve. (See Figure 25)

Using this value of R1 as the best estimate of the minimum of the error curve, the least squared error for this position is calculated and stored. R1 is incremented, once in the direction of increasing R1 and once in the direction of decreasing R1, and the least squared error at each of these positions is calculated, stored, and used to determine a Δ Error and a new R1 as before.

After the error is calculated with this second estimate of the minimum of the error curve, it is compared to the error calculated with the first estimate of the minimum. If these errors are close together and the absolute value of their difference is less than or equal to a given criterion, the

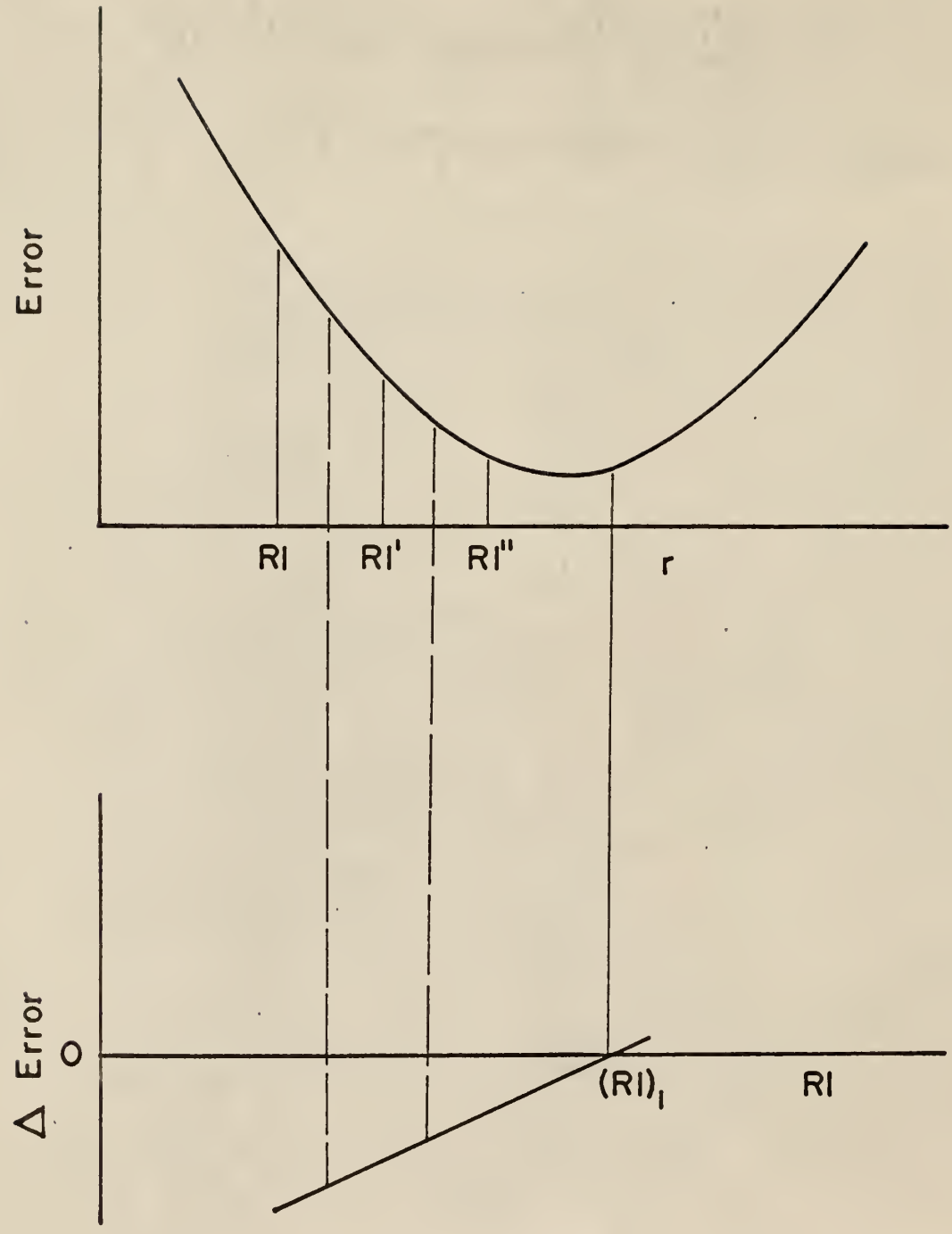

Fig. 25 Graphical Representation of How Iteration Procedure Progresses.

calculation is complete. Then the values of the unknown coefficients, α_j and β_j, the value of the effective rod radius, and the flux plot that results in the minimum least squared error is punched.

If the error criterion is not satisfied, the two radii that estimate the minimum error are compared. If they are close together and the absolute value of their difference is less than or equal to a preset value, the calculation is complete, and the required information is punched. If the radii accuracy criterion is not satisfied, the errors associated with these radii are compared to determine which is the smaller. The smallest error and the associated radius is stored, and the iteration to determine the minimum error proceeds.

The amount of output obtained during the iterations, and the type of analysis to be employed during the calculations can be controlled by the proper setting of the four sense switches. If sense switch 1 is ON while the input data is being read into the computer, the initial values of the count rate, the position, with respect to the center of the rod, at which the count was recorded, and the weighting factors are punched. If switch 1 is OFF, all of this output is omitted. When switch 1 is ON while the iterations are in progress,

the intermediate values of α_j and β_j from the solution of Eq. (F-4) are punched. This output is omitted if switch 1 is turned OFF during the iterations.

When sense switch 2 is turned ON during the iterations, the value of the least squared error and the radius at which it was calculated is punched. If switch 2 is OFF, this output is eliminated. Turning switch 2 ON as the input data is being read causes the transcendental equation for χ in the rod to be solved. If the switch is OFF as the data is read, the diffusion theory value for χ is calculated and used for the determination of the effective rod radius.

Turning sense switch 3 ON will cause an exit from the program during the iterative calculation for α_j and β_j or following the punching of the least squared error and R1. Sense switch 2 must be turned ON to exit following the punching of the error and R1. When this exit occurs, all of the output that results when the calculation ends in a normal fashion is punched. Care must be exercised when this exit is chosen. A minimum of eight iterations must have occurred before this type of exit is attempted. If sense switch 3 is OFF, the exit is omitted, and the end of calculation type output is eliminated.

The internal subroutine CRAM also operates on sense switch 3. If switch 3 is ON and the calculation of the unknown flux coefficients is in process, the value of the matrix elements (Eq. (F-12)) is typed before the matrix is solved. When switch 3 is OFF, this output is omitted.

Because of the nature of the operations connected with the use of sense switch 3, it must be used with caution.

If the program is compiled with the trace instructions included, sense switch 4 controls typed output. The compilation of the trace instructions and the use of sense switch 4 are primarily for the "debugging" of new programs. When switch 4 is ON, the values to the left of all equal signs are typed out. This type of output greatly slows the operation of the computer. So, unless a program is troublesome, sense switch 4 is normally left turned OFF.

Table 10. Input Data for the IBM 1620 Effective Rod Radius Program

Symbol	Explanation
SIGR	Total macroscopic cross section of the rod, cm^{-1}
SIGSR	Macroscopic scattering cross section of the rod, cm^{-1}
SIGAR	Macroscopic absorption cross section of the rod, cm^{-1}
SIGAG	Macroscopic absorption cross section of the moderator, cm^{-1}
SIGSG	Macroscopic scattering cross section of the moderator, cm^{-1}
AMUZ	Average cosine of the scattering angle in the rod
AMU1	Average cosine of the scattering angle in the moderator
R1	Radius of the rod, inches
R2	Outer boundary radius of the moderator, inches
N2	Number of data points
J1	Number of harmonics used in the analysis
IVD	Divisor to convert K1 to a distance from center of rod, inches
K1	Location of sample from center of rod
PHI	Corrected count rate of sample, cpm
M	Sample number
WT	Standard deviation of the corrected count rate, cpm

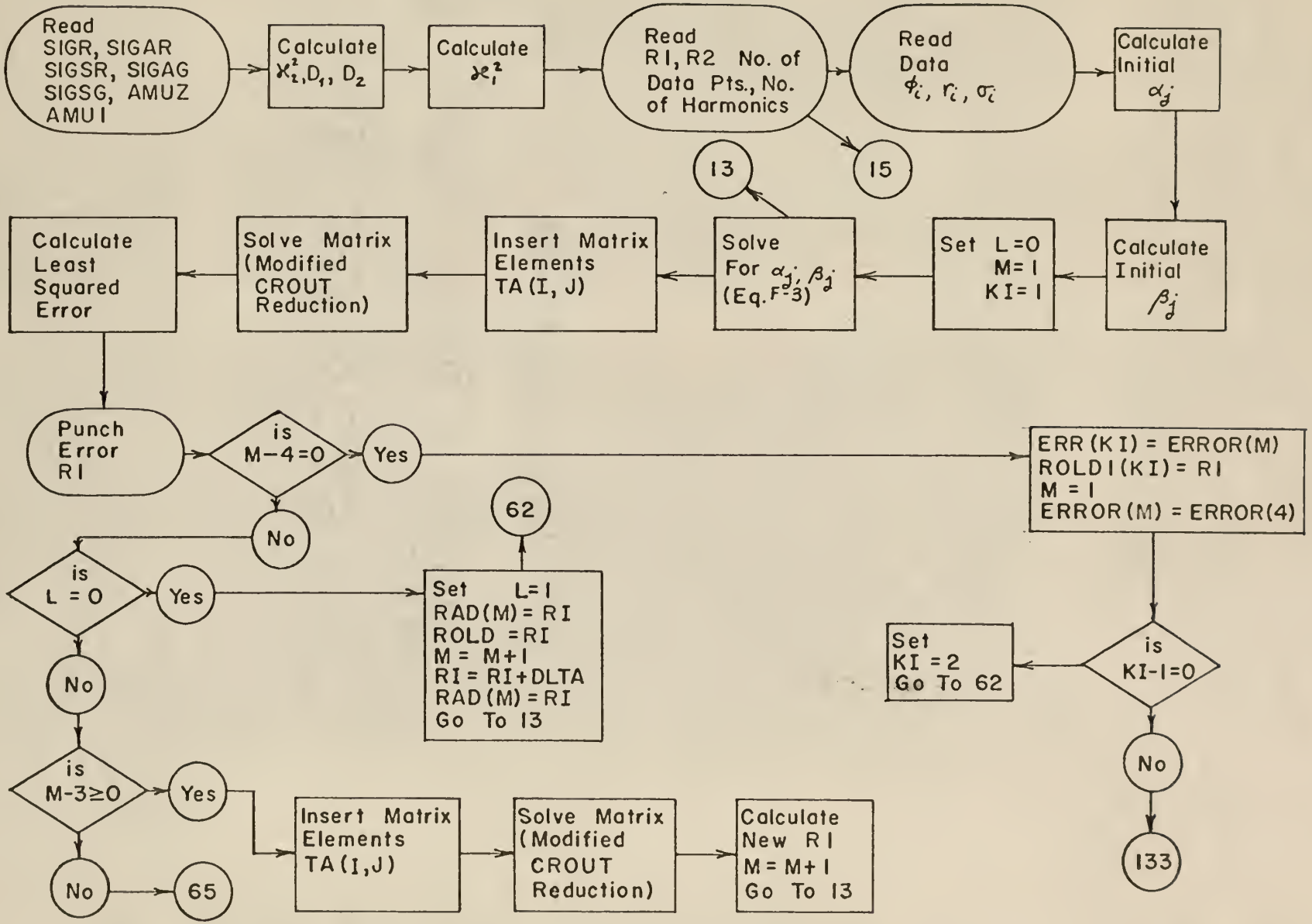

Logic Diagram for IBM 1620 Program to Determine Effective Rod Radius

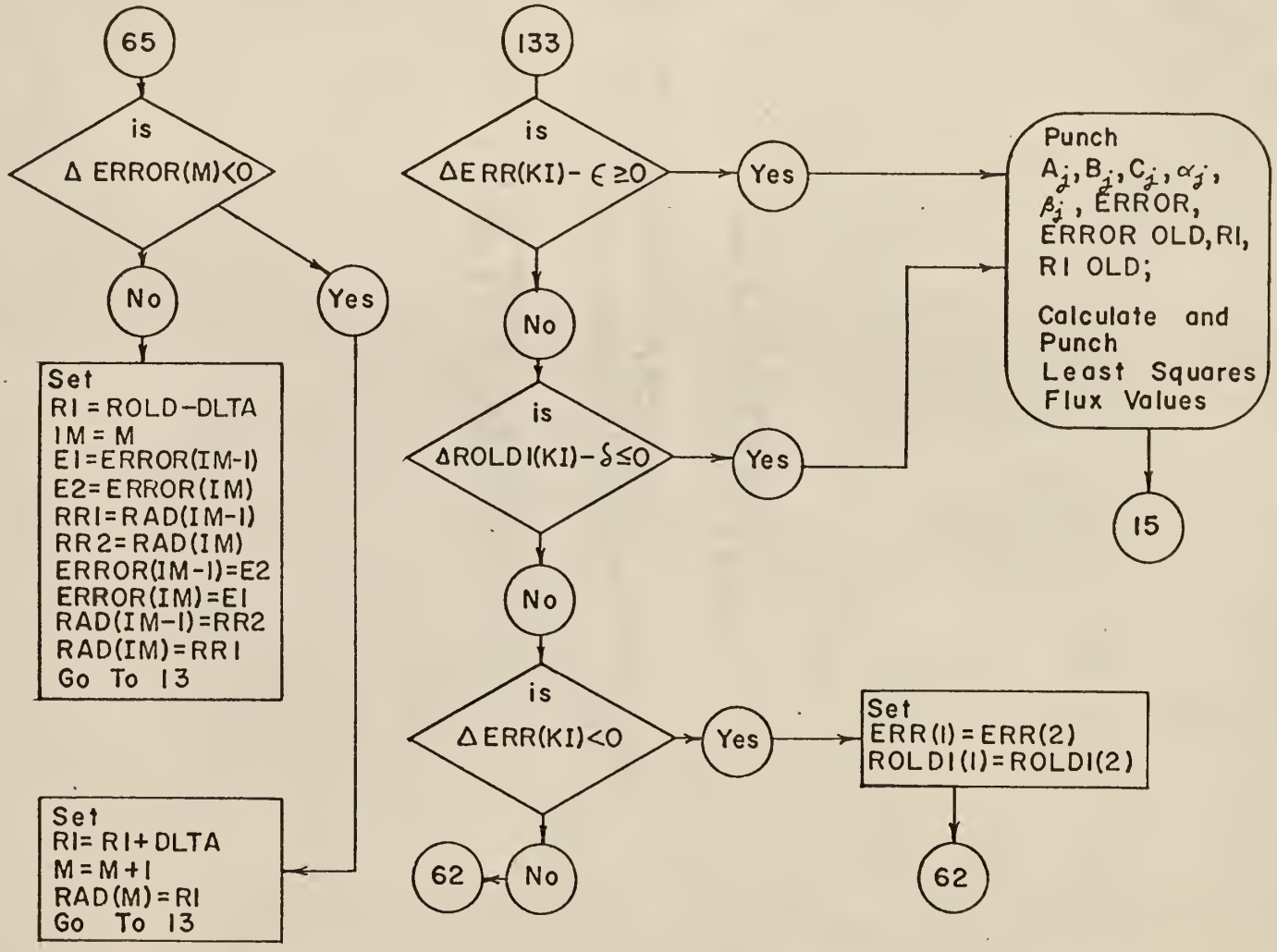

Logic Diagram for IBM 1620 Program to Determine Effective Rod Radius

```
C       EFFECTIVE ROD RADIUS PROGRAM      WW PORATH        5/1/63
        DIMENSION TA(5,6),B(5),PHI(70),RA(70),WW(70)
        DIMENSION AIZ(5,30),AJZ(5,70),AYZ(5,70),P(5,70)
        DIMENSION W(5),XX(5),YY(5),C(5),A(5),ROLD1(5)
        DIMENSION AA(5),BG(5),ALPHA(5),T(5),A1A(5)
        DIMENSION RAD(5),ERROR(5),ERR(5),DERR(5),CONST(5)
        G=0.
        N=1
        I1=G
        READ5,SIGR,SIGSR,SIGAR,SIGAG,SIGSG
        READ5, AMUZ, AMU1
        READ5,CRIT,DELTA,VAR
C       INPUT ABOVE IS 3 CARDS
        DZER=1./(3.*(SIGAR+SIGSR*(1.-AMUZ)))
        DONE=1./(3.*(SIGAG+SIGSG*(1.-AMU1)))
        AKP1=(SIGAG/DONE)*(2.54)**2
        AKP09=(SIGAR/DZER)*(2.54)**2
        AAKPO=SQRT(SIGAR/DZER)
        AKPO1=AAKPO+1.E-4
C       THIS SENSE SWITCH SELECTS THE TYPE OF
C       ANALYSIS FOR KAPPA OF ROD
        IF(SENSESWITCH2)29,2
    2   DZER=1./(3.*SIGSR)
        DONE=1./(3.*SIGSG)
        AKPO=(SIGAR/DZER)*(2.54)**2
        AKP1=(SIGAG/DONE)*(2.54)**2
        GO TO 15
C       TRANSCENTENTAL SOLUTION FOR KAPPA IN ROD TO STATEMENT 15
   29   TEST2=AAKPO-AKPO1
        IF(TEST2)28,33,26
   28   TEST2=-TEST2
   26   IF(TEST2/AAKPO-CRIT)33,33,27
   27   SOME=EXP(AAKPO/SIGSR)
        SOME=AAKPO/SIGR-(SOME-(1.0/SOME))/(SOME+(1.0/SOME))
        IF(SOME)36,33,36
   36   IF(I1)30,30,31
   30   I1=N
        AKPO1=AAKPO
        AAKPO=AAKPO+DELTA
        SOME1=SOME
        GO TO 29
   31   IF(AAKPO-AKPO1)32,33,32
   33   AKPO=(AAKPO*2.54)**2
        GO TO 15
   32   SLOP=(SOME-SOME1)/(AAKPO-AKPO1)
        IF(SLOP)37,38,37
   38   PUNCH95
        GO TO 30
   37   AKPO1=AAKPO
        SOME1=SOME
        AAKPO=AAKPO-SOME/SLOP
        GO TO 29
```

```
   15 READ5, R1, R2, ACC, DL, DLTA,VAL
      READ6,N2,J1,IVD
C     INPUT ABOVE IS 2 CARDS
      DIV=IVD
      DO 35 I=1,N2
      READ6,K1
      AB=K1
      RA(I)=AB/DIV
      IF(RA(I)-R1)34,34,35
   34 NROD=I
      L1=I+1
   35 CONTINUE
C     INPUT ABOVE IS N2 CARDS
      DO 41 I=1,N2
      READ 99, PHI(I),M,WT
   41 WW(I)=1./(WT*WT)
C     INPUT ABOVE IS N2 CARDS
      DZER=DZER/2.54
      DONE=DONE/2.54
C     THE FOLLOWING 7 CARDS PUNCH INPUT DATA
      PUNCH1,ACC,AKPO,AKP1,DIV
      PUNCH1,DZER,DONE,DL,AKPO9
      PUNCH1,R1,R2,DLTA,VAL
      PUNCH1,CRIT,DELTA,VAR,SIGR
      PUNCH1,SIGSR,SIGAR,SIGAG,SIGSG
      PUNCH1,AMUZ,AMU1
      PUNCH6,N2,J1
C     THIS SENSE SWITCH IS FOR THE PUNCHING OF R,PHI,WT
      IF(SENSE SWITCH 1)504,506
  504 PUNCH994
      DO 980 I=1,NROD
  980 PUNCH1,RA(I),PHI(I),WW(I)
      PUNCH993
      DO 981 I=L1,N2
  981 PUNCH1,RA(I),PHI(I),WW(I)
  506 ALPHA(1)=2.4048256
      ALPHA(2)=5.5200781
      ALPHA(3)=8.6537279
      ALPHA(4)=11.7915344
      ALPHA(5)=14.9309177
      L=G
      M=N
      KI=N
C     THIS LOOP CALCULATES THE INITIAL VALUES
C     OF ALPHA AND BETA
      DO 17 I=1,J1
      AA(I)=ALPHA(I)/R2
      A1A(I)=AA(I)+1.E-4
      ARG1=AKPO-AKP1-AA(I)**2
   17 BG(I)=SQRT(ARG1)
      III=G
```

```
C       THIS LOOP SOLVES THE TRANSCENDENTAL EQUATION
C       FOR ALPHA AND BETA
   13 DO 16 I=1,J1
      KKK=G
C       THIS SENSE SWITCH IS TO EXIT FROM THE PROGRAM BEFORE
C       THE CALCULATION IS COMPLETE
   10 IF(SENSESWITCH3)71,11
   11 W(I)=BG(I)*R1
      XX(I)=AA(I)*R1
      YY(I)=AA(I)*R2
      T(I)=JZER(YY(I))/YZER(YY(I))
      CONST(I)=(JZER(XX(I))-T(I)*YZER(XX(I)))/IZER(W(I))
      ANUM=DONE*AA(I)*(JONE(XX(I))-T(I)*YONE(XX(I)))
      ADEN=DZER*IONE(W(I))*CONST(I)
      SUM=BG(I)+ANUM/ADEN
      TEST1=(A1A(I)-AA(I))/AA(I)
      IF(TEST1)12,316,14
   12 TEST1=-TEST1
   14 IF(TEST1-ACC)316,316,298
  298 IF(SUM)299,316,299
  299 IF(III)300,300,304
  300 III=N
      A1A(I)=AA(I)
      AA(I)=AA(I)+DL
  254 SUM11=SUM
      ARG1=AKPO-AKP1-AA(I)**2
      BG(I)=SQRT(ARG1)
      GO TO 10
  304 IF(AA(I)-A1A(I))250,316,250
  250 SLOPE=(SUM-SUM11)/(AA(I)-A1A(I))
      IF(SLOPE)261,260,261
  260 PUNCH96
      GO TO 316
C       THIS SENSE SWITCH IS FOR PUNCHING INTERMEDIATE
C       VALUES OF ALPHA AND BETA
  261 IF(SENSESWITCH1)253,252
  253 IF(KKK)232,232,223
  232 KKK=N
      PUNCH117
  223 PUNCH1,SUM,SLOPE,BG(I),AA(I)
  252 A1A(I)=AA(I)
      AA(I)=AA(I)-SUM/SLOPE
      GO TO 254
  316 IF(I-1)255,255,16
  255 PUNCH 117
   16 PUNCH1,SUM,SLOPE,BG(I),AA(I)
C       THIS LOOP CHECKS ON THE POINTS IN THE ROD AND MODERATOR
      DO 21 I=1,N2
      IF(RA(I)-R1)22,22,21
   22 NROD=I
      L1=I+1
   21 CONTINUE
```

```
      J2=J1+1
C     THIS LOOP ZEROS THE MATRIX TA(I,J)
      DO 190 J=1,5
      DO 190 I=1,6
  190 TA(J,I)=G
      IF(J1-5)189,201,15
C     THIS LOOP PUTS ONES IN TA(I,I) AND TA(I,6)
  189 DO 200 I=J2,5
      TA(I,6)=N
  200 TA(I,I)=N
C     THIS LOOP CALCULATES THE MATRIX ELEMENTS TA(I,J)
  201 DO 194 K=1,J1
      DO 194 J=1,K
      DO 194 I=1,N2
      IF(I-NROD)191,191,192
  191 IF(J-1)208,207,208
  207 AIZ(K,I)=IZER(BG(K)*RA(I))
      TERM1=WW(I)*CONST(K)*AIZ(K,I)*PHI(I)
  208 TERM2=WW(I)*CONST(K)*AIZ(K,I)*CONST(J)*AIZ(J,I)
      GO TO 193
  192 IF(J-1)209,206,209
  206 AJZ(K,I)=JZER(AA(K)*RA(I))
      AYZ(K,I)=YZER(AA(K)*RA(I))
      P(K,I)=AJZ(K,I)-T(K)*AYZ(K,I)
      TERM1=WW(I)*P(K,I)*PHI(I)
  209 TERM2=WW(I)*P(K,I)*P(J,I)
  193 IF(J-1)216,215,216
  215 TA(K,6)=TA(K,6)+TERM1
  216 TA(K,J)=TA(K,J)+TERM2
  194 TA(J,K)=TA(K,J)
C     THIS SENSE SWITCH PUNCHES THE VALUES OF
C     THE MATRIX ELEMENTS TA(I,J)
      IF(SENSESWITCH4)241,240
  240 DO 242 I=1,J1
  242 PUNCH 1,TA(I,1),TA(I,2),TA(I,3),TA(I,6)
  241 IF(J1-1)211,211,212
  211 B(1)=TA(1,6)/TA(1,1)
      GO TO 213
C     THIS STATEMENT SOLVES THE MATRIX USING THE CRAM SUBROUTINE
  212 B(1)=CRAM(5.)
  213 DO 74 I=1,J1
      C(I)=-B(I)*T(I)
      A(I)=B(I)*CONST(I)
      IF(SENSESWITCH4)74,205
  205 PUNCH1,A(I),B(I),C(I)
   74 CONTINUE
C     THIS LOOP CALCULATES THE LEAST SQUARED ERROR
      ERROR(M)=G
      DO 196 I=1,N2
      SUMM=G
      DO 195 J=1,J1
```

```
      IF(I-NROD)197,197,198
  197 S=A(J)*AIZ(J,I)
      GO TO 195
  198 S=B(J)*AJZ(J,I)+C(J)*AYZ(J,I)
  195 SUMM=SUMM+S
  196 ERROR(M)=ERROR(M)+WW(I)*(PHI(I)-SUMM)**2
C     THIS SENSE SWITCH IS FOR THE PUNCHING OF THE ERROR AND R1
      IF(SENSESWITCH2)120,119
  120 PUNCH100,ERROR(M),R1
      PUNCH6,M
C     THIS SENSE SWITCH IS TO EXIT FROM THE PROGRAM BEFORE
C     THE CALCULATION IS COMPLETE
      IF(SENSESWITCH3)71,119
  119 IF(M-4)122,131,122
C     THIS SECTION DOWN TO STATEMENT 122 COMPARES THE ESTIMATES
C     OF THE MINIMUM ON THE ERROR CURVE
  131 ERR(KI)=ERROR(M)
      ROLD1(KI)=R1
      M=N
      ERROR(1)=ERROR(4)
      DLTA=DLTA*VAR
      IF(KI-1)133,132,133
  132 KI=KI+N
      GO TO 62
  133 TEST1=ERR(KI)-ERR(KI-1)
      IF(TEST1)134,135,135
  135 TEST=TEST1
      GO TO 141
  134 TEST=-TEST1
  141 IF(TEST/ERR(KI)-CRIT)71,71,136
  136 TEST=(ROLD1(KI)-ROLD1(KI-1))/ROLD1(KI)
      IF(TEST)137,138,138
  137 TEST=-TEST
  138 IF(TEST-VAL)71,71,139
  139 IF(TEST1)140,133,62
  140 ERR(KI-1)=ERR(KI)
      ROLD1(KI-1)=ROLD1(KI)
      GO TO 62
C     THIS SECTION INCREMENTS R1
  122 IF(L)64,62,64
   62 L=N
      RAD(M)=R1
      ROLD=R1
   63 R1=R1+DLTA
      M=M+N
      RAD(M)=R1
      GO TO 79
   64 IF(M-3)65,602,602
   65 IF(ERROR(M)-ERROR(M-1))63,67,67
   67 R1=ROLD-DLTA
      IM=M
      E1=ERROR(IM-1)
```

```
      E2=ERROR(IM)
      ERROR(IM)=E1
      ERROR(IM-1)=E2
      RR1=RAD(IM-1)
      RR2=RAD(IM)
      RAD(IM)=RR1
      RAD(IM-1)=RR2
      M=M+N
      RAD(M)=R1
C     THIS LOOP ADJUSTS THE VALUE OF ALPHA SO IT WILL PASS
C     THE CHECK AT THE BEGINNING OF THE ALPHA, BETA ITERATION
   79 DO 81 I=1,J1
   81 A1A(I)=AA(I)+1.E-4
      GO TO 13
  602 IP=M-1
C     THIS LOOP CALCULATES THE DELTA ERROR
      DO 68 K=1,IP
   68 DERR(K)=ERROR(K+1)-ERROR(K)
C     THIS LOOP ZEROS THE MATRIX TA(I,J)
      DO 69 I=1,5
      DO 69 J=1,6
   69 TA(I,J)=G
C     THIS LOOP PUTS ONES IN TA(K,K) AND TA(K,6)
      DO 70 K=1,5
      TA(K,6)=N
   70 TA(K,K)=N
C     THIS LOOP INSERTS THE MARTIX ELEMENTS TA(K,6) AND PUTS
C     ONES IN TA(1,K)
      DO 73 K=1,IP
      TA(K,6)=DERR(K)
      TA(K,1)=N
C     THIS LOOP CALCULATES THE AVERAGE RADIUS USED TO
C     DETERMINE THE DELTA ERROR
      DO 73 J=2,IP
   73 TA(K,J)=((RAD(K)+RAD(K+1))/2.)**(J-1)
C     THIS STATEMENT SOLVES THE MATRIX USING THE CRAM SUBROUTINE
      B(1)=CRAM(5.)
C     THIS STATEMENT ESTIMATES THE MINIMUM OF THE ERROR CURVE
      R1=-B(1)/B(2)
      M=M+N
      GO TO 79
C     THE FOLLOWING STATEMENTS PUNCH THE FINAL OUTPUT
C     WHEN A CALCULATION HAS BEEN COMPLETED
   71 PUNCH7
      DO 80 I=1,J1
   80 PUNCH1,A(I),B(I),C(I),AA(I)
      PUNCH 8
      PUNCH1,ERR(KI-1),ERR(KI),R1,ROLD1(KI-1)
      PUNCH 101
      DO 76 I=1,J1
   76 PUNCH1,BG(I)
      PUNCH93
```

```
      DO 500 I=1,NROD
      FLUXR=G
      DO 501 J=1,J1
  501 FLUXR=A(J)*AIZ(J,I)+FLUXR
  500 PUNCH99,FLUXR,I,RA(I)
      DO 502 I=L1,N2
      FLUXG=G
      DO 503 J=1,J1
  503 FLUXG=FLUXG+B(J)*AJZ(J,I)+C(J)*AYZ(J,I)
  502 PUNCH99,FLUXG,I,RA(I)
C     THIS STATEMENT RETURNS TO THE BEGINNING OF THE
C     PROGRAM TO READ NEW DATA TO BEGIN ANOTHER CALCULATION
      GO TO 15
C     THE FOLLOWING ARE THE FORMAT STATEMENTS USED TO READ
C     IN THE DATA AND PUNCH THE RESULTS
    1 FORMAT(E16.7,E16.7,E16.7,E16.7)
    5 FORMAT(E10.4,E10.4,E10.4,E10.4,E10.4,E10.4)
    6 FORMAT(I5,I5,I5,I5,I5,I5,I5,I5)
    7 FORMAT(7X3H A ,13X3H B ,13X3H C ,12X6H ALPHA)
    8 FORMAT(6X6H EROLD10X6H ERROR12X3H R112X6H ROLD )
  994 FORMAT(6X6H RADR ,10X6H PHIR ,10X4H WW )
  993 FORMAT(6X6H RADG ,10X6H PHIG ,10X4H WW )
   93 FORMAT(5X5H FLUX8X2H I6X2H R)
   95 FORMAT(  9H SLOP = 0)
   96 FORMAT( 10H SLOPE = 0)
   99 FORMAT(E14.7,I6,E14.7,I6)
  100 FORMAT(E16.7,8H = ERROR,E16.7,5H = R1)
  101 FORMAT( 7X5H BETA)
  117 FORMAT(8X4H SUM10X6H SLOPE10X6H BETA 10X6H ALPHA)
      END
```

APPENDIX G

Typical Output Results from IBM 1620 Effective Rod Radius Program

RESULTS FOR CASE 1C

1.0000000E-06	4.4059408E-00	6.0638201E-03	3.2000000E+01
1.1267290E-01	3.6023495E-01	1.0000000E-03	5.1623768E-00
4.9519509E-01	3.0000000E+01	5.0000000E-03	1.0000000E-05
1.0000000E-07	1.0000000E-04	8.0000000E-01	1.1760000E-00
9.4700000E-01	2.2900000E-01	8.6000000E-04	3.8500000E-01
1.1900000E-02	5.6000000E-02		

41 2

RADR	PHIR	WW
.0000000E-99	1.0115353E+04	9.5816865E-05
6.2500000E-02	1.0058883E+04	9.6392017E-05
1.2500000E-01	1.0001403E+04	9.6983427E-05
1.8750000E-01	1.0112435E+04	9.5973876E-05
2.5000000E-01	1.0438648E+04	9.3049491E-05
3.1250000E-01	1.0636582E+04	9.1377633E-05
3.7500000E-01	1.0950201E+04	8.8827885E-05
4.3750000E-01	1.1062097E+04	8.7978286E-05

RADG	PHIG	WW
5.0000000E-01	1.1593180E+04	8.4021765E-05
5.6250000E-01	1.1892787E+04	8.1958594E-05
6.2500000E-01	1.2100364E+04	8.0602182E-05
6.8750000E-01	1.2358013E+04	7.8972735E-05
7.5000000E-01	1.2423867E+04	7.8593324E-05
8.1250000E-01	1.2935179E+04	7.5554831E-05
8.7500000E-01	1.2982734E+04	7.5314384E-05
9.3750000E-01	1.3321534E+04	7.3448316E-05
1.0000000E-00	1.3671158E+04	7.1617831E-05
1.0625000E-00	1.3568959E+04	7.2185164E-05
1.1250000E-00	1.3658983E+04	7.1745558E-05
1.1875000E-00	1.3840301E+04	7.0842090E-05
1.2500000E-00	1.3682003E+04	7.1690302E-05
1.3125000E-00	1.3859986E+04	7.0805879E-05
1.3750000E-00	1.3949377E+04	7.0384294E-05
1.4375000E-00	1.3992222E+04	7.0202071E-05
1.5000000E-00	1.3958888E+04	7.0396815E-05
1.5625000E-00	1.4007022E+04	7.0188412E-05
1.6875000E-00	1.4375044E+04	6.8436376E-05
1.8125000E-00	1.4562405E+04	6.7590054E-05
1.9375000E-00	1.4762974E+04	6.6708813E-05
2.0625000E-00	1.4941096E+04	6.5949209E-05
2.1875000E-00	1.4768612E+04	6.6740481E-05
2.3125000E-00	1.4894300E+04	6.6211313E-05
2.4375000E-00	1.5080786E+04	6.5428052E-05
2.5625000E-00	1.5188922E+04	6.4991958E-05
2.6875000E-00	1.4766400E+04	6.6867407E-05
2.8125000E-00	1.4617184E+04	6.7575087E-05
2.9375000E-00	1.4260547E+04	6.9279635E-05
3.0625000E-00	1.4167774E+04	6.9757850E-05
3.1875000E-00	1.4060683E+04	7.0316495E-05

RESULTS FOR CASE 1C

```
 3.3125000E-00    1.4086218E+04    7.0221602E-05
 3.4375000E-00    1.3980354E+04    7.0780810E-05
       SUM              SLOPE             BETA              ALPHA
 1.2000000E-06   -6.2413793E+02    2.0958535E-00    8.5293118E-02
 3.9000000E-06   -5.2775842E+02    2.0889921E-00    1.8970686E-01
 4.0164002E+02 = ERROR    4.9519509E-01 = R1
  1
       SUM              SLOPE             BETA              ALPHA
 6.0000000E-07   -6.1272727E+02    2.0958508E-00    8.5359468E-02
 4.4000000E-06   -5.2321984E+02    2.0889849E-00    1.8978640E-01
 4.0333814E+02 = ERROR    5.0019509E-01 = R1
  2
       SUM              SLOPE             BETA              ALPHA
-6.0000000E-07   -6.2379839E+02    2.0958562E-00    8.5226589E-02
-3.8000000E-06   -5.3262975E+02    2.0889994E-00    1.8962727E-01
 4.0285732E+02 = ERROR    4.9019509E-01 = R1
  3
       SUM              SLOPE             BETA              ALPHA
-5.0000000E-07   -6.1623931E+02    2.0958537E-00    8.5287640E-02
 2.7000000E-06   -5.2889298E+02    2.0889927E-00    1.8970030E-01
 4.0162392E+02 = ERROR    4.9478277E-01 = R1
  4
       SUM              SLOPE             BETA              ALPHA
 1.1000000E-06   -6.2307692E+02    2.0958516E-00    8.5340744E-02
 4.1000000E-06   -5.2519726E+02    2.0889870E-00    1.8976394E-01
 4.0266891E+02 = ERROR    4.9878277E-01 = R1
  2
       SUM              SLOPE             BETA              ALPHA
-1.0000000E-06   -6.2303714E+02    2.0958559E-00    8.5234420E-02
-3.7000000E-06   -5.3226600E+02    2.0889985E-00    1.8963663E-01
 4.0255438E+02 = ERROR    4.9078277E-01 = R1
  3
       SUM              SLOPE             BETA              ALPHA
 7.0000000E-07   -6.2113821E+02    2.0958538E-00    8.5286098E-02
-1.0000000E-07   -5.2945212E+02    2.0889929E-00    1.8969846E-01
 4.0162228E+02 = ERROR    4.9466681E-01 = R1
  4
       SUM              SLOPE             BETA              ALPHA
-1.3000000E-06   -6.1687242E+02    2.0958521E-00    8.5328595E-02
 3.8000000E-06   -5.2661591E+02    2.0889883E-00    1.8974937E-01
 4.0225432E+02 = ERROR    4.9786681E-01 = R1
  2
       SUM              SLOPE             BETA              ALPHA
 2.0000000E-07   -6.2220039E+02    2.0958555E-00    8.5243527E-02
-2.5000000E-06   -5.3131034E+02    2.0889975E-00    1.8964752E-01
 4.0225559E+02 = ERROR    4.9146681E-01 = R1
  3
```

RESULTS FOR CASE 1C

SUM	SLOPE	BETA	ALPHA
-7.0000000E-07	-6.1875000E+02	2.0958538E-00	8.5286120E-02
2.8000000E-06	-5.2985978E+02	2.0889929E-00	1.8969848E-01
4.0162284E+02 = ERROR	4.9466840E-01 = R1		

4

A	B	C	ALPHA
-5.1614880E+02	-9.9121058E+02	-1.5629428E+02	8.5286120E-02
1.0033036E+04	1.7789112E+04	3.0815911E+03	1.8969848E-01

ERROLD	ERROR	R1	ROLD
4.0162228E+02	4.0162284E+02	4.9466840E-01	4.9466681E-01

BETA
2.0958538E-00
2.0889929E-00

FLUX	I	R
9.5168880E+03	1	.0000000E-99
9.5574740E+03	2	6.2500000E-02
9.6797510E+03	3	1.2500000E-01
9.8852860E+03	4	1.8750000E-01
1.0176711E+04	5	2.5000000E-01
1.0557766E+04	6	3.1250000E-01
1.1033352E+04	7	3.7500000E-01
1.1609594E+04	8	4.3750000E-01
1.2250533E+04	9	5.0000000E-01
1.2462748E+04	10	5.6250000E-01
1.2650846E+04	11	6.2500000E-01
1.2819234E+04	12	6.8750000E-01
1.2971160E+04	13	7.5000000E-01
1.3109092E+04	14	8.1250000E-01
1.3234944E+04	15	8.7500000E-01
1.3350235E+04	16	9.3750000E-01
1.3456185E+04	17	1.0000000E-00
1.3553797E+04	18	1.0625000E-00
1.3643895E+04	19	1.1250000E-00
1.3727174E+04	20	1.1875000E-00
1.3804218E+04	21	1.2500000E-00
1.3875524E+04	22	1.3125000E-00
1.3941526E+04	23	1.3750000E-00
1.4002591E+04	24	1.4375000E-00
1.4059047E+04	25	1.5000000E-00
1.4111176E+04	26	1.5625000E-00
1.4203434E+04	27	1.6875000E-00
1.4281052E+04	28	1.8125000E-00
1.4345384E+04	29	1.9375000E-00
1.4397531E+04	30	2.0625000E-00
1.4438401E+04	31	2.1875000E-00
1.4468752E+04	32	2.3125000E-00

RESULTS FOR CASE 1C

FLUX	I	R
1.4489227E+04	33	2.4375000E-00
1.4500378E+04	34	2.5625000E-00
1.4502678E+04	35	2.6875000E-00
1.4496543E+04	36	2.8125000E-00
1.4482336E+04	37	2.9375000E-00
1.4460383E+04	38	3.0625000E-00
1.4430972E+04	39	3.1875000E-00
1.4394367E+04	40	3.3125000E-00
1.4350804E+04	41	3.4375000E-00

DETERMINATION OF SHADOWING EFFECTS USING THE P_1 TRANSPORT MODEL

by

WILLIAM WALTER PORATH

B. S., Kansas State University, 1961

AN ABSTRACT OF A MASTER'S THESIS

submitted in partial fulfillment of the

requirements for the degree

MASTER OF SCIENCE

Department of Nuclear Engineering

KANSAS STATE UNIVERSITY
Manhattan, Kansas

1964

ABSTRACT

The usual method of treating the problem of self-absorption in an absorbing media is by use of an effective cross section which, when multiplied by the average neutron flux within the absorber, yields the proper magnitude of the flux depression. In this work, the problem of self-absorption was investigated from the stand point of an effective rod radius. This approach was developed by use of the P_1 transport model.

The mathematical theory of the P_1 transport model in cylindrical geometry for a two region, absorbing and moderating, system was developed, and analytical expressions for the neutron flux in each region were given. Two different source conditions were considered in the development, and the coefficients in the flux equations were presented.

The flux depression in the rod as the result of self-absorption was approached from the stand point of an effective rod radius instead of an effective cross section as is the usual case. Several sets of data for a one inch and a two inch diameter steel rod were analyzed by an IBM 1620 computer program that varied the radius of the absorbing rod in order to obtain the best neutron absorption as calculated using the P_1 transport model.

The data were analyzed by fitting the correct expression for the flux in each region while requiring that the weighted sum of the square of the residuals should be a minimum. All

of the data were analyzed using one harmonic and the value obtained from the asymptotic theory expression for $\varkappa$, the inverse diffusion length, in the rod. Selected sets of data were analyzed using two and three harmonics. A comparison was made between P_1 transport theory and diffusion theory by analyzing the data using one harmonic and the diffusion theory value for $\varkappa$ in the rod.

The results obtained for the effective rod radius indicated that this approach to the problem of the self-absorption effect was feasible. However, the amount of data used in this work were insufficient to fully verify the approach, and considerably more experimental data would be required to adequately support the concept of an effective rod radius.